2004

Rapid erosion at the Tsangpo Knickpoint and exhumation of southeastern Tibet

Margaret Malloy
Lehigh University

Malloy, Margaret

Rapid Erosion at the Tsangpo Knickpoint and Exhumation of Southeastern Tibet

May 2004

Rapid Erosion at the Tsangpo Knickpoint and Exhumation of Southeastern Tibet

By

Margaret Malloy

A Thesis
Presented to the Graduate and Research Committee
of Lehigh University
in Candidacy for the Degree of
Master of Science

in
Earth and Environmental Sciences

Lehigh University

April 26, 2004

This thesis is accepted and approved in partial fulfillment of the requirements for the Master of Science.

4/30/07
Date

Thesis Advisor

Chairperson of Department

Acknowledgments

I would like to thank Peter Zeitler for advising me. He introduced me to Namche Barwa and the exciting world of diffusion. He has been a wonderful advisor and is a fantastic scientist.

Much of the data I have would not have been possible without the expertise of Bruce Idleman. He is a wizard with lab equipment and gave exceptional advice.

I would also like to acknowledge Amanda Ault, Anne Meltzer, Brian Zurek, and Stephane Sol. They were great company in the field and their comments and advice were invaluable in interpreting my data. Anne Meltzer and Frank Pazzaglia deserve credit for being superb committee members. The entire Geodynamics of Indentor Corners group has been a great group to work with, especially Noah Finnegan, Mandy Booth, Bill Kidd, Peter Koons, and Dave Craw. Thank-you to Pete Reiners and Stefan Nicolescu for aiding in the analysis o zircon samples.

I would of course like to thank my family for supporting me. They listened to my crazy ranting about exotic places like the Tsangpo River and nodded and smiled at all the right times. My mom and dad deserve special credit for raising me to be unsatisfied with any job not done to the best of my capabilities. They also endured a number of late night phone calls about tests, grades, and papers.

Most importantly I would like to thank Robbie King. Not only is he the first roommate I ever had who could tolerate me for more than a year, he has continued to push me to improve as a scientist. He corrected my horrible grammar in every draft of my thesis, pushed when I needed a push and took me to the movies when I needed to breathe. He will make a wonderful professor one day.

Table of Contents

List of Tables

List of Figures

ABSTRACT

Located in the Himalayan-Tibetan Orogeny, the Tsangpo River flows east along the Indus-Tsangpo Suture Zone into the eastern Himalayan syntaxis but then abruptly reverses direction across the Namche Barwa antiformal massif and turns southwest towards the foreland. Associated with the change in the direction of the Tsangpo is a large knickpoint within the massif that drops 2,000 m in elevation. The abrupt change in the direction of the river at the massif suggests a past capture event. One proposed origin for the Namche Barwa massif involves tectonic and erosional feedbacks, which in turn may be linked to relatively recent capture of the Tsangpo River into the Brahmaputra system. In this model, the river is responsible for vigorous erosion that distorts local stress fields and focuses strain, thereby causing localized weakening of the crust and rock uplift. In an attempt to interpret the tectonic and geomorphic history of the Namche Barwa area, we have measured a suite of (U-Th)/He zircon and Ar/Ar K-feldspar ages from around this region. These data have been paired with currently unpublished Ar/Ar biotite ages. The zircon helium ages range from 0.22 Ma near this knickpoint to over 12 Ma at distal and higher-elevation locations. This age pattern extends across mapped terranes and structures and appears to define a regional-scale partial-retention zone with an inflection at ~3,000 m of elevation and 1-2 Ma in age. This inflection suggests at least several kilometers of erosion within the past few million years, consistent with the recent capture of the Tsangpo and propagation of incision into the SE Tibetan plateau. However, biotite ages of less than 5 Ma are trapped within the bounding structures of the Namche Barwa massif and suggest that the Tsangpo knickpoint is pinned by the exhumation of the massif. Furthermore, Ar/Ar feldspar thermal histories appear to

confirm the age relationships seen in both data sets. Here, we discuss a model for the Namche Barwa massif pairing biotite and zircon age patterns and their implications for the topography of southeastern Tibet.

CHAPTER 1 - INTRODUCTION

Recent research demonstrates that river incision establishes feedbacks with tectonics that collectively define how rocks will be exhumed (Avouac and Burov, 1996; Zaprowski et al., 2001; Zeitler et al., 2001; Vance et al., 2003). Molnar and England (1990) noted that climate change and stream incision are coincident with much of the rock uplift observed during the late Cenozoic in a number of orogens. Molnar and England (1990) further suggested that climatic variables could create a positive feedback on an existing orogenic system. Montogomery et al. (2001) debated the importance of such processes in the active Andean orogeny, while Zaprowski et al. (2001) demonstrated the importance of knickzones as the primary mechanism for the exhumation of the tectonically dead Black Hills, South Dakota. The relatively young and active Himalayan Orogeny, provides a premium setting for studying tectonic and erosional interactions and acts as a natural laboratory to investigate incision and uplift processes. Zeitler et al. (2001) examined the interplay of erosion and exhumation at Nanga Parbat within the western syntaxis (corner) of this tectonic belt. They proposed a model for Nanga Parbat as a "tectonic aneurysm" and suggested that erosion by the Indus River may be responsible for the 15-20 km of localized exhumation calculated for the past 3 Ma.

This study focuses on the eastern Himalayan syntaxis, where preliminary geomorphic and tectonic data suggest a setting similar to Nanga Parbat (Figure 1; Zeitler et al., 2001). Here, the Tsangpo River flows east along the Indus-Tsangpo Suture Zone (ITSZ). The arrival of the river to the Namche Barwa massif marks the location at which the river flows off of the Tibetan Plateau. Decreased riverbed elevations (a drop of

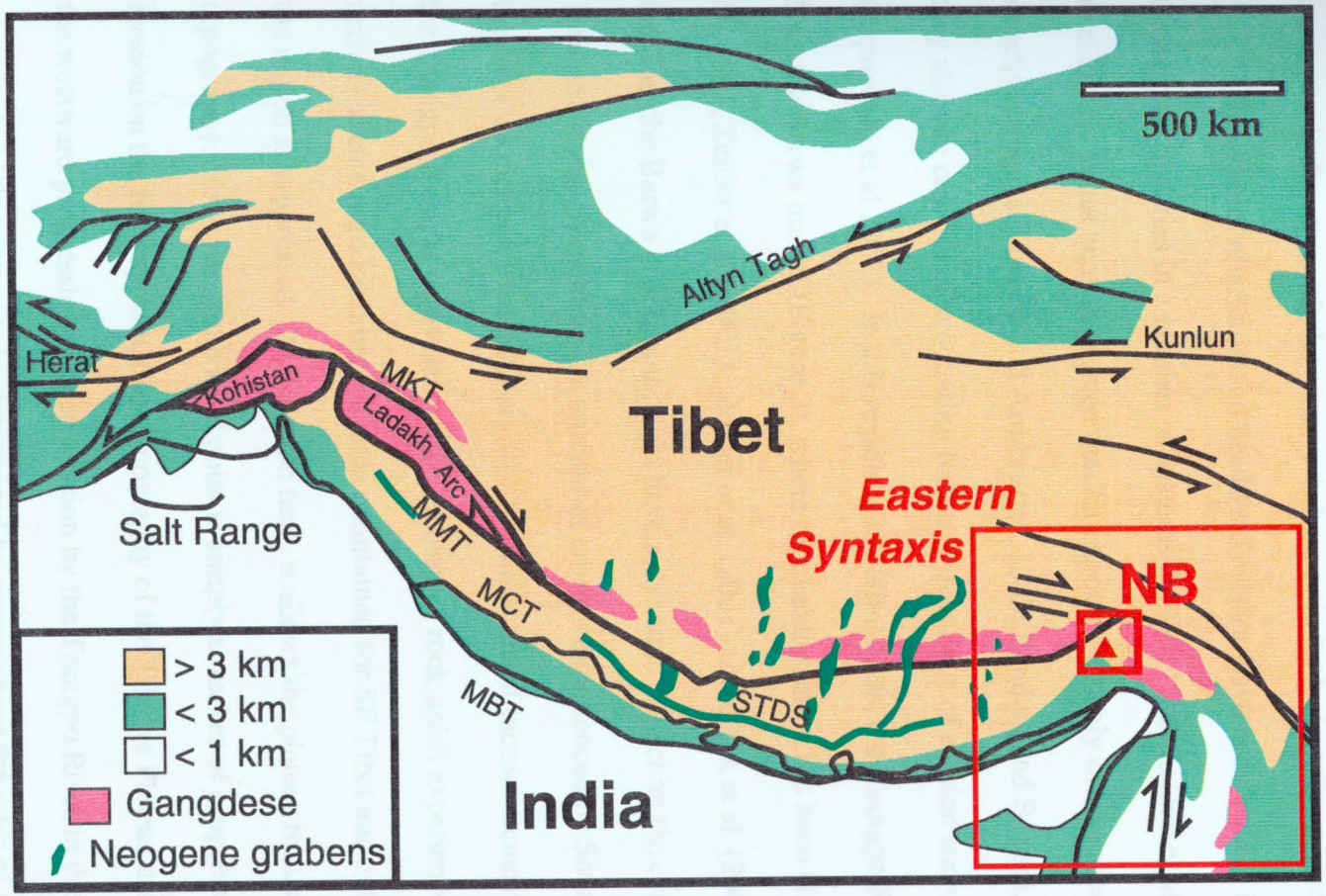

Figure 1: The Himalaya-Tibet Orogen. The field area for this study is located in the eastern syntaxis, around the Namche Barwa massif as is indicated. NB: Namche Barwa; MBT: Main Boundary Thrust; MCT: Main Central Thrust; MMT: Main Mantle Thrust; MKT: Main Karakorum Thrust; STDS: South Tibetan Detachment System. Figure taken from Zeitler et al., 2001

~2km) and increased topographic relief at the Namche Barwa massif, mark this transition and are delineated by a knickpoint on the river system (Figure 2a). The river's power corresponds directly with the observed changes in both elevation and relief (Figure 2b).

Knickpoint migration and headward erosion have been used to identify Quaternary histories in a number of systems (Miller, 1990; Leland et al, 1998; Zaprowski et al 2001). It has been suggested that knickpoints not only denote areas of recent uplift in active orogens (Seebert and Armbruster, 1983; Bendick and Bilham, 2001), but that they also are capable of accounting for large quantities of erosion and exhumation (Zaprowski et al 2001). In this region of the Himalayas, the Tsangpo River crosses the Namche Barwa massif (Figure 3), where rapid exhumation has been observed (Burg et al., 1998; Zeitler et al., 2001). Zeitler et al. (2001) and Clark et al. (2004) suggested that the Namche Barwa knickpoint might have a dynamic impact on the evolution of the Tibetan Plateau by limiting the amount of erosion experienced by Southeastern Tibet. If the river's knickpoint is stationary (the local amount of incision/removal of material by the Tsangpo River is equivalent to the amount of rock uplift experienced within the massif), then a high local base level is maintained for SE Tibet and extensive erosion of the region is suppressed. At the same time, it allows the plateau to sustain its high topography. However, if the knickpoint is simply a marker of progressive headward erosion on the river system, then topography of the Tibetan Plateau may be affected by the westward progression of deep incision by the Tsangpo River in the near future. The magnitude of this can only be determined by constraining the rates of this headward erosion. Furthermore, additional age constraints for exhumation upstream of the Tsangpo knickpoint can be used to further constrain the timing and distribution of plateau

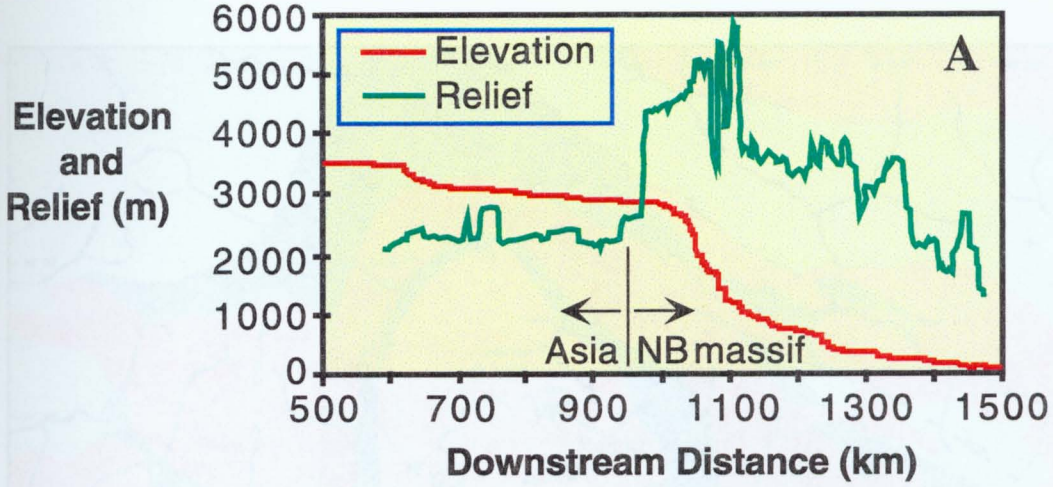

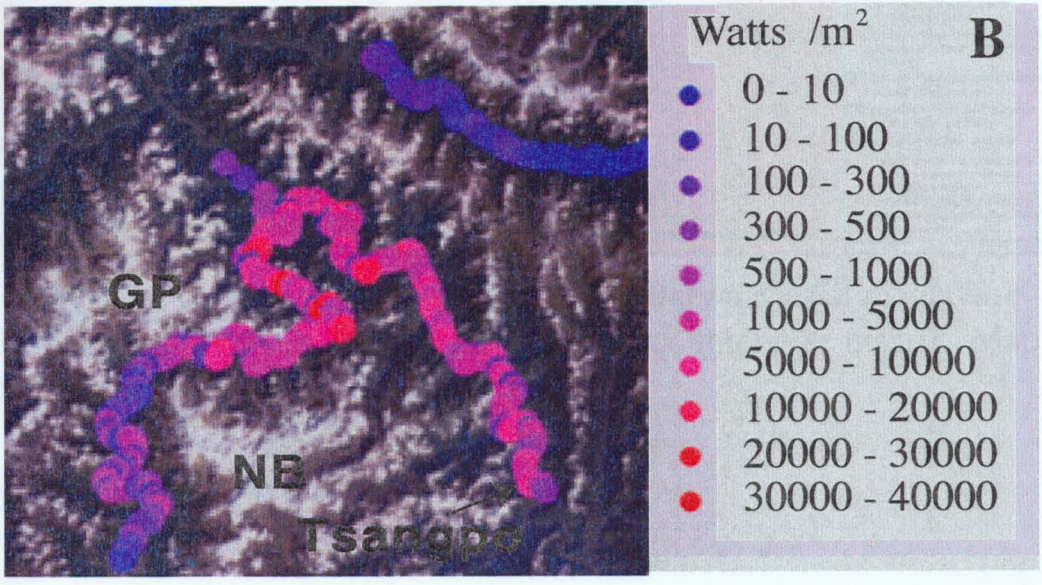

Figure 2a: Decreased river bed elevations (a drop of ~2km) and increased topographic relief at the Namche Barwa massif mark this transition and are deliniated by a knickpoint on the river system.
Figure 2b:The river's power corresponds directly with the observed changes in both elevation and relief. Figures courtesy of Noah Finnegan. NB: Namche Bawa; GP: Gyala Peri

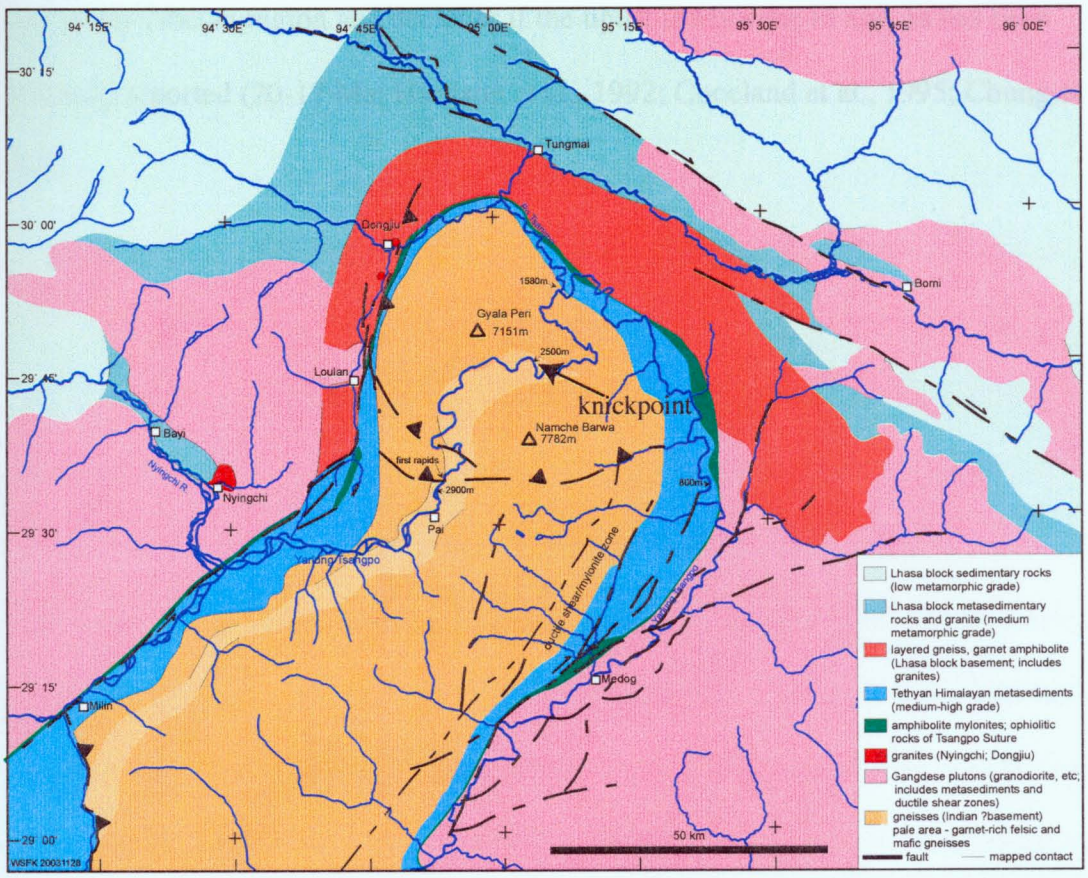

Figure 3: A geological map of the Namche Barwa Massif displaying the bend made by the Tsangpo River as it encounters the massif. Map courtesy of W. S. F. Kidd.

uplift in the Tibetan region and decipher if the uplift is Miocene in age, as has been previously reported (20-17 Ma; Harrison et al., 1992; Copeland et al., 1995; Chung et al., 1998).

CHAPTER 2 – BACKGROUND

2.1 GEOLOGIC SETTING

The Himalayan Orogeny is a relatively young continent-continent collisional system. India initially collided with Eurasia between ~40-50 Ma (Figure 1; Coward and Butler, 1985). At present, the Himalayas are divided by a series of north-dipping faults into different geological domains: the Subhimalayas, Lesser Himalayas, Greater Himalayas, and the Tethys Himalayas (from south to north; Figure 1). The Indus-Tsangpo Suture Zone, the northern boundary of the Tethys Himalayas, represents the location at which the two continents collided (Figure 1; Burchfiel et al., 1992; Searle and Treloar, 1993; Hodges, 2000). Directly north of the Tethys Himalayas is the Tibetan Plateau, which is believed to have been uplifted around 20-17 Ma (Harrison et al., 1992; Copeland et al., 1995; Chung et al., 1998) and is composed of a number of terranes added to the Eurasian Plate prior to the Himalayan orogeny proper (Hodges, 2000).

Approximately one-third of the area covered by the orogen is dominated by the two syntaxes, or corners (Zeitler et al., 2001). Nanga Parbat, a massif located in the western syntaxis, is described by Zeitler et al. (2001) as a "tectonic aneurysm", where erosion by the Indus River causes a positive feedback cycle that drives further exhumation of the massif. Erosion by river incision causes the crust to weaken and a topographic gap to develop. Crustal flow is then diverted towards this gap and can cause rapid rock uplift. This then drives more erosion and removal of material. Zeitler et al. (2001) hypothesized that Namche Barwa and the Tsangpo River, located within the Himalaya's eastern syntaxis, may represent a similar system. More importantly, the Tsangpo River may play

a significant role in the topographic evolution of the Tibetan Plateau through its erosion of much of the southeastern region of Tibet. Without the presence of other processes adding or restoring the crust, such erosional processes would result in the removal of a large amount of crust from the plateau, ultimately causing the plateau to shrink in size.

The Namche Barwa massif represents a geologic window of the Indian Plate in the Transhimalayan Plutonic Belt (Burg et al., 1998). The Namche Barwa massif (Figure 3) is composed of a 30 – 40 km wide antiform in Proterozoic gneisses derived from the Indian basement, which are overprinted by a Pleistocene metamorphic event (Burg et al., 1998). Thrust faults within the massif and strike-slip faults bounding the massif have been proposed (W. S. F. Kidd, personal communication); however, these faults have yet to be confirmed by field observations. A ductile shear zone and Tethyan Himalayan metasedimentary rocks surround the massif.

Where the Tsangpo River cuts across the Namche Barwa antiform, a major knickpoint is present. It is here that the river changes its easterly course along the Indus Tsangpo Suture Zone to head south towards the Bay of Bengal (Figure 3; Brookfield, 1998). Brookfield (1998) and Clark et al. (2004) suggest that this was not the original path of the river, which may have originally continued to flow east to connect with the present day Irrawaddy River (Figure 3), but its present turn to the south is a result of river capture. Clark et al. (2004) described the possible capture event as being caused by the capture of the Tsangpo, an orogen parallel river, by a steep transverse river, such as the Lhuit river, and then by the Brahmaputra river at the border between India, China and Burma (Figure 3).

The processes making river capture possible are suggested to have been brought on by the collision with India and Asia and the formation of the Tibetan Plateau, which caused major climate changes while also changing the drainages of a number of river systems. Clark et al. (2004) proposed that the rivers of eastern Tibet used to flow in a dendritic pattern. Many of the drainages subsequently were captured or reversed direction of flow in the same time frame as initiation of uplift of eastern Tibet (Koons, 1995; Brookfield, 1998; Hallet and Molnar, 2001; Clark et al., 2004). Here, Clark et al. (2004) calls for surface uplift as the cause for changes in river drainages, with shearing due to collision playing a secondary role. Hallet and Molnar's (2001) work in the three rivers area just east of the Namche Barwa massif, also calls for changes in drainage patterns as a result of collisional process. The three major rivers described by Hallet and Molnar (2001) are located within tens of kilometers to one another, and flow almost parallel. Hallet and Molnar (2001) expressed that this close proximity is result of right lateral shearing in response to collision and has forced the rivers to come unnaturally close to one another. Hallet and Molnar (2001) also noted that this indicated the presence of a large amount of crustal strain in the region of the eastern Himalayan syntaxis.

2.2 PRINCIPLES OF GEOCHRONOLOGY

Geochronology has been used in a number of tectonic settings to describe the timing of uplift events and to formulate regional cooling histories (e.g. Tjia et al., 1974; Mehta, 1980; Zeitler et al., 1989; Wolf et al., 1997; Spotila et al., 1998; Reiners et al., 2003). Thermochronology records an age of cooling for a given mineral phase through a given temperature. These temperatures can range from those representing rock

formation, to as low as 75 °C. These low-temperature systems have the ability to record cooling post crystallization. The cooling ages of a region can then be modeled and allow us to study processes that do not necessarily involve rock formation, such as river incision and exhumation.

Slowly cooling minerals gain radioactive products through radioactive decay (example: decay of U-Th to form Pb and alpha particles). However, these products, known as daughter products, may be lost from the system through thermally activated diffusion (McDougall and Harrison, 1999). This diffusion will slow as temperature falls, ultimately becoming negligible over even geologic time spans, such that virtually all radiogenic daughter product is retained with the crystal system. (Dodson, 1973; McDougall and Harrison, 1999). The physics and math of diffusion in a cooling system allows us to define a closure temperature for radiogenic isotopes. The apparent age given by these radiogenic isotopes represents the time at which a mineral had passed through its closure temperature (McDougall and Harrison, 1999).

Grain size and shape play a role in daughter-product retention, to a secondary degree. Upon thermal disturbance of a mineral, loss of diffusional products can occur at the surface of the mineral, while the mineral's interior will be less affected (Mcdougall and Harrison, 1999). The specific size and shape of a grain help to dictate how it will lose radiogenic information upon analysis and in nature. Size matters because diffusing atoms have a shorter distance to go in smaller grains. Shape matters because it is a measure of the surface/volume ratio; for equal volumes, the one with the higher surface area will experience greater diffusional loss. Because of this, we must take into account a mineral's size and dimensions when trying to obtain radiogenic information from it

If a mineral were to cool quickly through its closure temperature, the transition between which the mineral system is dominated by diffusional loss versus dominated by retention would be short. The age of such a grain would display the time at which the mineral experienced rapid cooling (when the daughter product began to be retained; McDougall and Harrison, 1999). However, in a slowly cooling system the time between total losses of the daughter product versus virtual total retention is very slow. Here, ages obtained represent a combination of when the system began to retain some radiogenic information (while diffusion was still taking place) and when diffusion became negligible.

One-way to examine slow cooling processes is to examine many samples from the same area over a vertical profile. A vertical profile through a system's closure temperature should display multiple cooling ages. These ages will reflect the region's cooling history (Figure 4). The zone in which minerals begin to retain radiogenic information (while still experiencing some diffusion) is called the partial retention zone (PRZ). In the PRZ, ages span from the actual ages of cooling to close to zero (the region in which the system is thermally active and complete outward diffusion occurs). Ages within the PRZ are not valid times of cooling. If an entire section of rocks- those experiencing no, partial, and full radioactive retention-were to be quickly incised, the entire data trend would be preserved and an image of the partial retention zone would be captured. The PRZ is less clear in younger systems that are undergoing rapid cooling. PRZ's are most diagnostic when cooling rates have slowed or become stagnant, so that their shape has a double-inflection. In young continuously cooling systems, the profile

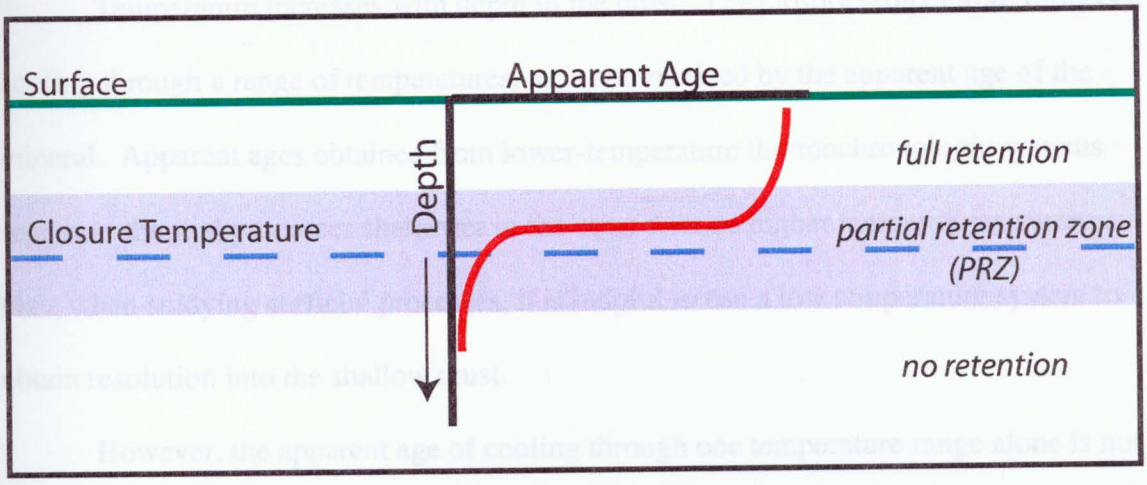

Figure 4: Profile of apparent ages through the closure temperature. As depth decreases, temperature increases. Above the closure temperature, the apparent age is zero. Cooling through the partial retention zone allows for the gradual retention of radiogenically produced products and eventual full retention.

just flattens out to reach the background age-elevation trend, and if exhumed even more rapidly, you won't see the classic PRZ shape.

Temperature increases with depth in the crust. The closure temperature reflects a cooling through a range of temperatures, as is summarized by the apparent age of the mineral. Apparent ages obtained from lower-temperature thermochronologic systems represent thermal processes shallower in the crust than do higher temperatures systems; thus, when studying surficial processes, it is helpful to use a low temperature system to obtain resolution into the shallow crust.

However, the apparent age of cooling through one temperature range alone is not enough to define the thermal history of a region. . In a tectonically inactive region, isotherms follow topography, but with depth the degree to which these isotherms are affected by the topography decreases (Braun, 2002). In tectonically active regions the cooling histories of the area may differ spatially and temporally. Isotherms, especially shallow isotherms, are affected by topography, advection of rock, and erosion. The response of isotherms to a change in either one of these variables may not be instantaneous (there may be a time lag before equilibrium is reattained). As these variables can also change spatially, the entire region's isotherms can vary four-dimensionally. In low temperature thermochronometry, this can lead to an overestimation of exhumation rates based on calculated apparent ages (Braun, 2002). Therefore, for tectonic systems where the topography is actively changing, it is helpful to employ the use of two radiogenic systems. A low temperature system will display how the topography has evolved, while a higher temperature radiogenic system will allow you to

constrain longer-term evolution and which is less sensitive to erosion, topography, and rock uplift (Braun, 2002).

To minimize these problems as much as possible, we developed a sampling strategy that encompasses a variety of elevations, as well as a broad area surrounding the Tsangpo knickpoint (both up and downstream). This allows us to view age relationships in three dimensions and examine spatial effects that might have affected parts of the study region. However, restrictions, and the nature of the field area, did not allow us as broad and specific a sampling as we would have liked. We were not able to sample much of the area south of Namche Barwa, nor immediately downstream of the knickpoint. Nevertheless, we were still able to sample a large swath of the field area. By following many of the Tsangpo's drainages we were also able to sample at a variety of different elevations, and we were even able to sample a vertical profile near Bayi (Figure 3), where a pack trail allowed us to climb up to higher elevations.

In this study, we consider the impact of erosion on active tectonics. Because the time scale at which geomorphic processes occur is extremely short, we have used a number of low temperature dating methods. The low closure temperature for some minerals allows them to be useful when studying exhumational processes (Wolf et al., 1997; Spotila et al., 1998) and has allowed us to obtain resolution into the first few kilometers of the crust.

The lowest temperature radiogenic system used was zircon (U-Th)/He. The closure temperature for zircon (U-Th)/He is between 175°C and 200°C (Reiners et al, 2002). (U-Th)/He radiogenic dating has only recently resurfaced as a low-temperature thermochronometer, but has been found to be reliable for creating low temperature

thermal histories (Zeitler et al., 1987; Farley et al., 1996; Reiners et al., 2002). The initial major concern with (U-Th)/He was alpha loss from a mineral's crystal lattice (Farley et al., 1996).

U and Th decay to form Pb and alpha particles. These alpha particles have a certain amount of kinetic energy when created, which causes them to move inside the crystal. The distance required for these particles to stop can be tens of microns (Farley et al., 1996). In very small grains, this can cause much of the daughter product to be lost, or ejected from the mineral by alpha loss (Farley et al., 1996). This can become a problem in trying to obtain the correct parent to daughter ratio for an apparent age of cooling. However, Farley et al. (1996) have proven that by examining the characteristics of the specific grains being analyzed (the minerals shape and size), possible alpha ejection problems can be corrected and the (U-Th)/He system can be used more reliably.

The use of zircon has proven to be very advantageous in (U-Th)/He dating (Reiners, 2002). Zircon contains higher concentrations of both U and Th than most other minerals used in low-temperature thermochronology (e.g. Titanite; Reiners, 2002). This means that a smaller amount of zircon is needed to produce a precise measurement. However, zircons can be zoned. Reiner (2002) noted that there seemed to be a temperature dependant release of gas in zircon that is consistent with either multiple domains or radiation damage to the mineral upon heating. Zoning can make calculations of an alpha correction complicated. A high uranium rim surrounding an older (less uranium) core is not assumed when making corrections because the grain is assumed to be homogenous. However, the higher uranium rim will eject more alpha particles from the system and our estimated alpha correction will be under correcting. The system could

also be reversed and cause an over correction. Correcting for the possible unique zoning of each individual zircon grain is both time consuming and complex. Thus, in order to try to minimize the problem, we have duplicated every sample. The hope is that each duplicate will be zoned differently (if at all). If the two samples' apparent ages agreed, we assumed zoning to have minimal effects. If the two ages did not agree, we took an average of the ages and assumed that this would be a closer estimate of the actual age.

The potassium feldspar $^{39}Ar/^{40}Ar$ system was also used. Ar/Ar ages are equivalent to those ages found by the K/Ar system (Merrihue, 1965; Merrihue and Turner, 1966). However, because only Ar is being analyzed, it is possible to conduct only one analysis per sample (as opposed to conducting two analyses in K/Ar; one for K content and a separate for Ar content; Merrihue and Turner, 1966). Alkali feldspar has proved unique in this dating method in that it has variable Ar retention characteristics (Sardarov, 1957; Foland, 1974; Zeitler, 1987). Lovera et al. (1989) showed that these Ar retention characteristics are controlled by a number of different domains inside the feldspar structure of different sizes and volumes. These domains begin Ar retention at different times and therefore have a range of different closure temperatures. We are able to interpret these kinetic data enclosed within feldspars because of irradiation, in which an even uniform distribution of ^{39}Ar is produced in the sample that then can be released during step heating. Lovera et al. (1997 and 2001) then went on to prove that by step heating feldspars and slowly releasing the gas of each domain, you can obtain a thermal history from one sample. By using the ^{39}Ar and ^{40}Ar obtained from step heating we can model the kinetic data of an individual sample (e. g. obtain an arrhenius plot, kinetic energy, the domains, etc.). We can then use this information to model a sample's

possible thermal history. The main range of temperature information attained by this system is between ~350-125°C.

Finally, biotite Ar/Ar was also used for this study and is courtesy of Zeitler (unpublished data). The closure temperature for this system is around 300°C and allows us to examine exhumation through higher temperatures.

By using all of these geothermometers, as opposed to only one, we are able to resolve the thermal history of the upper crust in the Namche Barwa Region. Each data set gives us a different layer of thermal information. By combining all three layers, we develop a temporal map of the field area, that when paired with spatial relationships can be used to construct a model of the thermal history of the area.

CHAPTER 3 - METHODS

3.1 SAMPLE COLLECTION

Samples of granite and gneiss containing zircon, biotite, and potassium feldspar were collected over three separate field seasons between 2001 and 2003 (Figure 5). Samples were obtained for a regional resolution (the area east of Lhasa and past Bomi) as well as for a more specific concentration on the massif itself. It was the hope that this would guarantee an unbiased picture of tectonic/geomorphic rock uplift processes believed to be taking place in the Namche Barwa system. Samples were also taken at a number of different elevations.

3.2 MINERAL SEPARATIONS

Minerals were separated from whole rocks using physical and heavy liquid techniques. Typical procedures consisted of using a jaw crusher to break the rock down to centimeter size particles. This was then crushed to less than 250 μm using a rock pulverizer. Samples were then washed with water and ethanol and dried. The more dense grains (> 2.55 g/cm^3) were separated using a Wilfley table. Zircons were obtained using methylene iodide (density 3.32 g/mL). Feldspars were separated using LST (density 2.85 g/mL). Final separation was done using a Franz magnetic separator.

Zircon grains were individually picked for (U-Th)/He analysis. After a trial set of samples we found that only one grain was needed per sample because typically zircons contain enough U and Th to produce detectable levels of ^{4}He, even in samples that are under 1 Ma in age. The system comes into equilibrium less than a million years after initial crystallization. All samples used in this study were crystallized more than a million years ago. Radon leakage is also not a concern in this study because of its high

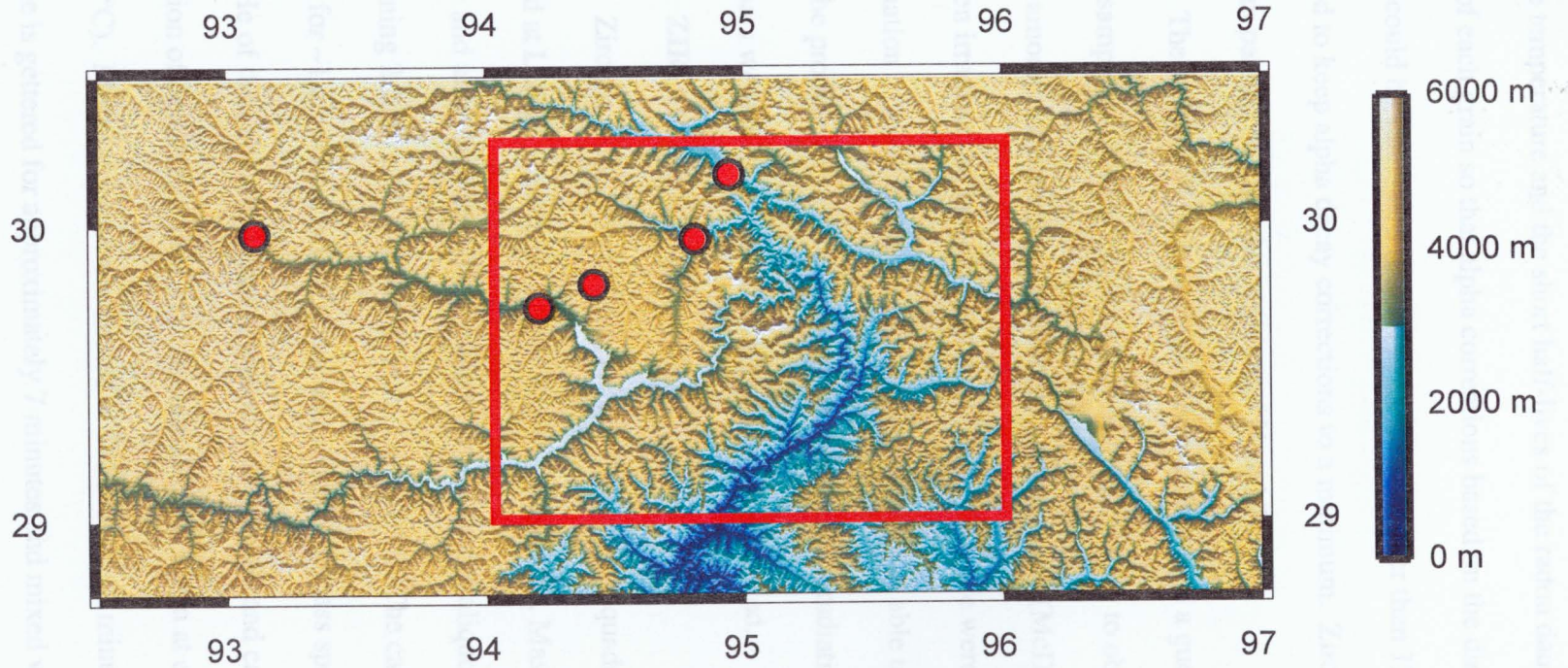

Figure 5: DEM of the Eastern Syntaxis with sample locations. Samples were collected and separated for feldspars (circles) and zircons (boxed area). To resolve the interaction of exhumation and river incision, both zircon (U-Th)/He thermochronometry and mica Ar/Ar thermochronometry were used to obtain low-temperature cooling histories. Feldspar Ar/Ar thermochronometry was also utilized to ensure capture of the regional cooling history.

closure temperature and the short half-lives of the radon daughter products. Pictures were taken of each grain so that alpha corrections based on the dimension and the size of the grains could be calculated (Figure 6). Grains smaller than 120 micron in width were avoided to keep alpha decay corrections to a minimum. Zircons were packaged in niobium packets to limit the addition of U and Th.

The amount of feldspar separated was based on a guess of the approximated age of the sample, as well as its potassium content. We try to obtain enough ^{40}Ar to ensure an ample amount for the numerous step-heating analyses (McDougall and Harrison, 1999). We then irradiate the sample to convert ^{39}K to ^{39}Ar. We were able to use preliminary information to make estimates of the expected ages in able to ensure that enough Ar could be produced in a short enough time period by irradiation to avoid this problem. Feldspars were then enclosed in tin packets and weighed.

3.3 ZIRCON ANALYSIS

Zircons were analyzed for ^{3}He and ^{4}He using a quadrupole mass spectrometer located at Lehigh University in the Geochronology lab. Mass discrimination is checked before and after each analytical session by measuring aliquots of a mixed helium standard containing 2.2234×10^{-13} moles of both ^{3}He and ^{4}He. The calibration gas is allowed to getter for ~1.5 minutes before it is released into the mass spectrometer. The measured $^{3}He/^{4}He$ of the calibration shot is typically about 0.80 and can be measured with a precision of better than 1% (1σ). An initial blank is run at extraction temperature (1350°C). Most samples were heated at 1350°C for 60 minutes. After heating, the sample is gettered for approximately 7 minutes and mixed with a 2.4987×10^{-13} mole spike of ^{3}He and then analyzed for He content. In any one batch standards are run last

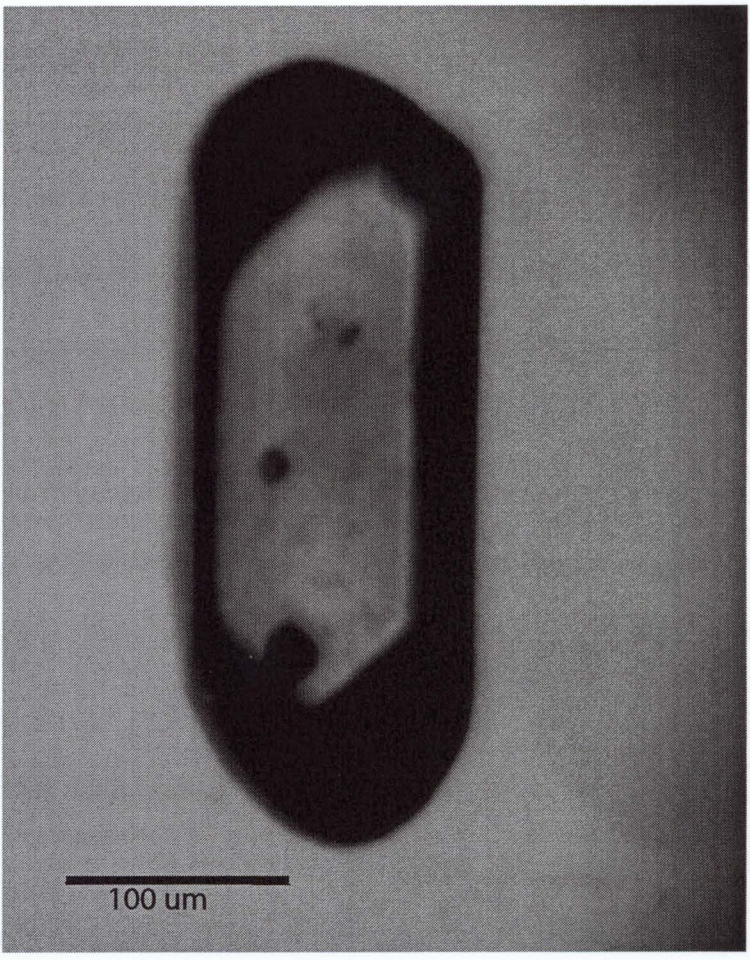

Figure 6: Typical zircon grain used for analysis.

because they have a much higher He content than most of our young zircons, and done in triplicate to assess analytical precision and the accuracy of our calibrations. The zircon standard for this study is the Fish Canyon tuff, with an approximate age of 27.9Ma formation found in Colorado (Carpéna and Mailhé, 1987). This standard has been shown to display (U-Th)/He ages consistent with other dating techniques (Reiners et al., 2002). Samples were then sent to Peter Reiners at Yale and analyzed by ICP-MS for U and Th. Effects due to alpha loss were assessed after all analyses are complete. The dimensions of the sample were compared to the U and Th concentrations to determine the effects of alpha loss (Ft), or the loss of the daughter product to a mineral due to alpha particle movement upon introduction into its crystal lattice (Farley et al., 1996). In smaller samples the effect of alpha recoil increases and can cause age corrections of up to 40%. To minimize this correction, zircons > 100 um diameter in size are used. All samples were replicated to give us an estimate of our precision.

3.4 FELDSPAR ANALYSIS

Feldspar samples were analyzed for Ar content using a VG 3600 mass spectrometer. Prior to analysis, feldspars were irradiated. K_2So_4 and CaF_2 were used as standards to calculate calcium and potassium interfering reactions. Step-heating analysis was conducted using the methods of Warnock and Zeitler (1998). Temperature can be controlled to better than 2-3 °C based on temperature measurements on the exterior base of the crucible. Previous experiments employing an internal thermal couple have shown a temperature offset of no more than 10 °C between the inside and outside of the crucible once crucible temperature had stabilized. After analysis the samples are corrected for

extraction line blanks, Ca and K interfering reactions from irradiation, decay of ^{37}Ar and ^{39}Ar, as well as for mass discrimination.

The number of domains in each sample was calculated by forward modeling. After obtaining the size, volume, and activation energy of each domain from the program, the feldspars thermal history can be modeled. In this study the Lovera forward model was used as well as the Arvert inverse model. Both models allow for the comparison of hypothetical thermal histories and the ^{39}Ar loss patterns that they would produce with that obtained from actual analysis.

CHAPTER 4 - RESULTS

Apparent ages of all samples in and around the Namche Barwa massif and the Tsangpo River's knickpoint show basic trends in the cooling histories of the region. Here we discuss the calculated ages found using both zircon (U-Th)/He and Ar/Ar thermochronometry. These ages are then compared to cooling histories obtained from feldspar analysis.

Table 1 summarizes (U-Th)/He age information obtained from zircon samples in and around the Namche Barwa massif (Figure 7, Appendix A provides full analytical data). All errors are recorded as 1σ errors. Error reported is based on the sample replicates, as the observed scatter in duplicates is large in comparison to analytical error and therefore dominates. The average error is consistent overall at ~ 10% of the age, but is seen as high as 30-100% in some samples. In these later samples we suspect that zoning is causing a greater than expected variation.

Zircon apparent ages are the youngest inside the massif (< 1 Ma), nearest the Tsangpo knickpoint. Ages gradually increase away from the knickpoint, and ages younger than 2 Ma are seen outside of the Namche Barwa massif. Zircon samples located at elevations lower than 2500m display ages between 0.2-2 Ma, with one exception, a 12 Ma sample located in the lower gorge ~60 km away from the Tsangpo knickpoint (Figure 8a). Those samples located above 2500m display ages older than 2 Ma and are scattered as high as 30 Ma. The age elevation relationship taken from a vertical profile near Bayi (figure 8b) displays little change in age over a ~ 1.5 km change in elevation.

Table 1: Zircon cooling ages obtained from (U-Th)/He analysis.
Details of analyses are located in appendix A.

sample	corrected age 1 (Ma)	corrected age 2 (Ma)	1σ	Average Age	RSD %
b115	1.31	1.01	0.21	1.16	18.29
b141	0.59	0.57	0.01	0.58	2.44
b-188	2.77	1.84	0.66	2.31	28.53
b-232	0.19	0.33	0.10	0.26	38.07
b-247	0.12	0.79	0.47	0.46	104.12
b-254	0.50	0.51	0.01	0.51	1.40
b-265	0.50	0.70	0.14	0.60	23.57
b35	13.07	11.15	1.36	12.11	11.21
BC-02-02	28.04	30.12	1.47	29.08	5.06
BC-03-02	11.44	13.07	1.15	12.26	9.41
BL-03-03	13.72	12.48	0.88	13.10	6.69
BL-05-03	9.10	16.99	5.58	13.05	42.77
BL-06-03	9.93	10.03	0.07	9.98	0.71
BL-07A-03	10.04	9.10	0.66	9.57	6.95
BL-09-03	9.34	2.50	4.84	5.92	81.70
BM-02-02	9.72	8.71	0.71	9.22	7.75
BM-03-02	9.78	10.86	0.76	10.32	7.40
BT-07-02	1.56	1.33	0.16	1.45	11.25
BT-08-02	4.95	4.27	0.48	4.61	10.43
BT-09-01	5.11	6.03	0.65	5.57	11.68
BT-12-02	4.34	5.32	0.69	4.83	14.35
BT-17-02	1.83	2.12	0.21	1.98	10.38
BT-18-01	0.30	0.42	0.08	0.36	23.57
BT-20-02	1.29	1.27	0.01	1.28	1.10
BT-20E-02	14.69	13.04	1.17	13.87	8.41
BT-21E-02	5.78	5.13	0.46	5.46	8.43
BT-23-02	1.77	1.33	0.31	1.55	20.07
BT-24-02	0.62	0.72	0.07	0.67	10.55
BT-29-02	1.02	1.73	0.50	1.38	36.51
BT-31-02	2.51	3.12	0.43	2.82	15.32
GP-09-03	0.58	0.63	0.04	0.61	5.84
GP-14-03	0.93	0.72	0.15	0.83	18.00
IG-15a-01	1.36	1.31	0.04	1.34	2.65
IG-19-01	2.24	2.64	0.28	2.44	11.59
IG-20b-01	2.97	2.81	0.11	2.89	3.91
NB02-102	7.31	6.79	0.37	7.05	5.22
NB02-120	14.37	12.84	1.08	13.61	7.95
NB02-159	5.20	5.64	0.31	5.42	5.74
NB02-35	1.87	1.68	0.13	1.78	7.57

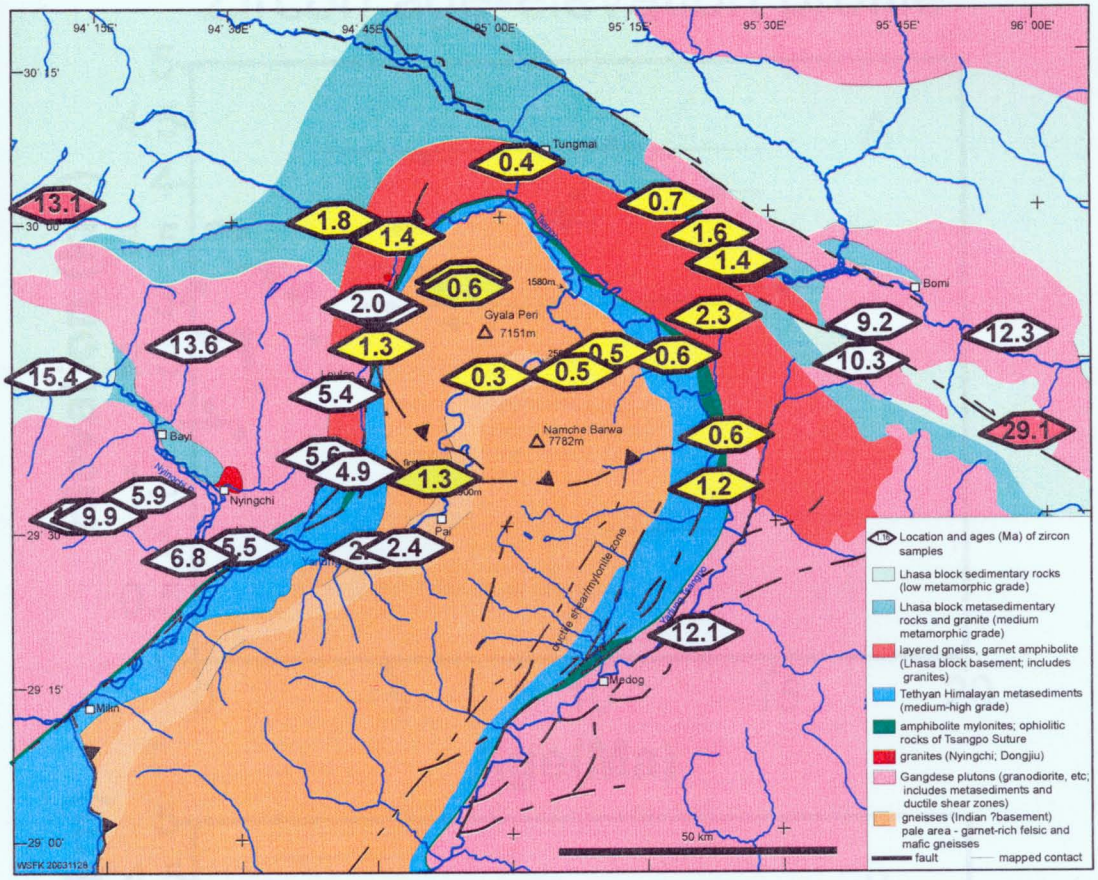

Figure 7: Zircon (U-Th)/He sample locations. The map shows the basic geology, structure and tributaries of the Namche Barwa massif. Prisms represent the location of zircon samples and their alpha-corrected (U-Th)/He cooling ages (closure temperature ~200°C) . Samples younger than 2 Ma have been shaded yellow. The red prisms denote samples located a few kilometers from the map boundaries. Younger ages occur within the Namche Barwa massif near the Tsangpo's knickpoint, and also at the lowest elevations along the river's main tributaries to the knickpoint. Note that the youngest ages are distributed across the proposed massif bounding structures. Map courtesy of W.S.F. Kidd

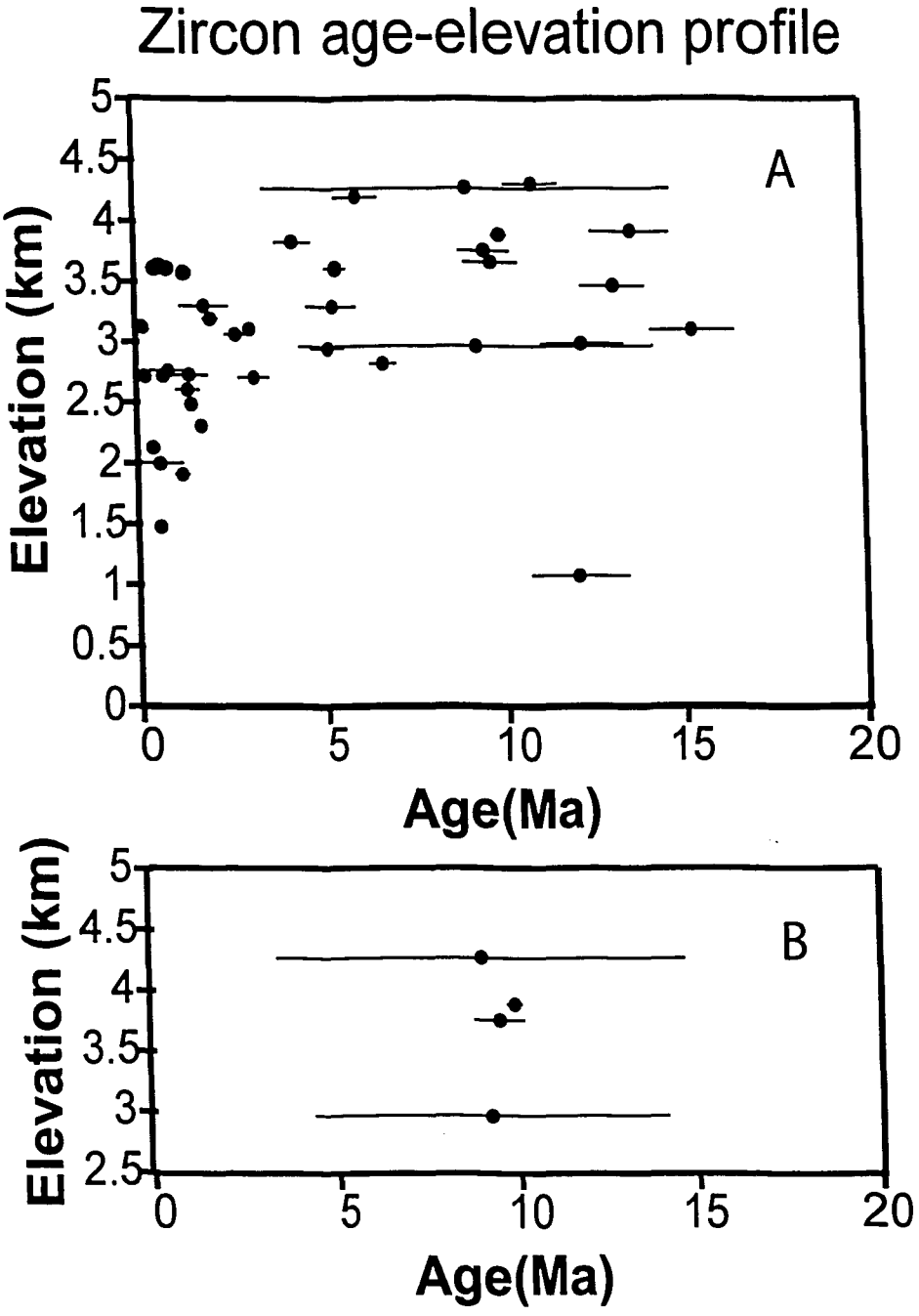

Figure 8: A. General age-elevation profile for zircon samples located in and around the NB massif. Trends in the zircon age- elevation profile show a steep gradient in ages at lower elevations (1500 - 2700 m), with a scatter of ages at higher elevations (~2700 m and up). B. Vertical profile of samples taken near Bayi. Bars represent 1σ error in ages. The error in elevations is smaller than the sample points.

Mica ages obtained from Peter Zeitler (unpublished data, Figure 9) display a central location of young ages (less than 5 Ma) inside the Namche Barwa antiformal massif, with the youngest ages (<2 Ma) located around the Tsangpo knickpoint. Samples located directly outside the massif display a dramatic jump to older ages (10-35 Ma).

Figures 10-14 summarize Ar/Ar feldspar results, showing age spectra, kinetic and domain information for each sample. Detailed feldspar analysis information is reported in appendix B. The Arrhenius relationships and R/Ro plots for each sample are used in determining the kinetic and diffusional parameters for each sample. All feldspar samples modeled have Ar distributions that suggest between 6 and 9 domains.

The first two modeled samples are located less than 20 km north, northwest of the massif (Figure 5). Sample BT-07-02, a garnet bearing granitic rock, displays initial cooling at approximately 10-8 Ma (Figure 15a). This is followed by a period of either isothermal equilibrium or slow cooling until approximately 2 Ma, when the sample was brought to the surface. Sample BT-33-02, a sample extracted from a granitic dike intruding metasediments, displays cooling during a similar time frame (Figure 15b). Here, the model suggests that there was initial cooling between 14 and 12 Ma. Again, either slow cooling or isothermal equilibrium follows this until approximately 2 Ma. Following this, a period of fast cooling is required to bring the sample to its current position on the surface. Both samples display periods of slow/no cooling for approximately 6 m.y. Then, in order for them to reach surface conditions, they experience rapid cooling starting near 2 Ma.

Two more feldspars samples are located within 50 km to the west of the massif, upstream of the Tsangpo knickpoint (Figure 5). The first, BT-20E-02, is a Gangdese Arc

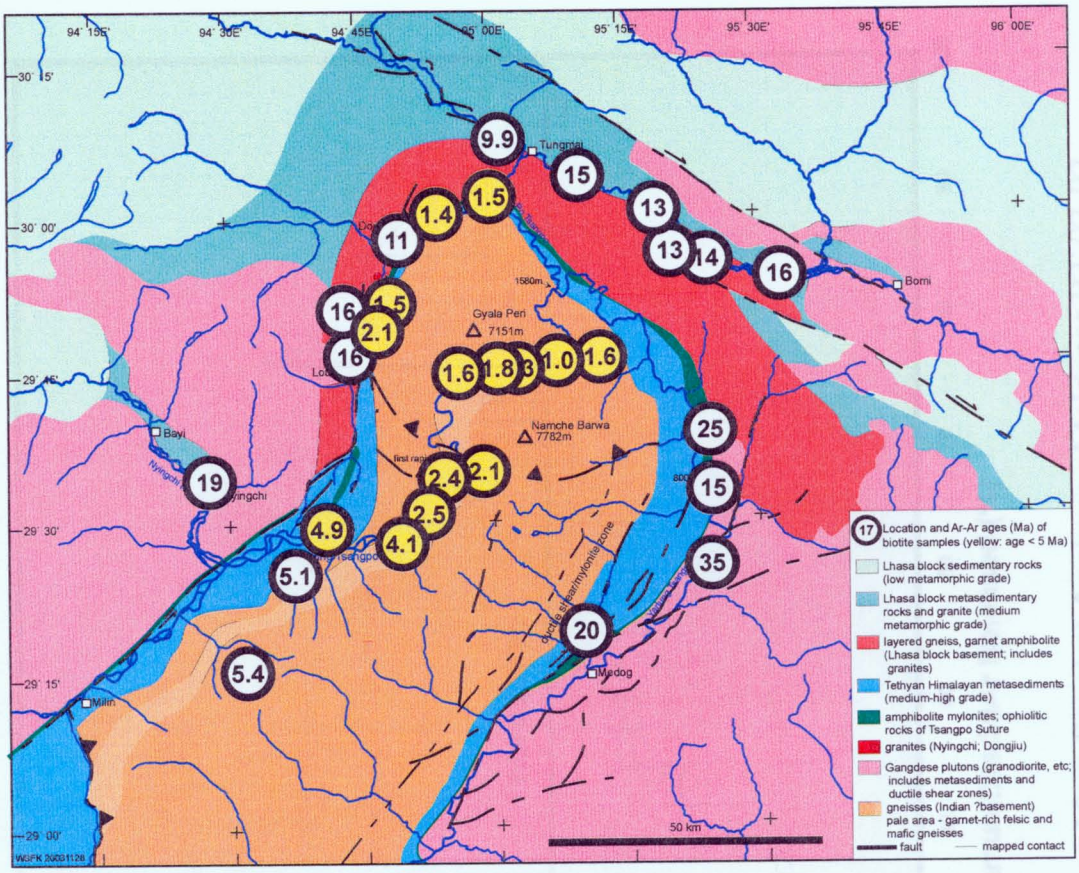

Figure 9: Ar-Ar Biotite Analyses (Zeitler, unpublished data). Circles show measured Ar-Ar cooling ages for biotites (closure temperature ~300°C). Ages younger than 5 million years have been highlighted to better show the distribution of young samples within and around the massif.

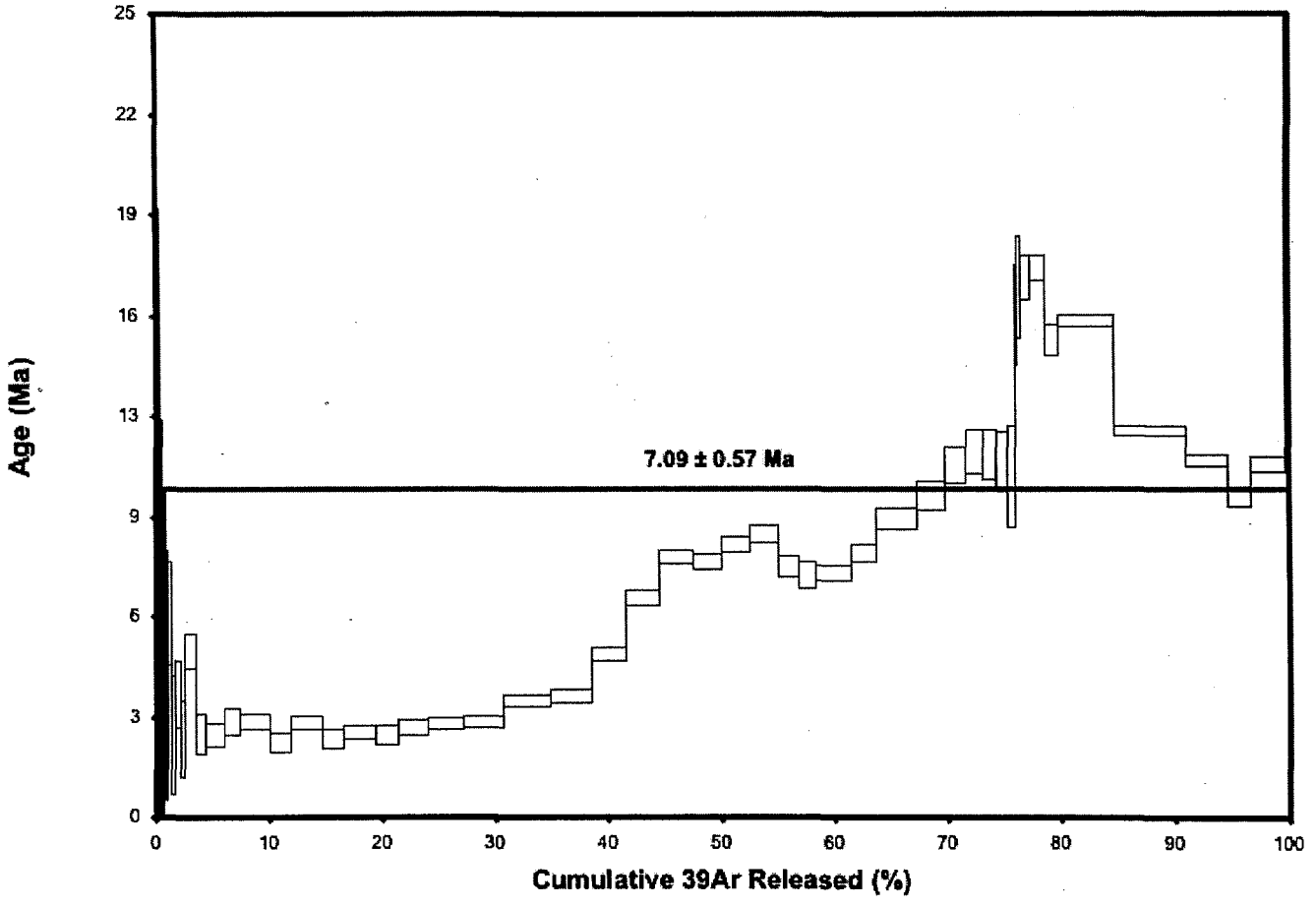

Figure 10a: Age Spectrum recorded from Mass Spectral Analysis of feldspar BT-07-02.

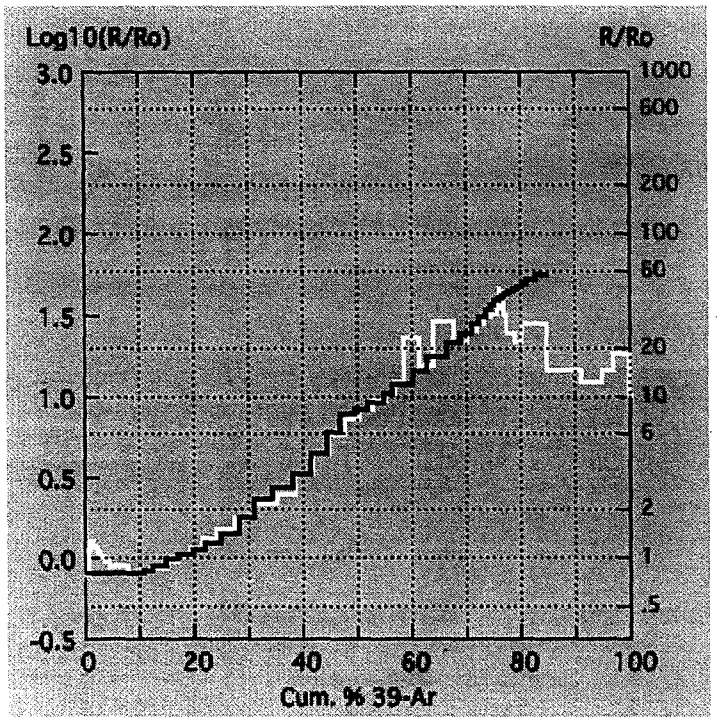

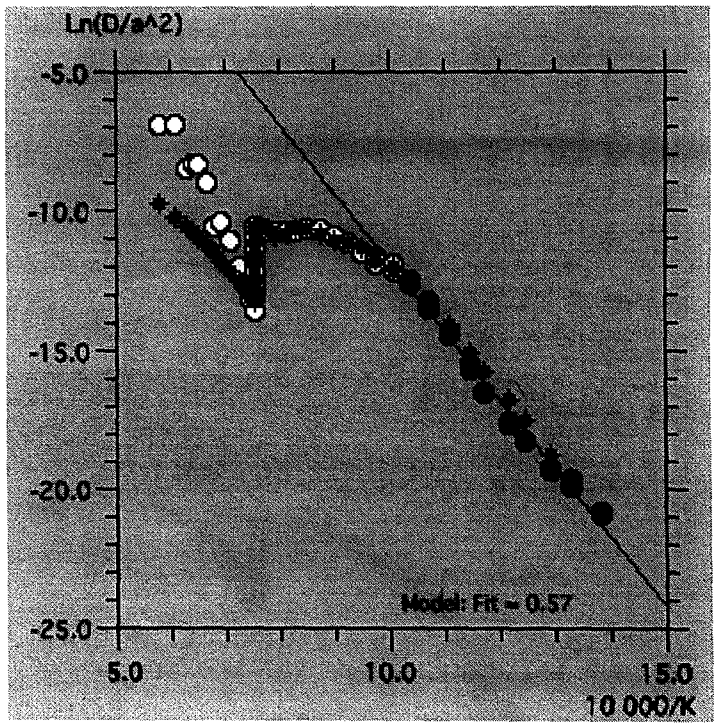

Figure 10b: Arhennius and R/Ro plot for feldspar BT-07-02.

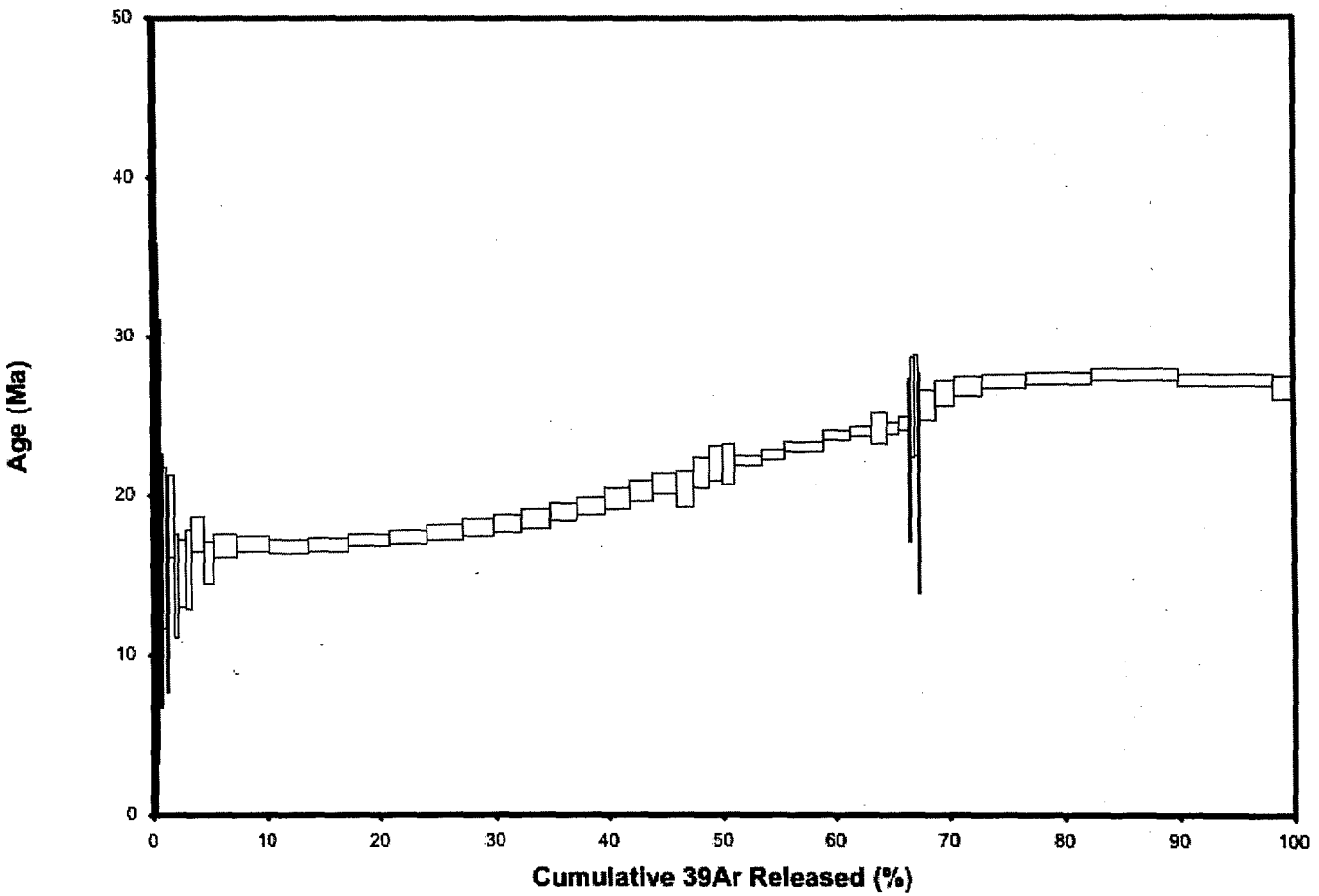

Figure 11a: Age Spectrum recorded from Mass Spectral Analysis of feldspar BT-20E-02

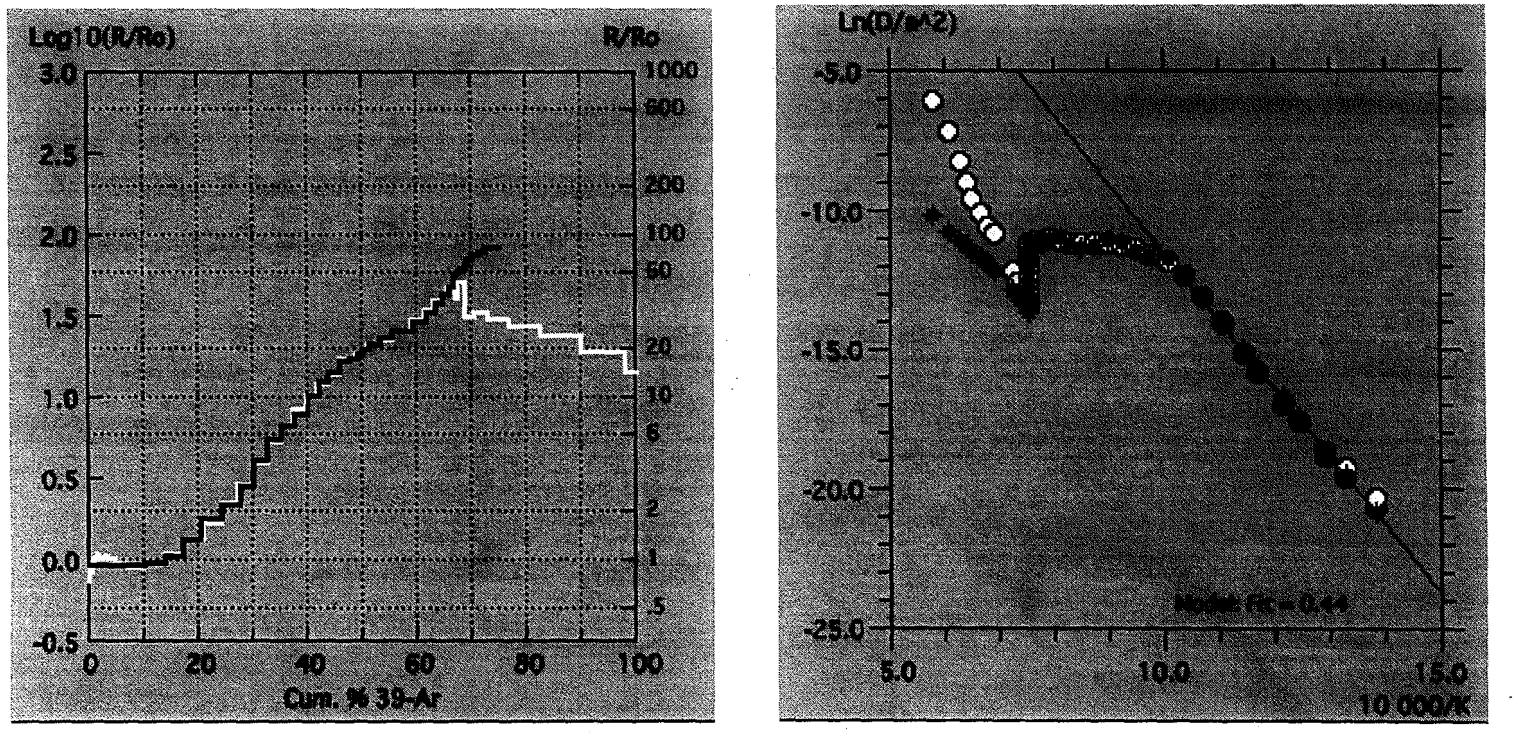

Figure 11b: Arrhenius and R/Ro plot for feldspar BT-20E-02

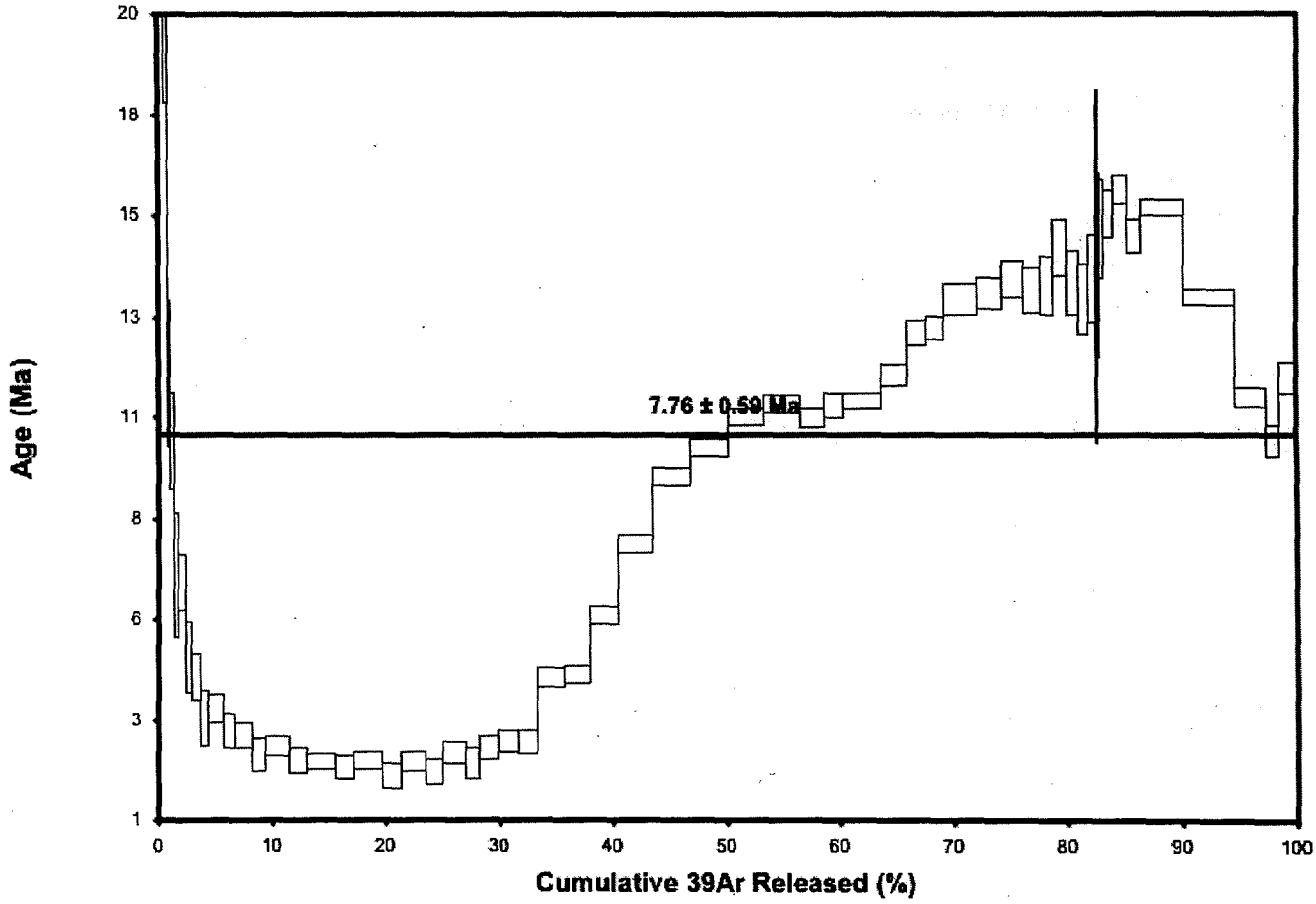

Figure 12a: Age Spectrum recorded from Mass Spectral Analysis of feldspar BT-33-02.

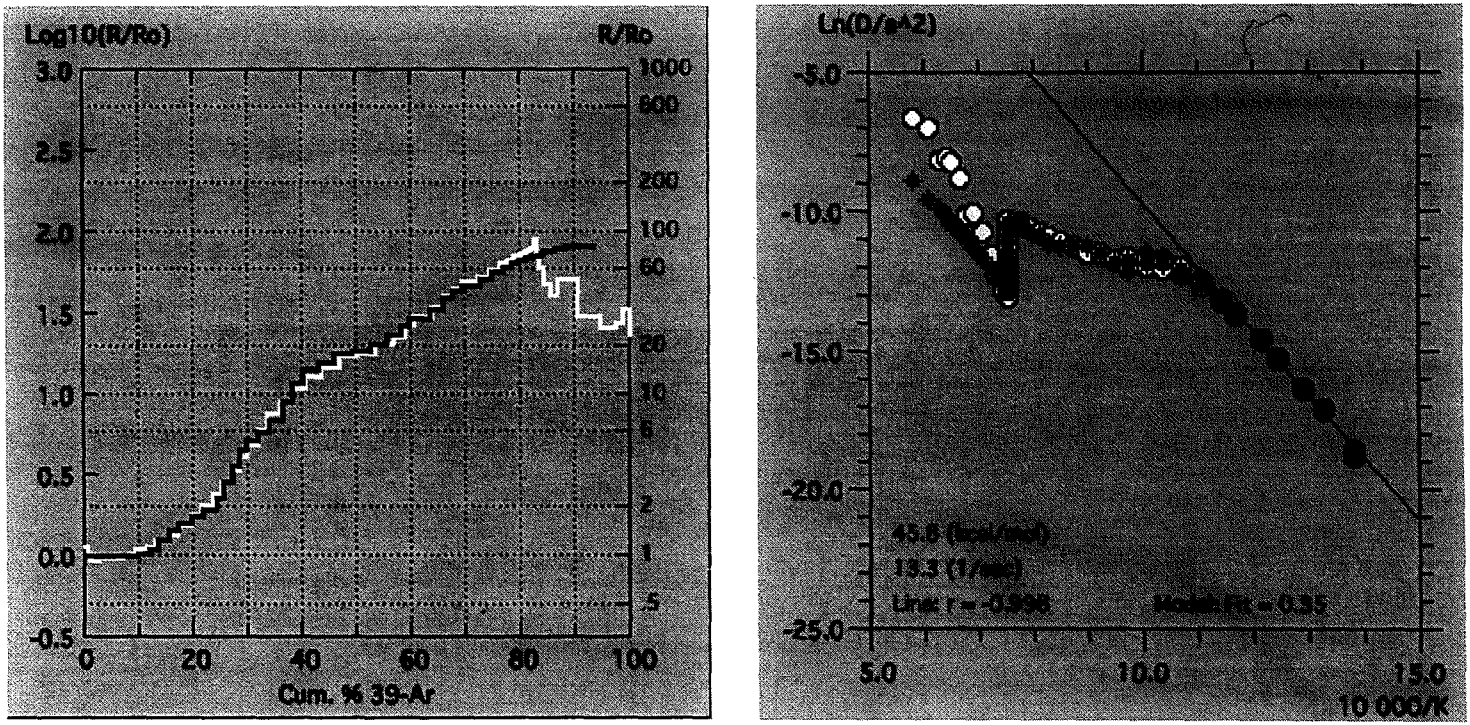

Figure 12b: Arrhenius plot and R/Ro plot for feldspar BT-33-02.

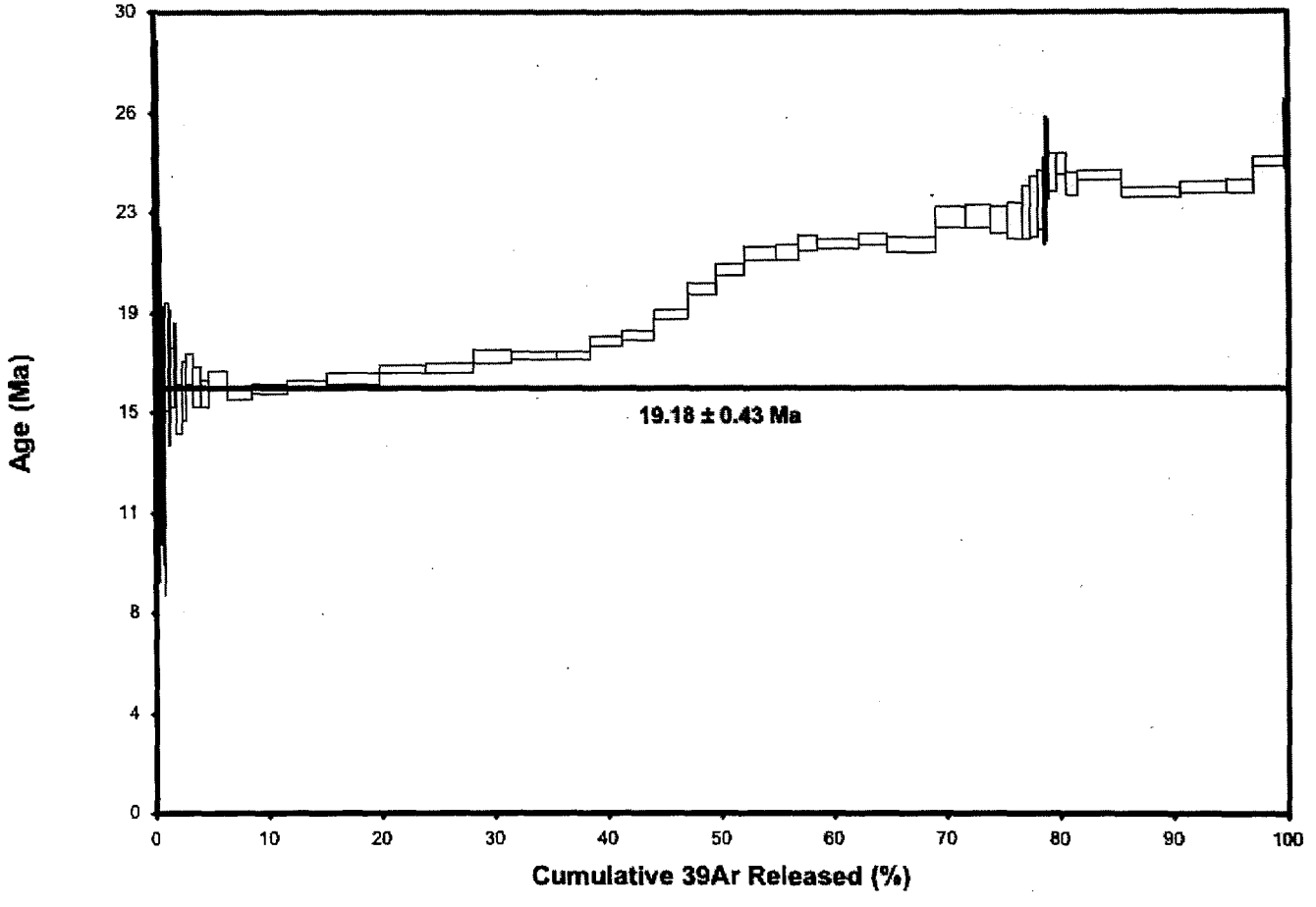

Figure 13a: Age Spectrum recorded from Mass Spectral Analysis of feldspar NB02-120.

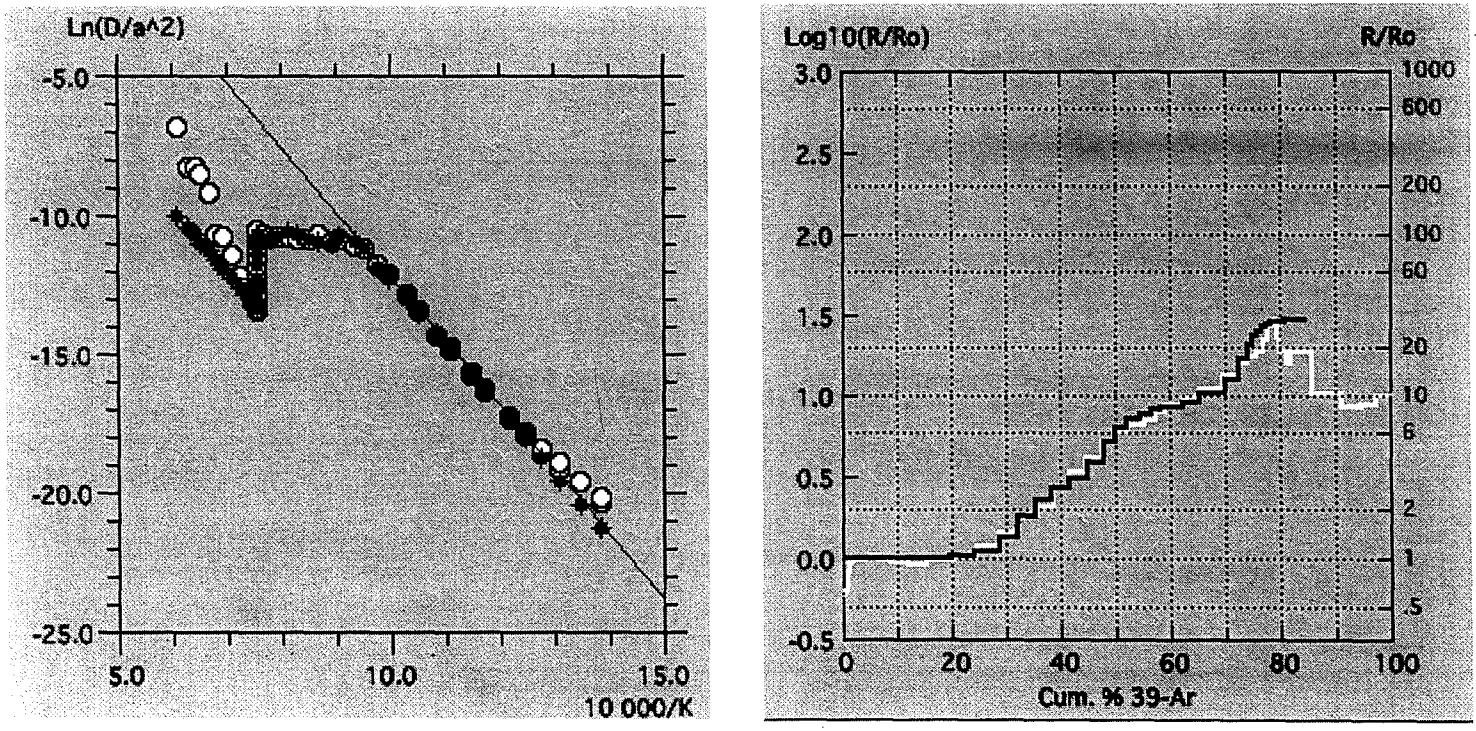

Figure 13b: Arrhenius and R/Ro plots for feldspar NB02-120

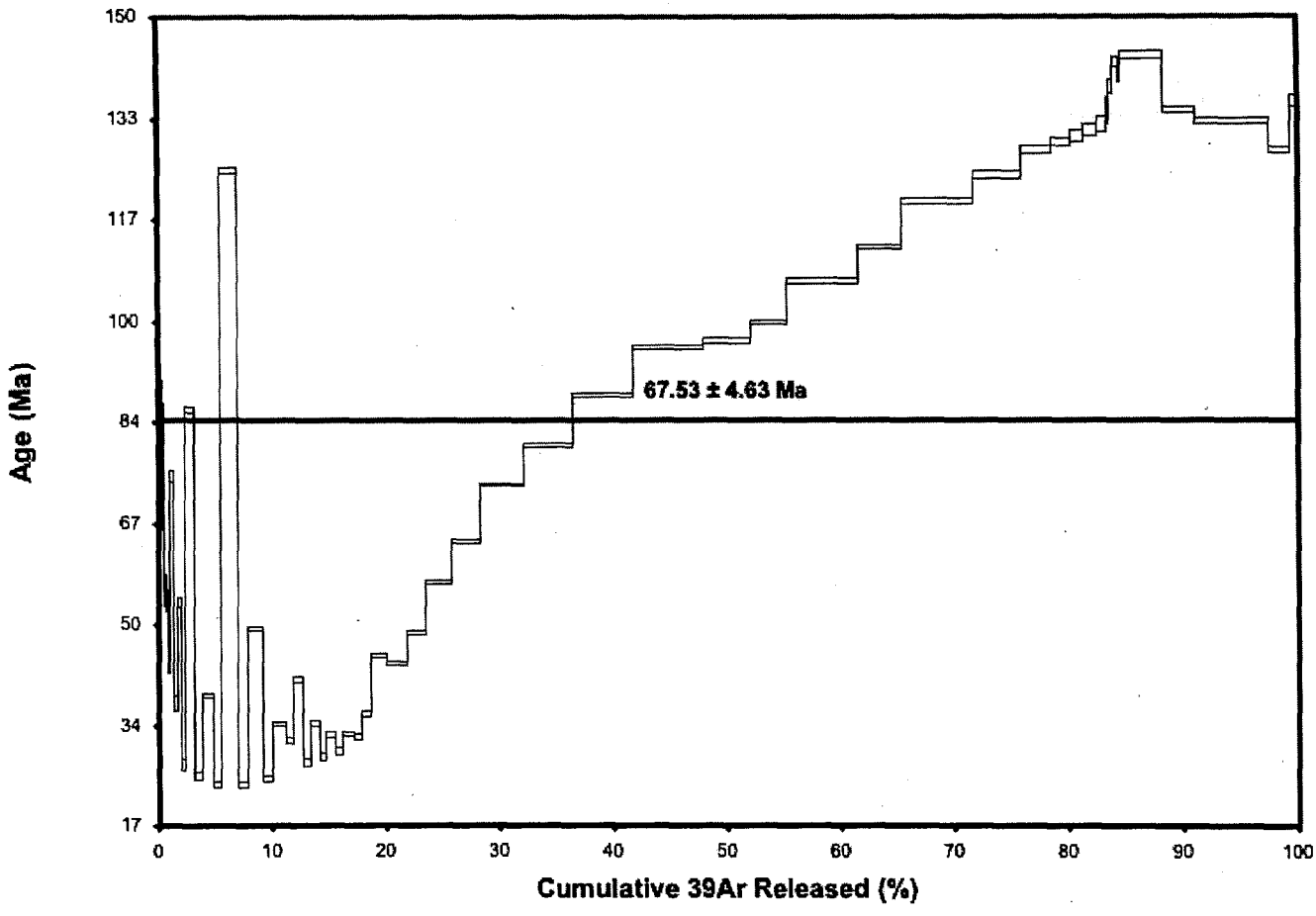

Figure 14a: Age Spectrum recorded from Mass Spectral Analysis of feldspar BT-36-02

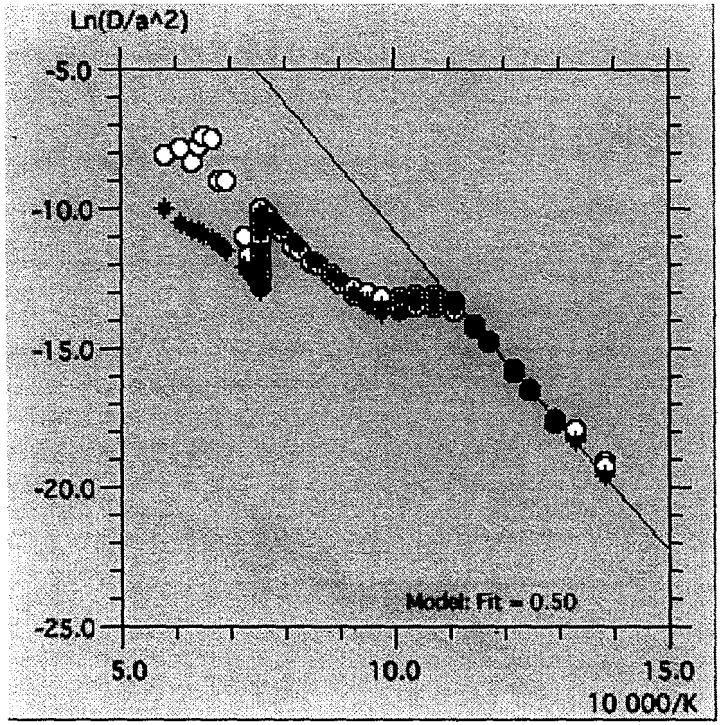

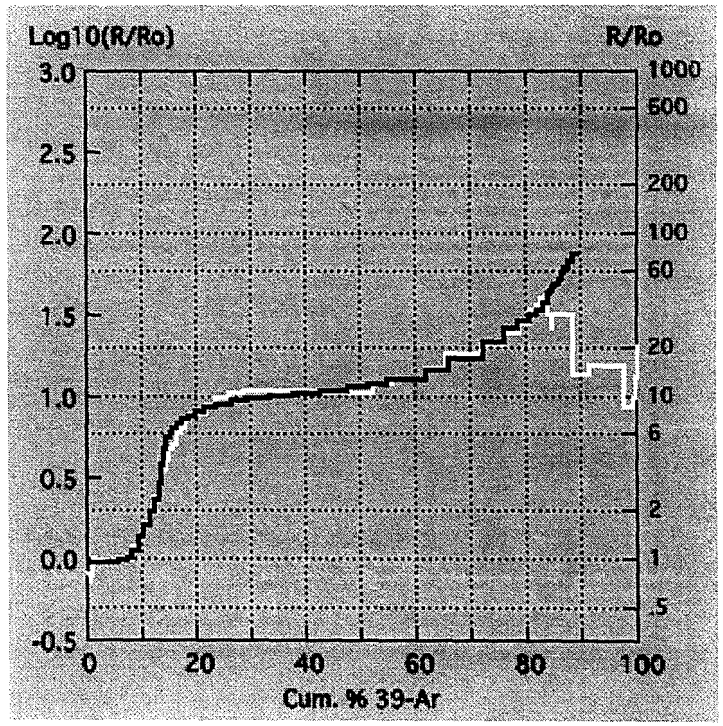

Figure 14b: Arhennius Plot and R/Ro plot for feldspar BT-36-02

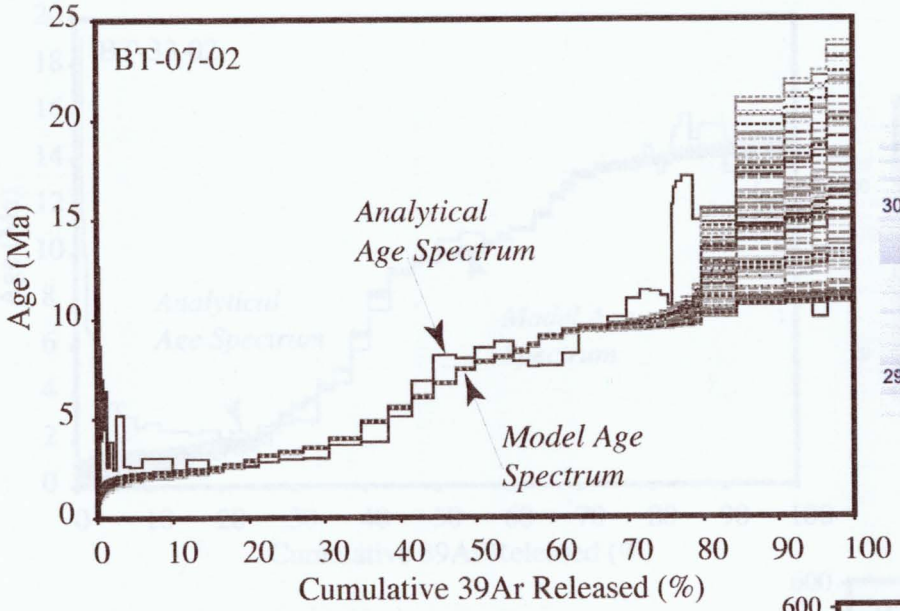

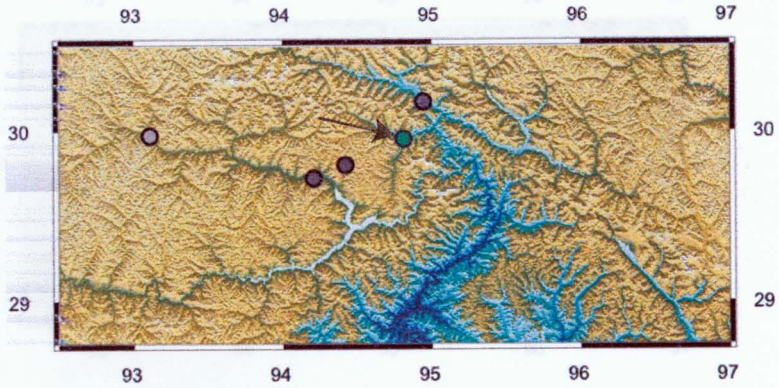

Figure 15a: Modeled Age Spectrum and thermal history for sample BT-07-02 using the Arvert Inverse Modeling program. The arrow on the DEM indicates the sample location.

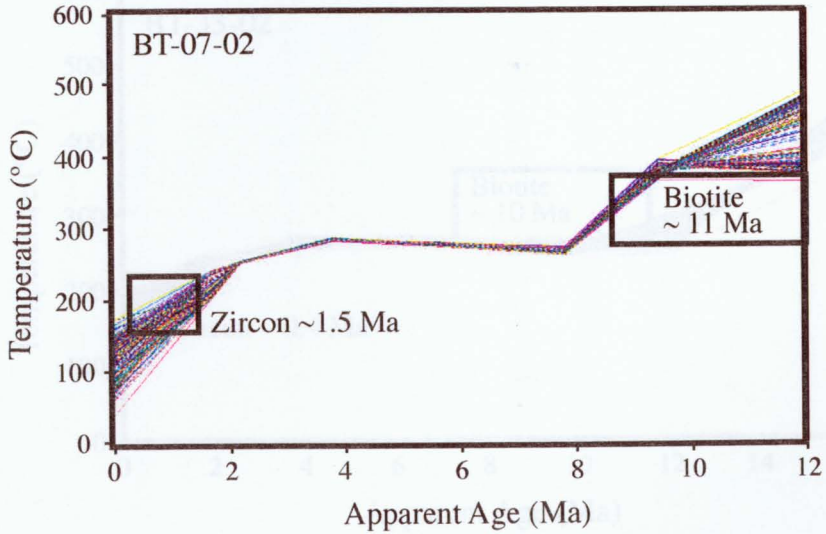

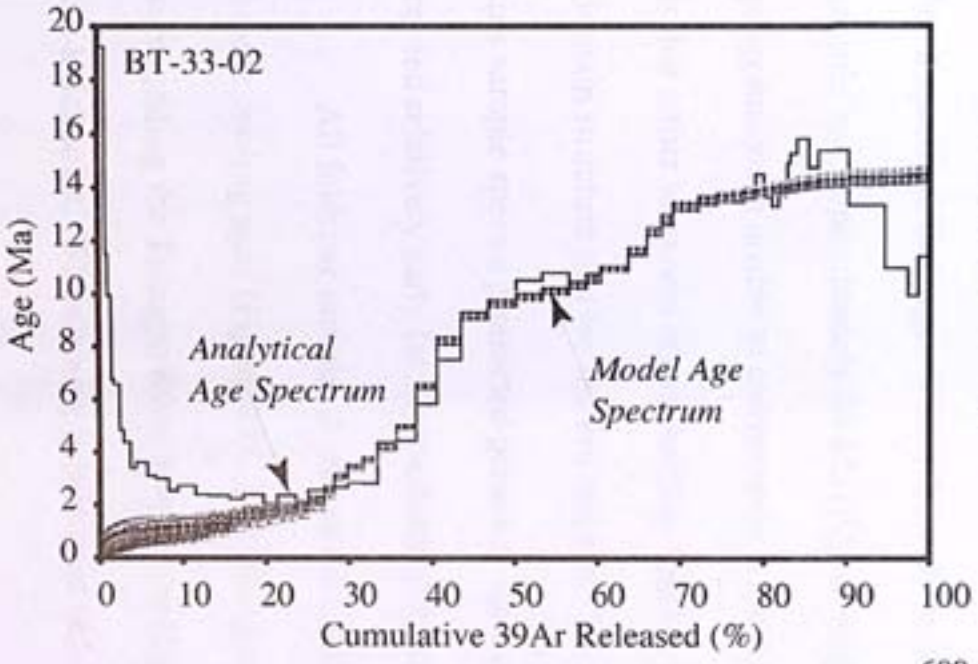

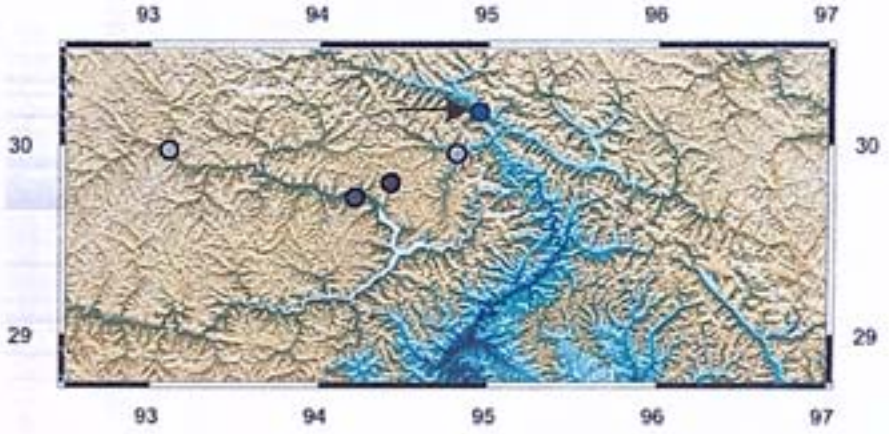

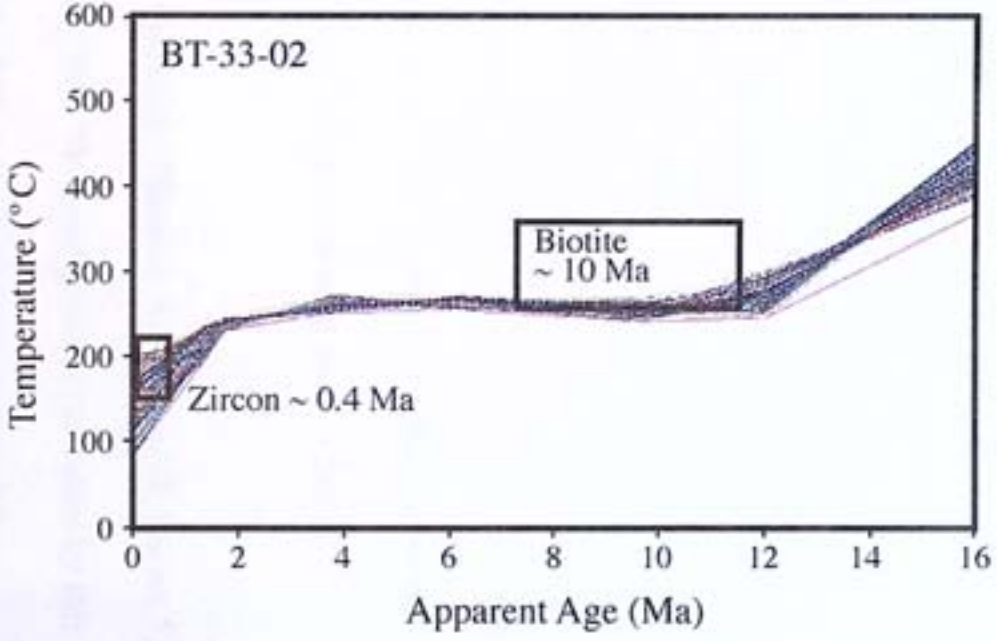

Figure 15b: Modeled Age Spectrum and thermal history for sample BT-33-02 using the Arvert Inverse Modeling program. The arrow on the DEM indicates the sample location.

granitoid. This sample does not record cooling as recently as those to the north of the massif (Figure 15c). Initial cooling of this feldspar is suggested to commence around 30 Ma. It confines the period between 24 and 20 Ma to slow cooling, but thermal interpretations following this period are difficult to make based on inverse and forward modeling. Sample NB02-120, another sample of Gangdese Arc granitoid, suggests a period of slow cooling (or isothermal equilibrium) between 21 and 17 Ma (Figure 15d). It then suggests a more rapid period of cooling until approximately 14 Ma. Both western samples display periods of slow to no cooling around 20 Ma. Sample NB02-120 further suggestion of rapid cooling corresponds well with the initial cooling seen in both northern feldspar modeled thermal histories.

BT-36-02, a granitoid (located to the west of the Namche Barwa massif, Figure 5) has a spectrum that rages widely from 24 to 140 Ma. The youngest age produced by this sample was approximately 24 Ma (Figure 14a). Both inverse and forward modeling programs were unable to converge on a close fit to the age spectrum. We believe that this is due either to excess argon that was trapped within the sample or to complexities in the domain structure that we did not resolve. Nonetheless, the age spectrum suggests that this sample spent a protracted period of time at relatively low temperatures and then cooled relatively early (at approximately 20 Ma).

All feldspar samples demonstrate cooling histories in agreement with zircon and biotite cooling ages (Figure 15). The youngest samples are seen within the massif and surrounding the Tsangpo River knickpoint (Figure 7 and 9). Ages increase away from the knickpoint. While young biotite ages (<5 Ma) are contained within the massif, young

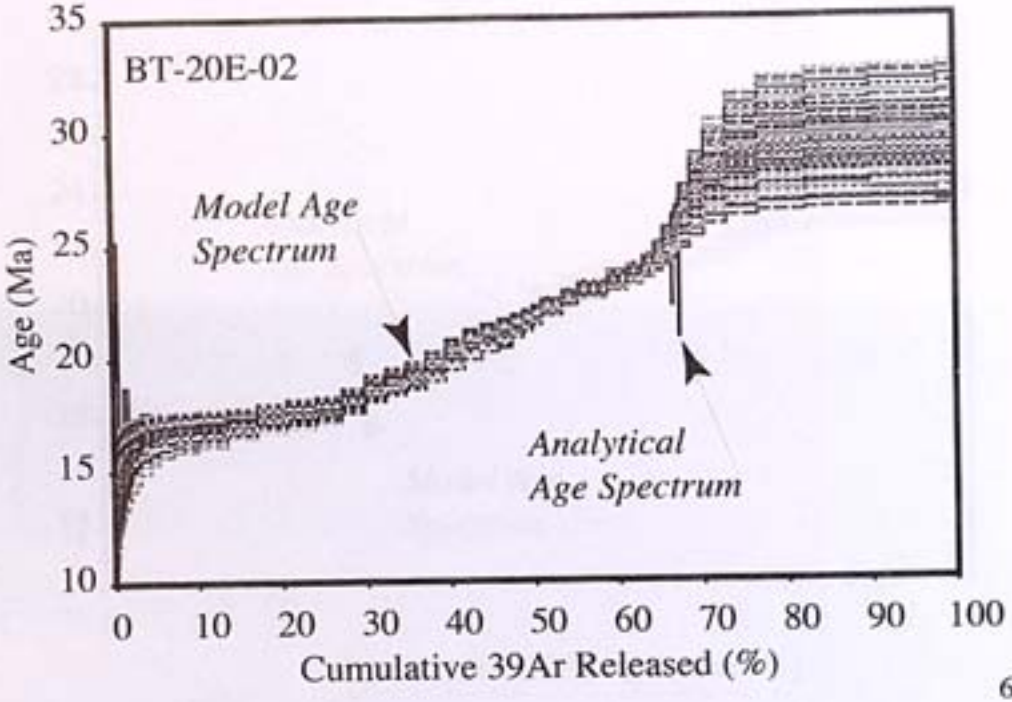

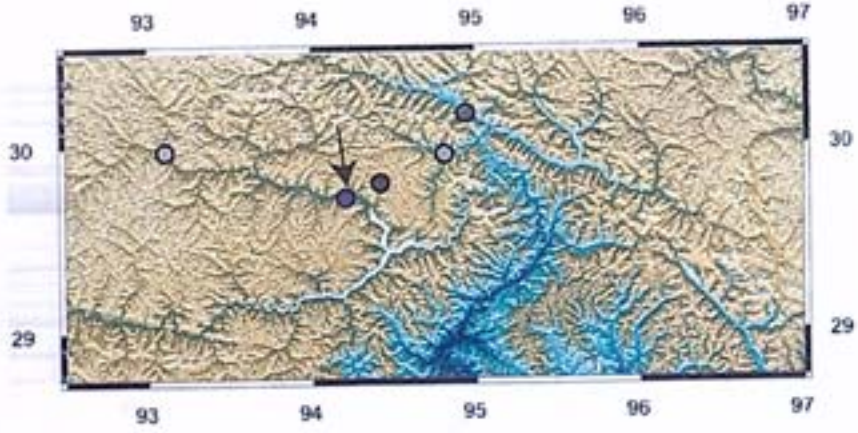

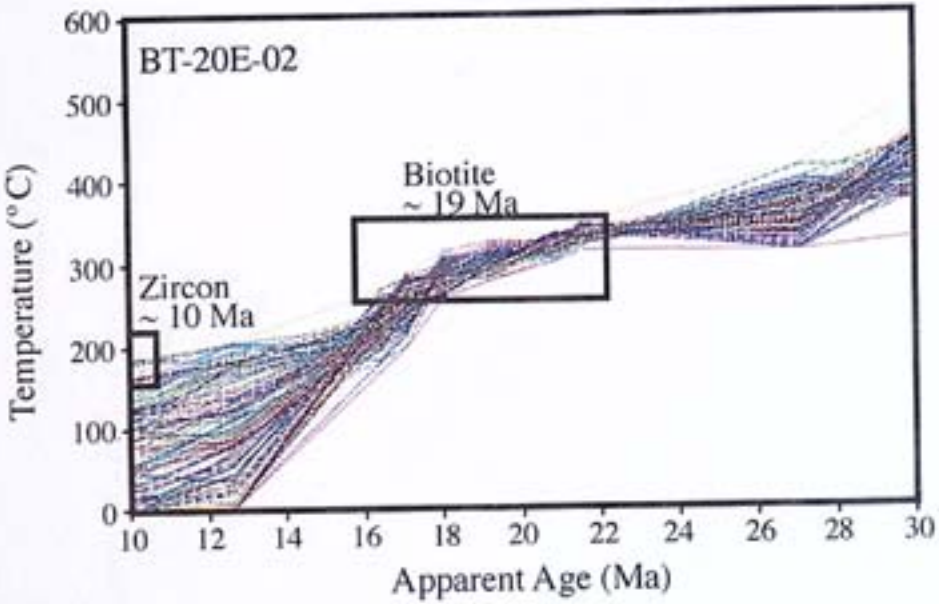

Figure 15c: Modeled Age Spectrum and thermal history for sample BT-20E-02 using the Arvert Inverse Modeling program. The arrow on the DEM indicates the sample location.

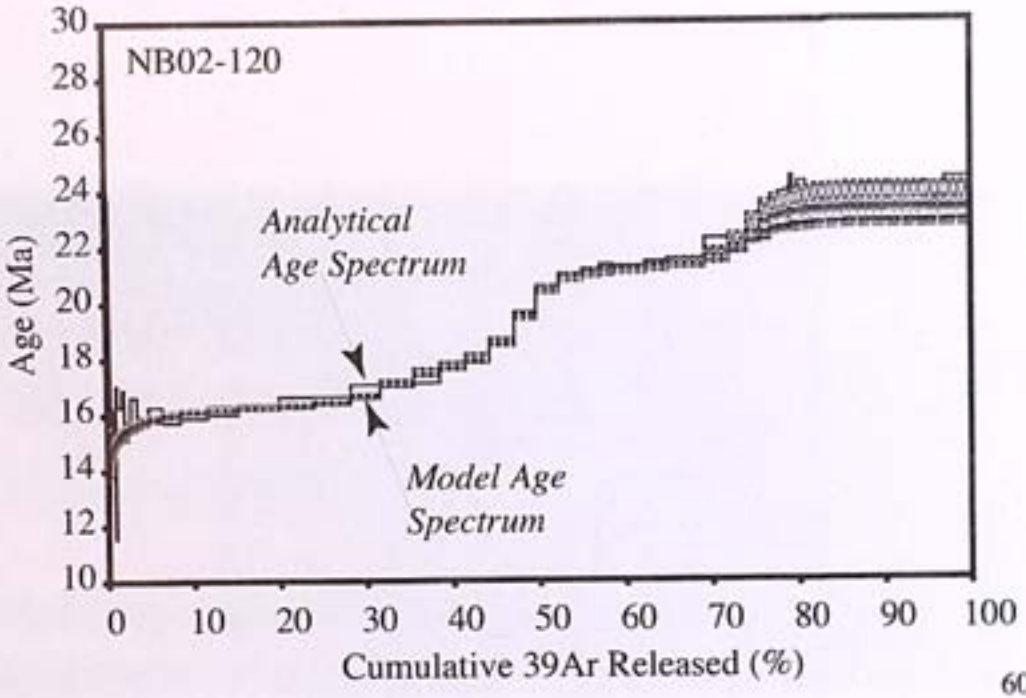

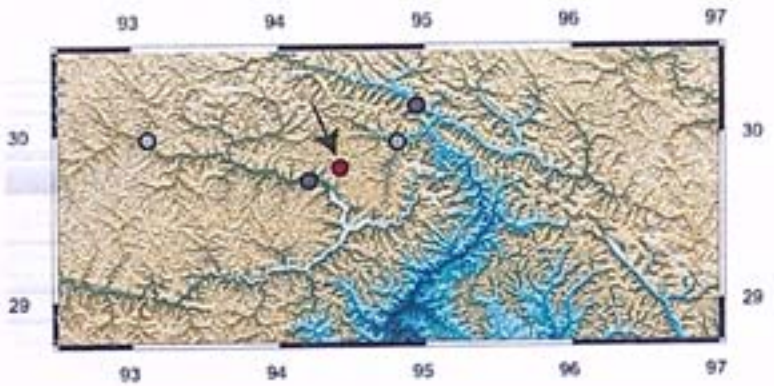

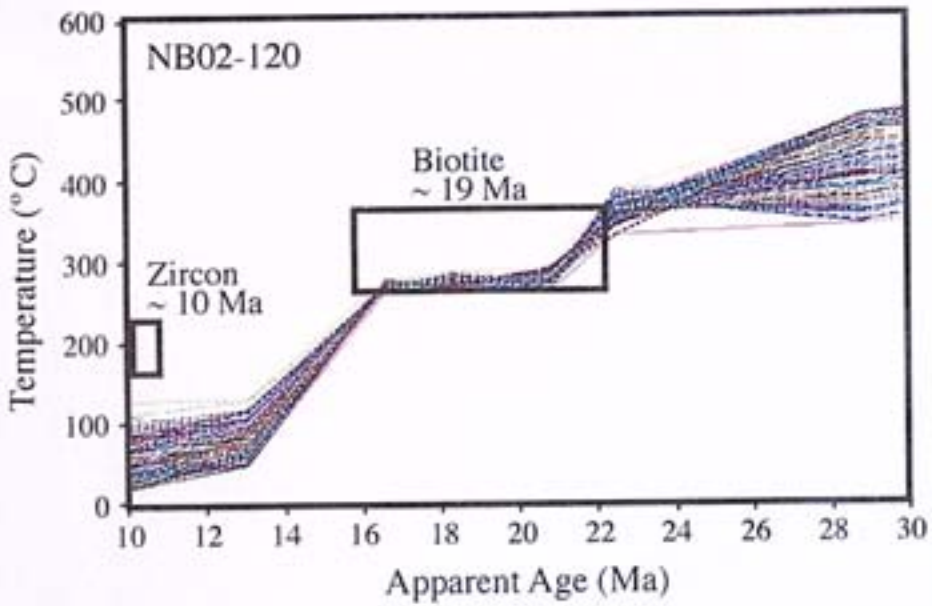

Figure 15d: Modeled Age Spectrum and thermal history for sample NB02-120 using the Arvert Inverse Modeling program. The arrow on the DEM indicates the sample location.

zircon ages (<2 Ma) continue outside of the Namche Barwa massif and extend out along the Tsangpo River's tributaries.

CHAPTER 5 - DISCUSSION

5.1 THE NAMCHE BARWA MASSIF

The distribution of zircon ages in the region surrounding Namche Barwa display extremely young zircons surrounding the Tsangpo River knickpoint (Figure 7). Young ages spread away from the knickpoint along tributaries of the Tsangpo River. Ages of less than 2 Ma can be found as far away from the knickpoint as near Bomi. General age/elevation patterns of zircons display a steep gradient in young samples (Figure 8a). Those samples between 0.2 and 2 Ma are at elevations between 1500 and 2500 meters. Above this elevation ages tend to follow a shallower gradient, ranging from 2 to 30 Ma. A more specific profile of age versus elevation (Figure 8b) does not display much change in age over a significant change in elevation and does not help to define the location of a regionally exposed (U-Th)/He partial retention zone. Both feldspar cooling histories, and zircon ages indicate that there has been 200-300 °C of cooling in the last two million years just outside the massif. One sample located farther away from the massif, but still at a lower elevation, is relatively old (> 10 Ma). The sample is most likely on the fringe of the active zone, and closer to the mountain front.

Biotite data collected by Zeitler in 2001 and 2002 (Zeitler, unpublished data) display an age pattern consistent with past work in the Nanga Parbat massif (Figure 9; Schneider et al., 1999). Young ages here (less than 5 Ma) are contained solely inside the Namche Barwa massif and around the Tsangpo knickpoint, while older ages abound (13+ Ma) less than 50 km downstream and outside of the massif. These trapped young ages suggest a recent cooling event affecting the deeper crust (to temperatures of 300° C) inside the Namche Barwa Massif, but not in the surrounding region.

Furthermore, zircon U-Pb ages obtained by Booth et al. (in review) also demonstrate the presence of extremely young granites within the Namche Barwa massif (less than 10 Ma) that are unique to this location in the Himalayas. Zircon crystallization ages outside the massif are > 20 Ma. These young ages within the massif Booth et al. (in review) proposes to be the result of decompression melting similar to that found by Zeitler et al. (2001) in Nanga Parbat. The presence of these young decompressional melts corresponds nicely with the presence of a tectonic aneurysm in the Namche Barwa massif.

Feldspar data taken just outside the massif shows an interesting series of events surrounding the Namche Barwa massif since its formation (Figure 15), Feldspars located near the knick point (BT-07-02 and BT-33-02) yield thermal histories having two periods of rapid cooling, at ~2 Ma and ~17 Ma. These were separated by a period of isothermal stagnation about 10 m.y. in duration. SHRIMP zircon U-Pb ages collected for these samples by Booth et al. (in review) show ages of at least 40 Ma for BT-07-02 and 20 Ma for BT-33-02. As these ages indicate time of mineral crystallization, it is clear that feldspar thermal histories are recording events after crystallization. Samples NB02-120 and BT-20E-02 are located upstream of and away from the knickpoint. NB02-120's thermal history is highlighted by rapid cooling from ~22-21 Ma, followed by a period of isothermal equilibrium. This sample's U-Pb age is 51 Ma (Booth et al., in review). The period of time in which temperature remains relatively constant is in good agreement with sample BT-20E-02, U-Pb age of 50 Ma (Booth et al., in review). Neither sample recorded any data within the last 2 to 3 Ma. The pattern of cooling experienced by the feldspars in this study is interesting in that the modeled thermal histories agree well with

both zircon and biotite data collected. Biotite data obtained near Tungmai (just north of the massif; located on a tributary which joins the Tsangpo River downstream of the knickpoint) show ages around 9.9 Ma with zircons of less than 1 Ma, very close to the observed spectrum of feldspar data obtained from the same area. The same is seen in ages obtained east of Bayi and upstream of the knickpoint. We see ages in biotites of ~19Ma and zircons between ~13.6 and 6 Ma. The fact that feldspar data strongly support both data sets suggests that patterns seen in both are valid and any tectonic interpretations made must fit not only observed young biotite ages trapped within the massif, but also the propagating young age pattern of zircon data extending outside of the massif.

Sample BT-36-02 is located well to the west of the Namche Barwa massif. Feldspars from this 250 Ma intrusive (Figure 5; U-Pb age obtained from Booth et al., in review) suggest that this region of Tibet was stable and experienced little or no exhumation-related cooling until activity on the Gangdese Thrust began in the early Miocene, when the feldspar begins closure. Although we were not able to successfully model this sample's thermal history with high precision, we still have control given the range of ages and we believe that basic interpretations from this data point are still valid. This old age to the west of the massif is significant in that it displays that the tectonic/geomorphic forces acting on the massif are local and not affecting regional tectonics.

A previously developed model by Zeitler et al. (2001), the tectonic aneurysm, links river incision with tectonics to explain young ages confined in a structurally bound massif (Figure 16). This model relates changes in crustal rheology to large degrees of erosion and evacuation of material by river incision. Such erosion weakens the crust and

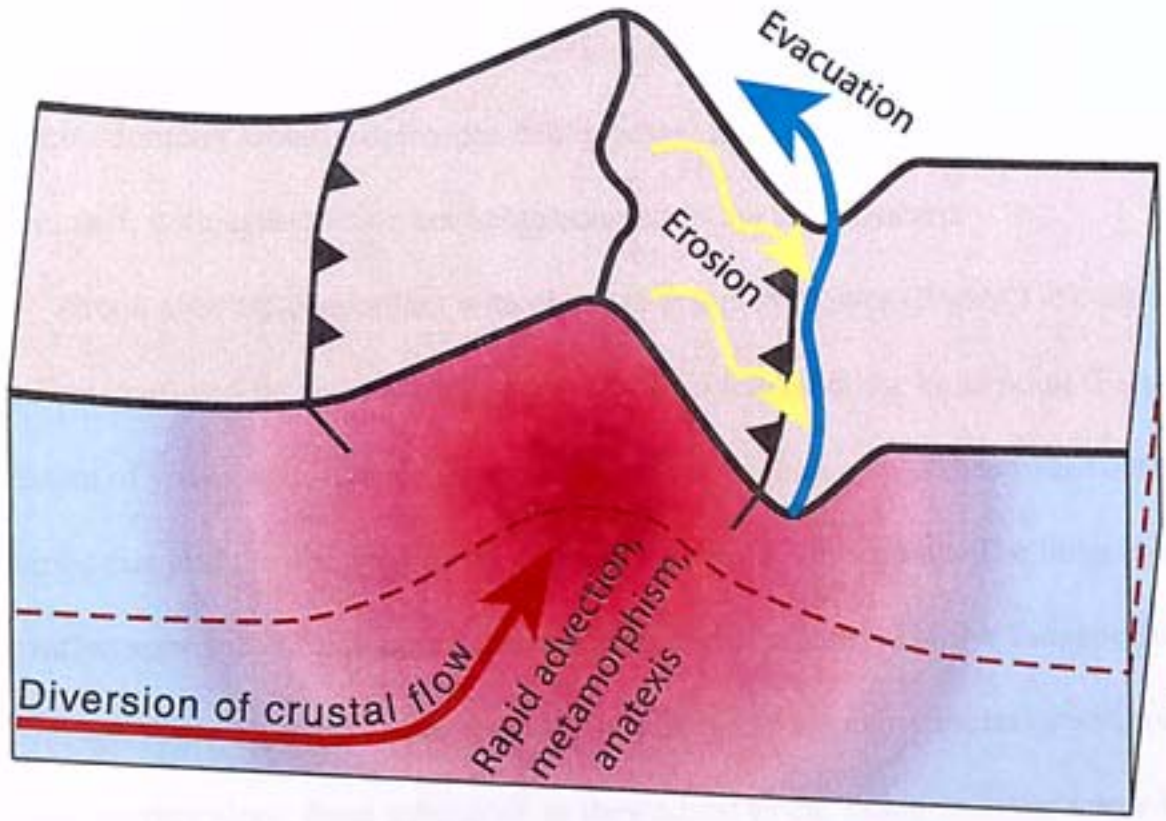

Figure 16: Zeitler et al.'s (2001) tectonic aneurysm model relates changes in crustal rheology to large degrees of erosion. Such erosion weakens the crust and diverts crustal flow towards the topographic gap, thus causing rapid rock uplift, more erosion and thus more removal of material. If actively occuring, ages found by low-temperature thermochronometry would display extremely young ages within the bounding structures of the massif and ages that are relatively unaffected in surrounding areas.

creates a topographic gap. Crustal flow then becomes diverted towards this topographic gap, thus causing a positive feedback cycle of rapid rock uplift, more erosion and then more removal of material. If actively occurring, ages found by low-temperature thermochronometry would display extremely young ages within the bounding structures of the massif, with ages outside not being coupled to the same system.

Zircon ages are concordant with changes in stream power (Figure 17; courtesy of Noah Finnegan) and increase to older ages steadily away from the knickpoint (Figure 7). The extent of young ages outside the massif could be explained with headward cutting of tributaries that join the Tsangpo River downstream of the knickpoint. The large change in elevation seen at the knickpoint creates a drop in the base level of the Tsangpo River downstream. This decreased base level would affect downstream tributaries and force headward cutting along these tributaries as they adjust to the Tsangpo River's new base level. In this way, it is possible to explain young ages outside the massif. However, for this model to apply to Namche Barwa, it means that local geothermal gradients must be extremely steep (as to allow the river to set ages at more than 175°C in the crust). In order to obtain such gradients, exhumation must have been fairly fast (and thus the local isotherms are currently decoupled from the topography) and/or have long-lived brisk exhumation in the region. The regional distribution of both zircon ages and feldspar data suggest modest rates of cooling until 2-3 Ma, where cooling rates experience a significant increase. Furthermore, samples taken near Tungmai (Figure 7) are at elevations of greater than 2000 meters, and are still less than 1 Ma. Without significant amounts of rock uplift being paired with rock incision, it is hard to explain these ages. These ages therefore don't support a suggested steep thermal gradient in the area.

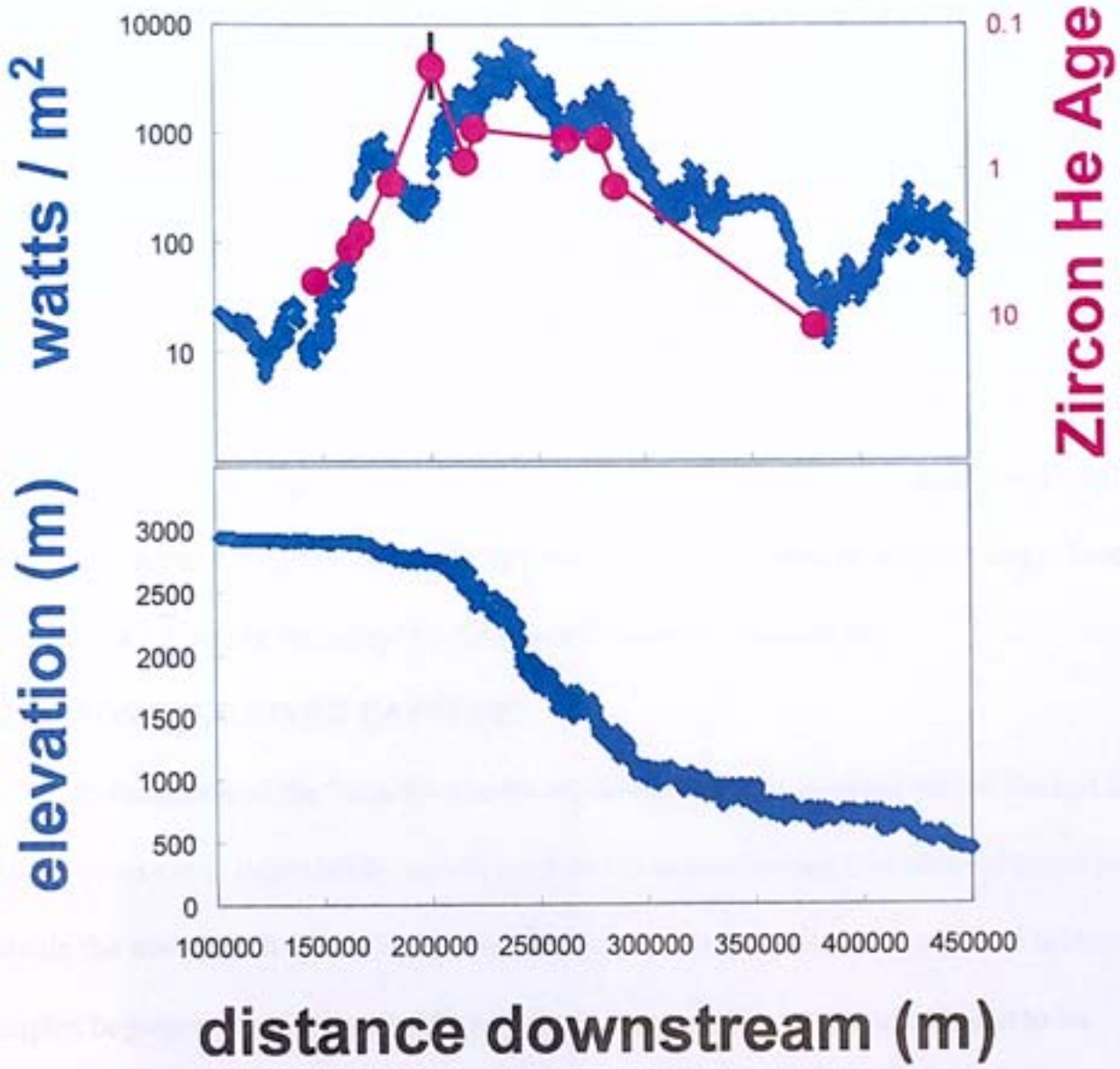

Figure 17: The relationship of Tsangpo river power and elevation upstream to dowstream versus zircon (U-Th)/He ages obtained along the river. Elevation and power data obtained from Noah Finnegan (personal communication).

We have developed a new model to show how both data sets can be combined to can explain both large changes in relief, as well as young ages propagating from the Tsangpo's knickpoint (Figure 18). In the Namche Barwa model, a tectonic aneurysm still controls much of the uplift seen within the massif and has affected cooling of more than 350°C in the upper crust. Prior to the localization of strain along the faults bounding the massif and advection within the massif, doming may have occurred regionally. This would allow for the large amount of rock uplift, paired with river incision, required for setting young ages at high elevations outside of the massif. Such a scenario may explain young ages surrounding the massif as defined in the zircon system, while younger biotite age patterns are solely delimited by the massif's tectonic boundaries.

5.2 POSSIBLE RIVER CAPTURE

Exhumation of the Namche Barwa Massif must have occurred within the last 3-5 million years (as is indicated by zircon ages and feldspar thermal histories collected just outside the massif). It is in this time frame that we see the thermal histories of feldspar samples beginning to display rapid cooling and when young zircon ages begin to be recorded. It is possible that exhumation of the massif is driven by the actual capture event speculated by Koons (1995), Brookfield (1998), and Clark et al. (2004). Prior to its capture, the Tsangpo River may have flowed westward at grade. The northeastward cutting Brahmaputra River then captured the Tsangpo River, creating the distinctive bend seen in the river system (Clark et al., 2004). After capture, the base level of the new system dramatically changed. This created a dramatic wave of incision (marked by a knickpoint) originating from the capture point. Upon arrival to the massif, the incision wave may have started to decrease as exhumation and regional doming began. At this

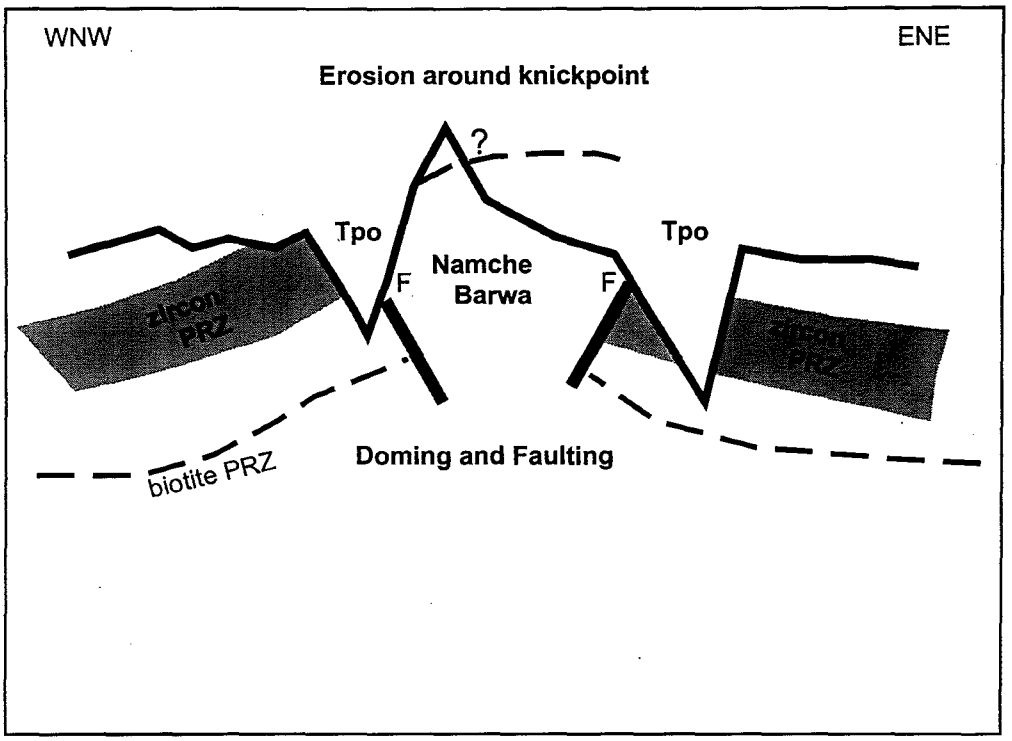

Figure 18: The Namche Barwa Model. This model pairs both doming and faulting to explain age distributions in and around the Namche Barwa massif.

point, rock uplift may still have been less than erosion by river incision, allowing for headward movement of river incision (and the knickpoint) after initial exhumation of the massif began. However, the knickpoint would have become stabilized and the incision wave would stop, as rock uplift began to match erosion by river incision. This would explain the location of the knickpoint within the massif today. Further propagation of incision would have occurred up tributaries of the Tsangpo connected downstream of the knickpoint (propagation seen in zircon age information). Upstream of the knickpoint, both data sets would reflect similar patterns, with samples inside the massif affected by the aneurysm and those outside affected by regional base level. If capture did not immediately precede the onset of doming and faulting, the incision wave prior to capture of the knickpoint would be more subdued. However, actual timing of river capture cannot be postulated from this data set, only restricted to before onset of exhumation inside the massif.

5.3 THE TIBETAN PLATEAU

The distribution of young ages around the Namche Barwa massif suggests that the knickpoint on the Tsangpo River has not moved headward in the last few million years. Exhumation within the massif seems to at least be pacing river incision. The location of zircon ages with respect to river power (Figure 17), then further shows that the youngest ages are a little upstream of the knickpoint and most powerful point in the river. The presence of this relationship could suggest that not only is exhumation equal to incision, but there may be more rock uplift then river incision and the knickpoint may in fact be moving downstream.

If the Tsangpo River were merely cutting back, it could only expose rocks from ~ 4 km depth. This amount of exhumation would not be sufficient to set the radiogenic zircon ages that we see present in the Namche Barwa massif. Some other mechanism had to carry the isotherms closer to the surface to allow the zircon ages to become set. If the river was captured and then triggered rock uplift, then the isotherms can move up and the river can assist in setting ages. Furthermore, the knickpoint is required to be inside the massif to obtain the 20 km of rock exposure in the last 3 Ma. It seems very coincidental if the Tsangpo had simply been cutting headward and ran into the growing antiform, where it was then pinned. Therefore, the connection of the two, the river and the aneurysm, seems much more feasible.

The large amount of exhumation within the Namche Barwa massif within the last 5 Ma demonstrates the river's power to evacuate weathered materials from a tectonically active setting. If the Tsangpo River were simply propagating westward, the amount of material that it would be able to evacuate would not allow the southeastern corner of the plateau to maintain its high elevation. This drop in elevation would propagate as the river continues to cut west through Tibet. Young ages within the massif imply that headward cutting by the Tsangpo River has been halted and the river cannot therefore continue to move westward onto the Tibetan Plateau. The mean elevation of the Tibetan Plateau is ~ 4,000 m. The implications that the river system has on the plateau could very well be to allow it to retain some of this topography.

The Tibetan Plateau is believed to have experienced uplift from 20-17 Ma (Harrison et al., 1992; Copeland et al., 1995, Chung et al., 1998). The current high elevation of the Plateau seems to have persisted since at least 8 Ma (Le Pichon et al.,

1997, Harrison et al., 1992). The fact that it has not lost much of this original elevation partly confirms that headward cutting and erosion have not been allowed a significant role in lowering the base-level elevation. If rivers, such as the Tsangpo, were allowed to continue headwards, the mean Tibetan elevation would be forced to fall in order for equilibrium to be attained. In general, given how fast erosion seems to be working at the edges, 8 m.y. let alone 15 m.y., could have dramatically changes the topography of the plateau.

5.4 STRUCTURAL EVOLUTION

Young cooling histories in the Namche Barwa area define rock uplift coupled with erosion over the past 5 Ma. Older ages and longer-term cooling histories surrounding the Namche Barwa massif then help to define the past structural evolution of this part of the eastern syntaxis. Lee et al. (2003) suggested that between 18 and 12 Ma there was shearing along the Jiali fault zone, just north of the Namche Barwa massif, which they believed to be an indicator of oblique convergence between India and Asia. Quidelleur et al. (1997) found feldspar thermal histories for granitoids of the gangdese batholith to display a period of cooling between 19 and 11 Ma. They believed this to be evidence for thrusting along the Renbu-Zedong thrust, located above the Indus-Tsangpo Suture Zone. Feldspar sample NB02-120, whose thermal history encompasses this later time frame (Figure 15d), does suggest a cooling event at approximately 17 Ma that is consistent with potential movement along these fault systems. Furthermore, Initial cooling of both BT-07-02 and BT-33-02 (Figure 15a and 15b) show initial cooling within this same time frame. Biotite ages surrounding the massif tend to agree with the distribution seen in the feldspar thermal history and help to support fault movement.

Furthermore, Zircon U-Pb data (Booth et al., in review) also agree with hypothesized fault movement at this time. Crystallization ages surrounding the Namche Barwa massif range from 20-25 Ma.

CHAPTER 6 – CONCLUSIONS

Within the eastern syntaxis of the Himalayan-Tibetan orogeny, the Namche Barwa massif is the location of a significant change in relief and base elevation, as well as the location of a large knickpoint and bend in the Tsangpo River. Zircon (U-Th)/He analyses of samples located in the massif and at low elevations along the river's main tributaries record cooling ages of less than 2 Ma and show an age-elevation profile similar to that of rocks exhumed from a partial retention zone ~2-3 Ma (Figures 7 and 8). This suggests incision-related rock uplift in the region. However, incision alone cannot explain the large change in relief in this region. Nor can it easily explain the He ages themselves given isotherm depths at start of rapid cooling, unless the geothermal gradient was extremely steep to start with. Biotite Ar/Ar cooling ages (Figure 9), within the same region, suggest fault-related uplift of the massif (i.e. young ages are found solely inside the massif suggesting an active tectonic aneurysm; Figure 16; Zeitler et al. 2001). This faulting may be coupled with incision-related doming to explain both local relief and cooling age distributions (Figure 18). Feldspar Ar/Ar cooling histories are consistent with both zircon partial retention zone data defining a period of rapid uplift at ~2-3 Ma and also with suggested recent capture of the Tsangpo River.

This research helps to support recent speculation that river incision can indeed play an important roll in rock uplift in active tectonic settings. Furthermore, we demonstrate that it is possible to use low temperature thermochronometry to study shallow crustal processes, such as erosion related rock uplift. Thermal histories obtained from these chronometers can define regional cooling patterns, which then can be used to model the tectonic processes responsible for age distributions.

REFERENCES CITED

Bendick, R. and R. Bilham, How perfect is the Himalayan arc?, Geology, 29, 791-794, 2001.

Booth, A. L., Zietler, P. K., Kidd, W. S. F., Wooden, J., Liu, Y., Idleman, B., Hren, M., and C. P. Chamberlain, U-Pb zircon constraints on the tectonic evolution of southeastern Tibet, Ms in review.

Booth, A. L., Zeitler, P. K., Kidd, W. S. F., Wooden, J. L., Idleman, B., Yuping, L., and C. P. Chamberlain, Geochemical and geochronologic constraints on the tectonic evolution of Southeastern Tibet, Eos Trans. AGU, 84(46), Fall Meet. Suppl., Abstract T42B-0288, 2003.

Braun, J., Quantifying the effect of recent relief changes on age-elevation relationships, Earth and Planetary Science Letters, 200, 331-343, 2002.

Brookfield, M. E., The evolution of the great river systems of southern Asia during the Cenozoic India-Asia collision: rivers draining southwards, Geomorphology, 22, 285-312, 1998.

Burchfiel, B. C., C. Zhiliang, K. V. Hodges, L. Yuping, L. H. Royden, D. Changrong, and X. Jiene, The South Tibetan Detachment System, Himalayan orogen: Extension contemporaneous with and parallel to shortening in a collisional mountain belt, Special Paper Geol. Soc Am. 269, 48pp., 1992.

Burg, J., Nievergelt, P., Oberli, F., Seward, D., Davy, P., Maurin, J., Diao, Z., and M. Meier, The Namche Barwa syntaxis: evidence for exhumation related to compressional crustal folding, Journal of Asian Earth Sciences, 16, 239-252, 1998.

Carpéna, J., and D. Mailhé, Fission-track dating calibration of the Fish Canyon Tuff standard in French reactors, Chemical Geology, 66, 53-59.

Chen, C., DePaolo, D., and C. Lan, Rb-Sr microchrons in the Manaslu granite: implications for Himalayan thermochronology, Earth and Planetary Science Letters, 143, 125-135, 1996.

Chung, S. L., Lo, C. H., Lee, T. Y., Zhang, Y., Xie, Y., Li, X., Wang, K. L., and Wang, P. L., Diachronous uplift of the Tibetan plateau starting 40 Ma ago, Nature, 394, 769-773, 1998.

Clark, M. K., Schoenbohm, L. M., Royden, L. H., Whipple, K. X., Burchfiel, B. C., Zhang, X., Tang, W., Wang, E., and L. Chen, Surface uplift, tectonics, and erosion of eastern Tibet from large-scale drainage patterns, Tectonics, 23, TC1006, 2004.

Copeland, P., Harrison, M., Yun, P., Kidd, W.S.F., Roden, M., and Yuquań, Z., Thermal evolution of the Gangdése batholith, southern Tibet: A history of episodic unroofing, Tectonics, 14, 223-236, 1995.

Coward, M. P., and R. W. H. Butler, Thrust tectonics and the deep structure of the Pakistan Himalaya, Geology, 13, 417-420, 1985.

Dodson, M. H., Closure temperature in cooling geochronological and petrological systems, Contrib Mineral Petrol, 40, 259-274, 1973.

England, P., and P. Molnar, Surface uplift, uplift of rocks, and exhumation of rocks, Geology, 18, 1173-1177, 1990.

Farley, K. A., Wolf, R. A., and L. T. Silver, The effects of long alpha-stopping distances on (U-Th)/He ages, Geochimica et Cosmochimica Acta, 60, 4223-4229, 1996.

Foland, K. A., 40ar diffusion in homogeneous orthoclase and an interpretation of Ar diffusion in K-feldspar, Geochimica et Cosmochimica Acta, 38, 151-166, 1974.

Hallet, B., and P. Molnar, Distorted drainage basins as markers of crustal strain east of the Himalaya, Journal of Geophysical Research, 106, 13,697-13,709, 2001.

Harrison, T. M., Copeland, P., Kidd, W. S. F., and A. Yin, Raising Tibet, Science, 225, 1663-1670, 1992.

Hodges, K. V., Tectonics of the Himalaya and southern Tibet from two perspectives, GSA Bulletin, 112, no. 3, 324-350, 2000.

Kirby, E., and K. Whipple, Quantifying differential rock-uplift rates via stream profile analysis, Geology, 29, 415-418, 2001.

Koons, P. O., Modeling the topographic evolution of collisional belts, Annual Review of Earth and Planetary Science, 23, 375-408, 1995.

Lee, H.-Y., Chung, S. L., Wang, J. R., Wen, D. – J., Lo, C. – H., Yang, T. F., Zhang, Y., Xie, Y., Lee, T. – Y., Wu, G., and J. Ji, Miocene Jiali faulting and its implications for Tibetan tectonic evolution, Earth and Planetary Science Letters, 205, 185-194, 2003.

Leland, J., Reid, M. R., Burbank, D. W., Finkel, R., and M. Caffee, Incision and differential bedrock uplift along the Indus River near Nanga Parbat, Pakistan Himalaya, from 10Be and 26Al exposure age dating of bedrock straths, Earth and Planetary Science Letters, 154, 93-107, 1998.

Le Pichon, X., Henry, P., and B. Goffe, Uplift of Tibet, from eclogites to granulites; implications for the Andean Plateau and the Variscan belt, Tectonophysics, 273, 57-76, 1997.

Lin, D., Dalai, Z., Yin, A., Kapp, P, and Harrison, T. M., Cenozoic structural and metamorphic evolution of the eastern Himalayan syntaxis (Namche Barwa), Earth and Planetary Sciences, in review.

Lovera, O. M., Richter, F. M., and T. M. Harrison, the 40Ar/39Ar thermochronometry for slow cooled samples having a distribution of diffusional domain sizes, J. Geophys. Res., 94, 17917-17935, 1989.

Lovera, O. M., Grove, M., Harrison, T. M., and K. I. Mahon, Systematic analysis of K-feldspar 40Ar/39Ar step heating results: I. Significance of activation energy determinations, Geochimica et Cosmochimica Acta, 61, 3171-3192, 1997.

Lovera, O. M., Grove, M., and T. M. Harrison, Systematic analysis of K-feldspar 40Ar/39Ar step heating results: II. Relevance of laboratory argon diffusion properties to nature, Geochimica et Cosmochimica Acta, 66, 1237-1255, 2002.

McDougall, I., and T. M. Harrison, Geochronology and thermochronology by the 40Ar/39Ar method, Oxford University Press, New York, 261 p, 1999.

Mehta, P. K., Tectonic significance of the young mineral dates and the rates of cooling and uplift in the Himalaya, Tectonophysics, 62, 207-217, 1980.

Merrihue, C., Trace-element determinations and potassium-argon dating by mass spectroscopy of neutron-irradiated samples, Trans. Am. Geophys. Un. 46, 125, 1965 (abstract).

Merrihue, C., and G. Turner, Potassium-argon dating by activation with fast neutrons, The Journal of Geophysical Research, 71, 2852-2857, 1966.

Miller, J. R., The influence of bedrock geology on knickpoint development and channel-bed degradation along downcutting streams in south-central Indiana, Journal of Geology, 99, 591-605, 1990.

Molnar, P., and P. England, Late Cenozoic uplift of mountain ranges and global climate change: chicken or egg?, Nature, 346, 29-34, 1990.

Montgomery, D. R., Balco, G., and S. D. Willett, Climate, tectonics, and the morphology of the Andes, Geology, 29, 579-582, 2001.

O'Brien, P. J., Subduction followed by collision: Alpine and Himalayan examples, Physics of The Earth and Planetary Interiors, 127, 277-291, 2001.

Quidelleur, X., Grove, M., Lovera, O. M., Harrison, T. M., Yin, A., and F. J. Ryerson, Thermal evolution and slip history of the Renbu Zedong Thrust, southeastern Tibet, Journal of Geophysical Research, 102, 2659-2679, 1997.

Reiners, P. W., Farley, K. A., and H. J. Hickes, He diffusion and (U-Th)/He thermochronometry of zircon: initial results from Fish Canyon Tuff and Gold Butte, Tectonophysics, 349, 297-308, 2002.

Reiners, P. W., Zhou, Z., Ehlers, T. A., Xu, C., Brandon, T. M., Donelick, R. A., and S. Nicolescu, Post-orogenic evolution of the Dabie Shan, eastern China, from (U-Th)/He and fission-track thermochronology, American Journal of Science, 303, 489-518, 2003.

Sardarov, S. S., Retention of radiogenic argon in microcline, Geochemistry, 3, 233-237, 1957.

Schneider, D. A., Edwards, M. A., Zeitler, P. K., and C. D. Coath, Mazeno Pass pluton and Jutial pluton, Pakistan Himalaya: age and implications for entrapment mechanisms of two granites in the Himalaya, Contrib Mineral Petrol, 136, 273-284, 1999.

Searle, M. P., and Treloar, P. J., Himalayan Tectonics – an introduction, from P.J. Treloar and M. P. Searle (eds), Geological Society Special Publication, 74, 1-7, 1993.

Spotila, J. A., Farley, K. A., and K. Sieh, Uplift and erosion of the San Bernardino Mountains associated with transpression along the San Andreas fault, California, as constrained by radiogenic helium thermochronometry, Tectonics, 17, 360-378, 1998.

Stewart, R., Hallet, B., and D. Trippett, Extraordinarily rapid exhumation rates in the Tsangpo Gorge, eastern Himalaya syntaxis: Evidence from detrital zircon fission-track geochronology and geothermometry, pre-press, 16 p.

Tagami, T., Farley, K. A., and D. F., Stockli, (U-Th)/He geochronology of single zircon grains of known Tertiary eruption age, Earth and Planetary Science Letters, 207, 57-67, 2003.

Tjia, H. D., Fujii, S., Kigoshi, K., and A. Sugimura, Late Quaternary uplift in eastern Indonesia, Tectonophysics, 23, 427-433, 1974

Warnock, A. C. and P. K. Zeitler, 40Ar/39Ar thermochronometry of K-feldspar from the KTB borehole, Germany, Earth and Planetary Science Letters, 158, 67-79, 1998.

Whipple, K., Kirby, E., and S. H. Brocklehurst, Geomorphic limits to climate-induced increases in topographic relief, Nature, 401, 39-43, 1999.

Wolf, R. A., Farley, K. A., and L. T. Silver, Assessment of (U-Th)/He thermochronometry: the low-temperature history of the San Jacinto mountains, California, Geology, 25, 65-68, 1997.

Zaprowski, B. J., Evenson, E. B., Pazzaglia, F. J., and J. B. Epstein, Knickzone propagation in the Black Hills and northern High Plains: A different perspective on the late Cenozoic exhumation of the Laramide Rocky Mountains, Geology, 29, 547-550, 2001.

Zeitler, P. K., Argon diffusion in partially outgassed alkali feldspars: Insights from 40Ar/39Ar analysis, Chemical Geology, 65, 167-181, 1987.

Zeitler, P. K., Herczig, A. L., McDougall, I., and M. Honda, U-Th-He dating of apatite: a potential thermochronometer, Geochimica et Cosmochimica Acta, 51, 2865-2868, 1987.

Zeitler, P. K., Sutter, J. F., Williams, I. S., Zartman, R., and Tahirkheli, R. A. K., Geochronology and temperature history of the Nanga Parbat-Haramosh Massif, Pakistan, Geological Society of America Special Paper 232, 1-22, 1989.

Zeitler, P. K., Koons, P. O., Bishop, M. P., Chamberlain, C. P., Craw, D., Edwards, M. A., Hamidullah, S., Jan, M. Q., Khan, M. A., Khattak, M. U. K., Kidd, W. S. F., Mackie, R. L., Meltzer, A. S., Park, S. K., Pecher, A., Poage, M. A., Sarker, G., Schneider, D. A., Seeber, L., and Shroder, J. F., Crustal reworking at Nanga Parbat, Pakistan: Metamorphic consequences of thermal-mechanical coupling facilitated by erosion, Tectonics, 20, no. 5, 712-728, 2001.

Appendix A: Zircon (U-Th)/He data

* Sample heated to 1150 C for 45 minutes ** Sample heated to 1200 C for 20 minutes
^ sample heated to 1250 C for 20 minutes

Sample	4-He (mol)	U (ng)	Th (ng)	Geometry	Grain #	Width (um)	length (um)	Ft	Raw age (Ma)	Corrected age (Ma)
b115*	3.4005E-14	5.32258876	1.66888298	prism	3	155.00	345.00	0.843	1.10	1.31
b115				prism		112.00	282.00			
b115				prism		107.00	316.00			
b115*	8.3743E-14	18.7198701	2.10117283	prism	4	126.00	263.00	0.799	0.81	1.01
b115				prism		76.00	283.00			
b115				prism		78.00	245.00			
b115				prolate spheroid		101.00	318.00			
b141*	4.1804E-14	12.5631214	8.71054238	prism	2	220.00	280.00	0.900	0.53	0.59
b141				prolate spheroid		225.00	315.00			
b141*	5.331E-14	11.7575586	33.0745335	prolate spheroid	2	198.00	290.00	0.895	0.51	0.57
b141				prolate spheroid		223.00	262.00			
b-188	1.7157E-14	1.30136502	0.36598635	prism	1	120.6	207.91	0.829	2.29	2.77
b-188	2.6823E-14	3.15754703	0.67515926	prolate spheroid	1	113.92	167.27	0.818	1.50	1.84
b-232	2.0949E-14	23.1172288	0.24246835	prism	2	153.00	502.00	0.873	0.17	0.19
b-232	4.3834E-14	29.1017943	8.6313976	prism	1	96.82	382.81	0.803	0.26	0.33
b-247	2.3183E-15	3.85556911	1.76995607	prism	1	110.86	261.72	0.814	0.10	0.12
b-247	1.734E-14	4.429E+00	2.833E+00	prism	1	104.88	237.79	0.801	0.63	0.79
b-254*	5.9694E-13	200.190895	189.198095	prism	3	211.00	452.00	0.910	0.45	0.50
b-254				prism		164.00	439.00			
b-254				prism		202.00	393.00			
b-254*	5.8856E-13	214.567143	129.050619	prism	3	144.00	378.00	0.883	0.45	0.51
b-254				prism		216.00	357.00			
b-254				prism		191.00	264.00			
b265*	6.4406E-14	26.9458793	8.61048134	prism	3	134.00	231.00	0.832	0.41	0.50
b265				prism		148.00	179.00			
b265				prism		119.00	199.00			
b-265*	5.086E-14	13.1040253	10.3022541	prism	2	197.00	240.00	0.864	0.61	0.70
b-265				prism		132.00	301.00			

Appendix A: Zircon (U-Th)/He data

* Sample heated to 1150 C for 45 minutes ** Sample heated to 1200 C for 20 minutes
^ sample heated to 1250 C for 20 minutes

Sample	4-He (mol)	U (ng)	Th (ng)	Geometry	Grain #	Width (um)	length (um)	Ft	Raw age (Ma)	Corrected age (Ma)
b35*	1.2291E-12	16.8585392	25.7963464	prism	3	91.00	451.00	0.761	9.95	13.07
b35				prism		60.00	659.00			
b35				prism		87.00	391.00			
b35*	6.5244E-13	9.7881167	12.9495117	prolate spheroid	1	134.00	517.00	0.846	9.43	11.15
BC-02-02	4.9011E-13	3.60557464	2.15559828	prism	1	102.81	184.02	0.788	22.08	28.04
BC-02-02	4.8538E-12	29.8765268	17.6710174	prism	1	175.41	326.40	0.877	26.41	30.12
BC-03-02	4.9988E-13	8.27897975	6.17577171	prism	1	128.00	258.00	0.833	9.53	11.44
BC-03-02	4.4854E-13	6.38021686	4.41881758	prism	1	155.00	275.00	0.858	11.21	13.07
BL-03-03	1.0944E-12	18.2761967	4.47068731	prism	1	88.56	192.04	0.765	10.50	13.72
BL-03-03	1.0612E-12	17.9807627	4.53199014	prism	1	127.48	214.61	0.828	10.33	12.48
BL-05-03	3.3306E-13	7.62276637	2.19003828	prism	1	122.09	311.86	0.834	7.59	9.10
BL-05-03	6.6615E-13	7.5031873	4.34958579	prism	1	136.45	384.2	0.853	14.49	16.99
BL-06-03	3.7611E-11	9.01634509	3.26882879	prism	1	139.62	303.31	0.851	8.45	9.93
BL-06-03	4.2664E-13	8.54603298	2.99342153	prism	1	146.12	276.24	0.853	8.55	10.03
BL-07A-03	3.3359E-13	6.29716377	3.66592364	prism	1	154.77	299.12	0.861	8.64	10.04
BL-07A-03	2.1658E-12	10.6593385	3.35738493	prism	1	174.47	323.25	0.883	8.04	9.10
BL-09-03	4.3309E-14	3.58105181	0.62469967	prolate spheroid	1	148.65	284.5	0.863	2.16	2.50
BL-09-03	1.3346E-13	2.80340056	2.12633115	prolate spheroid	1	110.5	203.38	0.803	7.49	9.34
BM-02-02	2.6722E-13	6.00360095	3.37152723	prism	1	137.34	223.61	0.838	7.29	8.71
BM-02-02	2.8346E-13	5.39881894	4.98816346	prism	1	111.21	390.60	0.823	8.00	9.72
BM-03-02	1.4987E-13	2.78585175	3.32658928	prism	1	109.61	190.66	0.797	7.79	9.78
BM-03-02	2.2428E-13	5.49186195	1.37399413	prism	1	59.67	145.57	0.659	7.15	10.86
BT-07-02**	2.2622E-13	30.5928246	4.62613359	prism	2	108.00	329.00	0.851	1.33	1.56
BT-07-02				prism		100.00	490.00			
BT-07-02**	1.535E-13	24.4913715	2.49029909	prism	2	148.00	250.00	0.856	1.14	1.33
BT-07-02				prism		148.00	313.00			
BT-08-02	8.0357E-14	3.0985757	2.24905436	prism	1	124.33	270.76	0.831	4.11	4.95
BT-09-01	1.1855E-13	4.84294164	1.53263089	prism	1	120.80	269.28	0.828	4.23	5.11

Appendix A: Zircon (U-Th)/He data

* Sample heated to 1150 C for 45 minutes ** Sample heated to 1200 C for 20 minutes
^ sample heated to 1250 C for 20 minutes

Sample	4-He (mol)	U (ng)	Th (ng)	Geometry	Grain #	Width (um)	length (um)	Ft	Raw age (Ma)	Corrected age (Ma)
BT-09-01	2.1734E-13	7.79926974	0.5991716	prolate spheroid	1	128.00	298.00	0.842	5.08	6.03
BT-12-02	2.1908E-13	10.4633488	4.90902215	prism	1	99.32	375.74	0.806	3.50	4.34
BT-12-02	1.7269E-13	7.49110371	2.06682349	prism	1	80.47	242.00	0.755	4.02	5.32
BT-17-02^	2.3465E-13	27.7197838	2.31764475	prism	2	157.00	337.00	0.844	1.54	1.83
BT-17-02				prism		132.00	303.00			
BT-17-02^	2.0635E-13	20.946686	2.16842518	prism	2	129.00	333.00	0.840	1.78	2.12
BT-17-02				prism		123.00	285.00			
BT-18-01*	3.4776E-14	23.0276489	7.95594262	prism	2	145.00	350.00	0.850	0.26	0.30
BT-18-01				prism		124.00	341.00			
BT-18-01*	3.7921E-14	17.822471	6.22122428	prism	2	146.00	402.00	0.860	0.36	0.42
BT-18-01				prism		149.00	286.00			
BT-20-02^	8.3844E-14	13.4545143	8.20500523	prism	3	81.00	284.00	0.787	1.01	1.29
BT-20-02				prism		100.00	264.00			
BT-20-02				prism		93.00	383.00			
BT-20-02^	8.0572E-14	13.2388347	2.89130624	prism	2	156.00	280.00	0.849	1.07	1.27
BT-20-02				prism		120.00	263.00			
BT-20E-02	2.3098E-12	33.302304	0.23673076	prism	1	157.00	454.00	0.874	12.84	14.69
BT-20E-02	3.1744E-13	3.23208285	3.03475194	prism	1	106.69	341.77	0.813	14.92	18.35
BT-20E-02	2.3186E-12	37.2688162	0.26492687	prism	1	176.00	393.00	0.883	11.52	13.04
BT-21E	2.0594E-13	7.60047326	2.31728167	prism	1	110.78	238.95	0.812	4.69	5.78
BT-21E-02	1.8005E-13	7.09562545	2.77025306	prism	1	125.00	373.00	0.841	4.31	5.13
BT-23-02	6.5405E-14	7.9379447	2.3545016	prism	1	101.22	337.95	0.808	1.43	1.77
BT-23-02	1.2852E-13	20.5470721	3.23746493	prism	1	123.00	424.00	0.843	1.12	1.33
BT-24-02	4.1092E-14	14.8559755	0.11330324	prism	2	118.00	322.00	0.831	0.51	0.62
BT-24-02	1.0434E-13	31.9077408	2.59158342	prism	1	115.97	351.45	0.831	0.60	0.72
BT-29-02	7.1001E-15	1.37705355	1.81944218	prism	1	70.52	247.74	0.719	0.73	1.02
BT-29-02	1.4769E-13	19.0845087	2.58121954	prism	1	108.50	211.57	0.805	1.39	1.73
BT-31-02	1.684E-12	150.798582	8.79708182	prism	1	104.07	336.16	0.814	2.04	2.51

Appendix A: Zircon (U-Th)/He data

* Sample heated to 1150 C for 45 minutes ** Sample heated to 1200 C for 20 minutes
^ sample heated to 1250 C for 20 minutes

Sample	4-He (mol)	U (ng)	Th (ng)	Geometry	Grain #	Width (um)	length (um)	Ft	Raw age (Ma)	Corrected age (Ma)
BT-31-02	2.9482E-12	204.777624	13.7686986	prism	1	128.39	338.16	0.844	2.63	3.12
BT-8-02	1.5697E-13	8.33558436	0.2433141	prism	2	100.00	441.00	0.812	3.47	4.27
GP-09-03	2.2832E-13	83.2042472	15.5149238	prism	1	123.67	367.05	0.841	0.49	0.58
GP-09-03	6.0721E-14	20.1495075	7.36250827	prism	1	113.85	281.07	0.821	0.52	0.63
GP-14-03	1.1815E-13	27.0864462	6.67127806	prism	1	121.13	246.26	0.826	0.77	0.93
GP-14-03	1.0722E-13	32.0652329	12.2415962	prism	1	109.6	167.78	0.795	0.57	0.72
IG-19-01	3.2896E-14	3.44401334	0.61688384	prism	1	84.31	199.02	0.758	1.70	2.24
IG-19-01	8.4225E-14	7.90075495	0.17046443	prism	1	80.47	179.02	0.745	1.97	2.64
IG-20b-01	7.8014E-14	5.91631617	0.34101981	prism	3	107.00	288.00	0.812	2.41	2.97
IG-20b-01	2.0325E-14	1.67286063	0.57173423	prism	1	75.14	280.95	0.744	2.09	2.81
IG-15a-01	2.8693E-12	427.47856	1.83979334	prism	1	254.00	453.00	0.915	1.24	1.36
IG-15a-01	1.7183E-12	261.908652	1.20040548	prism	1	325.00	400.00	0.927	1.22	1.31
NB02-102	6.346E-13	18.7204968	3.34801222	prism	1	120.75	248.13	0.826	6.03	7.31
NB02-102	6.2716E-13	19.1839646	4.17842466	prism	1	139.00	336.00	0.853	5.77	6.76
NB02-120	3.0509E-12	42.624342	8.89137164	prism	1	163.00	513.00	0.880	12.65	14.37
NB02-120	7.8873E-13	13.0438535	3.01223123	prism	1	119.35	275.77	0.828	10.64	12.84
NB02-159**	1.028E-12	41.6022084	8.93475323	prism	1	117.00	518.00	0.839	4.36	5.20
NB02-159**	7.5856E-13	27.2199931	5.62151203	prism	1	158.00	450.00	0.874	4.93	5.64
NB02-35	2.8629E-14	3.22832399	1.1710143	prism	1	108.24	268.37	0.812	1.52	1.87
NB02-35	6.201E-14	7.5458468	2.25379577	prism	1	134.00	354.00	0.850	1.43	1.68

Standards	4-He (mol)	U (ng)	Th (ng)	Geometry	Grain #	Width (um)	Length (um)	Ft	Raw age (Ma)	Corrected age (Ma)
Published age of Fish Canyon zircon: 29.7 Ma (Carpéna and Mailhé, 1987) Average age of standards: 28.2 Ma; 1s: 1.689; RSD %: 5.99.										
Fish Canyon 59/03	1.98E-13	1.58E+00	8.84E-01	prolate spheroid	1	105	200.00	0.803	20.54	25.57
Fish Canyon 59/03-2	2.41E-13	1.85E-100	9.38E-01	prolate spheroid	1	111	208.00	0.804	21.54	26.79
FC-1 197/03	7.1203E-13	5.053266	0.49980053	prism	1	146	274	0.852	25.5	29.93
FC-2 197/03	1.8398E-12	12.5459775	0.58005815	prism	1	157	539	0.875	26.86	30.69

Appendix A: Zircon (U-Th)/He data

* Sample heated to 1150 C for 45 minutes ** Sample heated to 1200 C for 20 minutes
^ sample heated to 1250 C for 20 minutes

Sample	4-He (mol)	U (ng)	Th (ng)	Geometry	Grain #	Width (um)	length (um)	Ft	Raw age (Ma)	Corrected age (Ma)
FC-3 197/03	1.9047E-12	12.671213	0.65189366	prism	1	148	529	0.868	27.5	31.68
FC-1 227/03	1.6515E-12	11.738403	7.0383788	prism	1	179	456	0.886	22.84	25.78
FC-1 239/03	7.8239E-13	5.46769274	2.74925867	prism	1	100.36	216.09	0.791	23.7	29.97
FC-2 239/03	9.8104E-13	6.94315555	3.95186444	prism	1	117.54	286.62	0.825	23.09	27.98
FC-1 batch013	4.1756E-13	3.20516229	1.34423919	prism	1	92.65	229.98	0.78	21.97	28.16
FC-2 batch013	9.2777E-13	6.71259612	3.63693964	prism	1	128.02	292.93	0.838	22.71	27.1
FC1-014	4.9787E-13	3.82416286	2.51939057	prism	1	110.14	228.05	0.807	20.89	25.88
FC1-15	4.6285E-13	3.38404411	1.65017916	prism	1	110.65	182.48	0.800	22.73	28.43
FC1-16	1.6785E-12	11.8942221	4.42954735	prism	1	116.92	222.8	0.817	24.03	29.42
FC2-014	3.7085E-13	2.61367616	1.77814874	prism	1	93.36	168.1	0.766	22.66	29.59
FC2-15	5.4323E-13	3.97309564	2.14019631	prism	1	113.16	188.78	0.804	22.48	27.96
FC2-16	6.5333E-13	4.61167282	2.65942895	prism	1	111.13	239.88	0.811	23.11	28.05
FC3-014	4.0513E-13	3.01547203	1.79019618	prism	1	100.54	166.07	0.779	21.84	28.05
FC3-15	3.6668E-13	2.59763322	2.12209844	prism	1	119.4	223.63	0.818	21.94	26.83
FC3-16	9.6026E-13	6.81548341	3.4778587	prism	1	128.18	257.98	0.834	23.03	27.94

* Sample heated to 1150 C for 45 minutes ** Sample heated to 1200 C for 20 minutes
^ sample heated to 1250 C for 20 minutes

Appendix B: Isotopic analysis of feldspars from SE Tibet

Temperature °C	duration min	$^{40}Ar/^{39}Ar$	$^{38}Ar/^{39}Ar$	$^{37}Ar/^{39}Ar$	$^{36}Ar/^{39}Ar$	^{39}Ar 10^{-13} mol	^{39}Ar Released %	$^{40}Ar^*$ %	Age +/- 1σ Ma
BT-36-02. K-feldspar; wt= 0.039 g; Irradiation: J = 0.0095; $(^{36}Ar/^{37}Ar)_{Ca} = 2.641 \times 10^{-4}$; $(^{39}Ar/^{37}Ar)_{Ca} = 6.792 \times 10^{-4}$; $(^{40}Ar/^{39}Ar)_K = 2.98 \times 10^{-2}$; $(^{38}Ar/^{39}Ar)_K = 0.01$.									
450	15	35.47898	0.24737	0.03639	0.78742	0.05025	0.22	13.23	524.02 ± 35.85
450	15	4.65945	0.04601	0.00999	0.19034	0.02612	0.11	7.65	78.14 ± 12.23
480	15	5.03538	0.03643	0.00660	0.02256	0.04835	0.21	42.92	84.30 ± 2.26
480	15	3.31367	0.02485	0.01442	0.00550	0.02870	0.13	66.70	55.92 ± 2.65
500	15	3.20949	0.02221	0.00528	0.00252	0.04187	0.18	80.57	54.18 ± 1.82
500	15	2.66011	0.01926	0.00872	0.00192	0.03037	0.13	81.68	45.02 ± 2.75
530	15	4.45164	0.03169	0.00804	0.00149	0.07830	0.34	90.45	74.73 ± 0.99
530	15	2.20182	0.01520	0.00982	0.00102	0.06114	0.27	86.95	37.35 ± 1.26
550	15	3.18999	0.02091	0.00747	0.00078	0.10334	0.45	92.43	53.86 ± 0.76
550	15	1.60350	0.00835	0.01032	0.00062	0.08063	0.35	88.27	27.27 ± 0.96
580	15	5.10551	0.03301	0.01049	0.00117	0.18851	0.83	93.12	85.45 ± 0.50
580	15	1.48778	0.00667	0.00949	0.00046	0.14163	0.62	89.96	25.32 ± 0.56
600	15	2.27493	0.01227	0.01101	0.00049	0.20987	0.92	92.86	38.57 ± 0.40
600	15	1.39864	0.00527	0.00974	0.00040	0.16054	0.71	90.47	23.81 ± 0.49
630	15	7.53551	0.05397	0.00897	0.00129	0.33700	1.48	94.84	124.74 ± 0.49
630	15	1.39416	0.00497	0.00729	0.00027	0.19892	0.87	92.71	23.74 ± 0.41
660	15	2.92811	0.01732	0.00675	0.00061	0.31349	1.38	93.27	49.50 ± 0.33
660	15	1.45607	0.00536	0.00896	0.00043	0.18127	0.80	90.27	24.78 ± 0.45
690	15	1.98725	0.01030	0.00949	0.00068	0.24975	1.10	89.64	33.74 ± 0.35
690	15	1.83290	0.00763	0.01000	0.00060	0.15472	0.68	89.91	31.14 ± 0.51
720	15	2.43212	0.01239	0.01274	0.00076	0.21234	0.93	90.49	41.21 ± 0.46
720	15	1.60948	0.00482	0.01282	0.00265	0.12759	0.56	66.41	27.38 ± 0.66
750	15	1.99197	0.00799	0.01533	0.00186	0.18321	0.81	77.49	33.82 ± 0.45
750	15	1.67777	0.00484	0.01536	0.00137	0.12847	0.56	79.44	28.53 ± 0.66
780	15	1.87956	0.00670	0.01916	0.00111	0.19494	0.86	83.97	31.93 ± 0.46
780	15	1.72835	0.00505	0.01819	0.00109	0.14171	0.62	83.10	29.38 ± 0.57
810	15	1.89875	0.00705	0.02032	0.00101	0.21418	0.94	85.23	32.25 ± 0.42
810	15	1.86327	0.00587	0.01877	0.00097	0.15207	0.67	85.47	31.65 ± 0.53
840	15	2.08990	0.00720	0.01810	0.00092	0.22398	0.98	87.43	35.47 ± 0.38
860	15	2.67327	0.01205	0.01719	0.00110	0.30250	1.33	88.30	45.24 ± 0.39
890	15	2.58666	0.01017	0.01639	0.00088	0.38361	1.69	89.92	43.80 ± 0.35

Appendix B: Isotopic analysis of feldspars from SE Tibet

Temperature °C	duration min	$^{40}Ar/^{39}Ar$	$^{38}Ar/^{39}Ar$	$^{37}Ar/^{39}Ar$	$^{36}Ar/^{39}Ar$	^{39}Ar 10^{-13} mol	^{39}Ar Released %	$^{40}Ar^*$ %	Age +/- 1σ Ma
910	15	2.89501	0.01175	0.01472	0.00090	0.39581	1.74	90.71	48.95 ± 0.29
940	15	3.39536	0.01534	0.01330	0.00096	0.53202	2.34	91.56	57.27 ± 0.30
960	15	3.79974	0.01830	0.01092	0.00105	0.58266	2.56	91.76	63.97 ± 0.28
990	15	4.35801	0.02319	0.01062	0.00131	0.84127	3.70	91.25	73.19 ± 0.28
1010	15	4.74891	0.02610	0.00960	0.00132	0.98779	4.34	91.89	79.61 ± 0.30
1030	15	5.24930	0.03009	0.00919	0.00126	1.21872	5.36	92.89	87.79 ± 0.33
1050	15	5.74309	0.03417	0.01034	0.00126	1.40429	6.17	93.48	95.84 ± 0.36
1050	15	5.81358	0.03319	0.00963	0.00131	0.94053	4.13	93.33	96.98 ± 0.35
1050	15	5.99829	0.03457	0.00990	0.00145	0.72839	3.20	92.88	99.98 ± 0.42
1050	45	6.41379	0.03759	0.01052	0.00154	1.42879	6.28	92.98	106.71 ± 0.41
1050	45	6.75811	0.04161	0.01066	0.00190	0.87793	3.86	91.96	112.26 ± 0.42
1050	120	7.22955	0.04610	0.01060	0.00232	1.46583	6.44	90.99	119.84 ± 0.50
1050	120	7.48981	0.04904	0.01082	0.00295	0.92113	4.05	89.26	124.00 ± 0.64
1050	120	7.74298	0.04960	0.01003	0.00259	0.60724	2.67	90.69	128.05 ± 0.64
1050	120	7.82445	0.04955	0.01047	0.00062	0.37667	1.66	97.36	129.35 ± 0.70
1050	120	7.88484	0.05010	0.00927	0.00059	0.29526	1.30	97.47	130.31 ± 0.92
1050	120	7.95349	0.04948	0.00996	0.00053	0.23674	1.04	97.71	131.41 ± 0.99
1050	120	8.00339	0.05112	0.00857	0.00050	0.19985	0.88	97.84	132.20 ± 1.29
1070	15	8.14405	0.05158	0.01184	0.00071	0.03625	0.16	97.14	134.44 ± 2.11
1090	15	8.39723	0.05524	0.00906	0.00083	0.06813	0.30	96.82	138.47 ± 1.21
1110	15	8.64965	0.05808	0.00766	0.00073	0.12976	0.57	97.24	142.47 ± 0.73
1050	15	8.56627	0.05852	0.01179	0.00083	0.04193	0.18	96.89	141.15 ± 1.82
1170	15	8.71921	0.06121	0.01070	0.00089	0.83643	3.68	96.74	143.57 ± 0.64
1200	15	8.16068	0.05557	0.00831	0.00071	0.64265	2.83	97.14	134.71 ± 0.45
1230	15	8.04304	0.04881	0.00520	0.00057	1.44937	6.37	97.61	132.83 ± 0.53
1260	15	7.73733	0.03944	0.00611	0.00048	0.41289	1.82	97.81	127.96 ± 0.52
1290	15	8.25261	0.03814	0.01527	0.00064	0.09097	0.40	97.43	136.17 ± 0.96
1320	15	8.61506	0.04207	0.01583	0.00038	0.02238	0.10	98.39	141.92 ± 3.38
1370	15	14.56182	0.08441	0.07202	0.00441	0.01815	0.08	91.61	233.75 ± 4.24
1450	15	28.14075	0.20773	0.04759	0.01273	0.00773	0.03	88.13	427.42 ± 10.23

NB02-120. K-feldspar; wt= 0.083 g; Irradiation: J = 0.0095; $(^{36}Ar/^{37}Ar)_{Ca} = 2.641 \times 10^{-4}$; $(^{39}Ar/^{37}Ar)_{Ca} = 6.792 \times 10^{-4}$; $(^{40}Ar/^{39}Ar)_K = 2.98 \times 10^{-2}$; $(^{38}Ar/^{39}Ar)_K = 0.01$.

Appendix B: Isotopic analysis of feldspars from SE Tibet

Temperature °C	duration min	$^{40}Ar/^{39}Ar$	$^{38}Ar/^{39}Ar$	$^{37}Ar/^{39}Ar$	$^{36}Ar/^{39}Ar$	^{39}Ar 10^{-13} mol	^{39}Ar Released %	$^{40}Ar^*$ %	Age +/- 1σ Ma
450	15	22.10389	0.07293	0.04735	0.48932	0.05582	0.14	13.26	343.87 ± 25.27
450	15	1.41319	0.02831	0.00494	0.12881	0.02054	0.05	3.58	24.06 ± 12.35
470	15	1.39598	0.01957	0.00609	0.02942	0.03003	0.08	13.80	23.77 ± 5.14
470	15	0.89942	0.01391	0.01620	0.01356	0.02178	0.06	18.22	15.35 ± 6.73
490	15	0.95697	0.01040	0.00681	0.00668	0.03451	0.09	32.32	16.33 ± 4.24
490	15	0.94956	0.00752	0.00929	0.00576	0.02534	0.06	35.42	16.20 ± 5.82
510	15	0.79894	0.00636	0.01762	0.00409	0.04141	0.11	39.24	13.64 ± 3.57
510	15	0.80871	0.00428	0.00839	0.00387	0.03242	0.08	40.83	13.81 ± 4.51
530	15	0.95254	0.00383	0.01181	0.00326	0.05292	0.14	48.96	16.25 ± 2.76
530	15	0.67716	0.00293	0.01582	0.00332	0.04264	0.11	40.13	11.57 ± 3.45
550	15	1.00198	0.00294	0.01071	0.00208	0.07201	0.18	60.81	17.09 ± 2.05
550	15	0.95708	0.00272	0.00953	0.00175	0.05845	0.15	63.68	16.33 ± 2.54
580	15	0.95597	0.00271	0.00755	0.00193	0.13090	0.34	61.38	16.31 ± 1.13
580	15	0.99307	0.00216	0.00634	0.00248	0.10555	0.27	56.52	16.94 ± 1.44
600	15	0.88691	0.00216	0.00754	0.00124	0.16723	0.43	69.07	15.14 ± 0.92
600	15	0.92632	0.00237	0.00567	0.00075	0.13553	0.35	78.72	15.81 ± 1.12
630	15	0.97578	0.00243	0.00640	0.00113	0.28397	0.73	72.80	16.65 ± 0.56
630	15	0.93540	0.00225	0.00551	0.00074	0.21763	0.56	78.98	15.96 ± 0.73
650	15	0.92046	0.00219	0.00544	0.00058	0.30795	0.79	81.97	15.71 ± 0.49
680	15	0.95574	0.00222	0.00580	0.00046	0.62322	1.60	85.11	16.31 ± 0.29
700	15	0.92296	0.00231	0.00588	0.00039	0.82587	2.12	86.51	15.75 ± 0.22
730	15	0.93261	0.00241	0.00592	0.00023	1.25352	3.21	90.45	15.91 ± 0.17
750	15	0.93946	0.00224	0.00561	0.00026	1.37244	3.52	89.72	16.03 ± 0.16
780	15	0.95426	0.00229	0.00599	0.00019	1.83518	4.70	91.78	16.28 ± 0.20
800	15	0.97659	0.00217	0.00551	0.00019	1.59397	4.09	91.87	16.66 ± 0.15
830	15	0.97798	0.00220	0.00513	0.00026	1.63444	4.19	90.17	16.68 ± 0.15
850	15	1.00249	0.00237	0.00466	0.00027	1.33941	3.43	90.08	17.10 ± 0.25
880	15	1.00553	0.00224	0.00436	0.00036	1.52278	3.90	88.10	17.15 ± 0.15
900	15	1.00518	0.00225	0.00341	0.00043	1.17204	3.00	86.41	17.15 ± 0.17
930	15	1.03648	0.00225	0.00326	0.00055	1.13035	2.90	84.32	17.68 ± 0.20
960	15	1.04804	0.00229	0.00318	0.00071	1.11809	2.87	81.41	17.87 ± 0.19
990	15	1.09676	0.00227	0.00284	0.00084	1.11294	2.85	79.70	18.70 ± 0.19
1010	15	1.15322	0.00233	0.00311	0.00100	0.99569	2.55	78.00	19.66 ± 0.22
1030	15	1.19554	0.00233	0.00377	0.00129	1.00263	2.57	74.46	20.37 ± 0.22

Appendix B: Isotopic analysis of feldspars from SE Tibet

Temperature °C	duration min	$^{40}Ar/^{39}Ar$	$^{38}Ar/^{39}Ar$	$^{37}Ar/^{39}Ar$	$^{36}Ar/^{39}Ar$	^{39}Ar 10^{-13} mol	^{39}Ar Released %	$^{40}Ar^*$ %	Age +/- 1σ Ma
1050	15	1.22894	0.00253	0.00353	0.00134	1.06726	2.74	74.22	20.94 ± 0.24
1050	15	1.23298	0.00243	0.00349	0.00161	0.78461	2.01	70.94	21.01 ± 0.31
1050	15	1.25434	0.00267	0.00366	0.00152	0.64002	1.64	72.36	21.37 ± 0.29
1050	45	1.25231	0.00250	0.00341	0.00152	1.43560	3.68	72.33	21.34 ± 0.20
1050	45	1.26070	0.00237	0.00337	0.00161	1.00219	2.57	71.34	21.48 ± 0.21
1050	120	1.24897	0.00255	0.00326	0.00197	1.68439	4.32	67.16	21.28 ± 0.27
1050	120	1.30933	0.00259	0.00347	0.00225	1.06923	2.74	65.31	22.30 ± 0.40
1050	120	1.31324	0.00257	0.00321	0.00247	0.79111	2.03	63.32	22.37 ± 0.44
1050	120	1.30450	0.00258	0.00329	0.00267	0.64345	1.65	61.40	22.22 ± 0.51
1050	120	1.30315	0.00264	0.00332	0.00190	0.45636	1.17	68.74	22.20 ± 0.67
1050	120	1.32136	0.00254	0.00311	0.00014	0.29634	0.76	94.94	22.51 ± 1.02
1050	120	1.33470	0.00244	0.00248	0.00007	0.25424	0.65	96.26	22.73 ± 1.13
1050	120	1.34972	0.00232	0.00329	0.00000	0.21681	0.56	97.84	22.99 ± 1.12
1070	15	1.34653	0.00221	0.00395	0.00000	0.03952	0.10	97.83	22.93 ± 1.66
1090	15	1.39563	0.00250	0.00418	0.00005	0.06238	0.16	96.93	23.76 ± 2.34
1110	15	1.43784	0.00274	0.00342	0.00015	0.09859	0.25	95.05	24.48 ± 1.50
1140	15	1.41019	0.00283	0.00362	0.00052	0.20421	0.52	88.52	24.01 ± 0.73
1170	15	1.42817	0.00276	0.00363	0.00054	0.38063	0.98	88.23	24.31 ± 0.41
1200	15	1.38515	0.00276	0.00342	0.00071	0.36842	0.94	85.24	23.58 ± 0.42
1230	15	1.40343	0.00266	0.00286	0.00066	1.47211	3.77	86.23	23.89 ± 0.19
1260	15	1.36376	0.00257	0.00210	0.00064	2.02313	5.19	86.12	23.22 ± 0.17
1290	15	1.37446	0.00284	0.00169	0.00068	1.56508	4.01	85.59	23.40 ± 0.21
1320	15	1.37788	0.00286	0.00169	0.00079	0.88853	2.28	84.02	23.46 ± 0.23
1370	15	1.43322	0.00288	0.00220	0.00095	1.08697	2.79	82.18	24.40 ± 0.21
1450		1.49397	0.00398	0.00183	0.00196	0.11372	0.29	71.01	25.42 ± 1.31
BT-33-02. K-feldspar; wt=0.10 g; Irradiation: J = 0.0095; $(^{36}Ar/^{37}Ar)_{Ca} = 2.641 \times 10^{-4}$; $(^{39}Ar/^{37}Ar)_{Ca} = 6.792 \times 10^{-4}$; $(^{40}Ar/^{39}Ar)_K = 2.98 \times 10^{-2}$; $(^{38}Ar/^{39}Ar)_K = 0.01$.									
450	15	28.51711	0.13513	0.01241	0.40095	0.13251	0.28	19.40	432.50 ± 19.63
450	15	2.57402	0.01974	0.00209	0.05070	0.06804	0.14	14.64	43.58 ± 4.18
480	15	1.12956	0.01136	0.00144	0.00749	0.15931	0.34	33.50	19.26 ± 1.32
480	15	0.67523	0.00884	0.00114	0.00445	0.11517	0.24	33.43	11.54 ± 1.73
500	15	0.58339	0.00677	0.00162	0.00304	0.17838	0.38	38.63	9.97 ± 1.13
500	15	0.39698	0.00634	0.00166	0.00310	0.13589	0.29	29.57	6.79 ± 1.46

Appendix B: Isotopic analysis of feldspars from SE Tibet

Temperature °C	duration min	$^{40}Ar/^{39}Ar$	$^{38}Ar/^{39}Ar$	$^{37}Ar/^{39}Ar$	$^{36}Ar/^{39}Ar$	^{39}Ar 10^{-13} mol	^{39}Ar Released %	$^{40}Ar^*$ %	Age +/- 1σ Ma
530	15	0.38697	0.00502	0.00144	0.00224	0.30863	0.65	35.91	6.62 ± 0.66
530	15	0.28460	0.00463	0.00109	0.00212	0.24071	0.51	30.25	4.87 ± 0.84
550	15	0.25694	0.00378	0.00149	0.00142	0.37806	0.80	36.44	4.40 ± 0.54
550	15	0.19897	0.00344	0.00121	0.00140	0.30675	0.65	30.96	3.41 ± 0.65
580	15	0.21346	0.00328	0.00132	0.00107	0.65012	1.38	38.08	3.65 ± 0.33
580	15	0.18278	0.00292	0.00101	0.00091	0.48728	1.03	38.08	3.13 ± 0.42
600	15	0.17642	0.00302	0.00103	0.00089	0.71176	1.51	37.58	3.02 ± 0.30
600	15	0.15059	0.00245	0.00114	0.00079	0.53734	1.14	36.45	2.58 ± 0.38
630	15	0.16099	0.00277	0.00127	0.00086	0.99007	2.10	36.25	2.76 ± 0.23
630	15	0.14115	0.00264	0.00136	0.00061	0.72185	1.53	40.34	2.42 ± 0.29
660	15	0.14037	0.00232	0.00098	0.00064	1.19329	2.53	38.97	2.40 ± 0.20
660	15	0.13193	0.00255	0.00112	0.00045	0.81284	1.72	44.66	2.26 ± 0.26
690	15	0.14148	0.00257	0.00110	0.00049	1.13320	2.40	44.92	2.42 ± 0.20
690	15	0.12076	0.00234	0.00136	0.00062	0.76881	1.63	36.14	2.07 ± 0.28
720	15	0.14039	0.00243	0.00138	0.00048	1.05996	2.25	45.06	2.40 ± 0.22
720	15	0.12634	0.00244	0.00138	0.00044	0.69765	1.48	44.32	2.16 ± 0.30
750	15	0.15192	0.00245	0.00172	0.00051	0.91395	1.94	45.82	2.60 ± 0.24
750	15	0.13744	0.00233	0.00202	0.00047	0.58119	1.23	44.82	2.35 ± 0.36
780	15	0.15899	0.00232	0.00215	0.00058	0.75746	1.61	44.20	2.72 ± 0.28
810	15	0.16778	0.00255	0.00284	0.00056	0.85433	1.81	46.20	2.87 ± 0.26
840	15	0.16641	0.00255	0.00297	0.00062	0.86176	1.83	44.02	2.85 ± 0.26
870	15	0.25625	0.00314	0.00366	0.00104	1.06012	2.25	43.24	4.39 ± 0.22
900	15	0.26094	0.00296	0.00356	0.00079	1.10048	2.33	49.72	4.47 ± 0.21
930	15	0.34295	0.00369	0.00359	0.00111	1.21488	2.58	48.94	5.87 ± 0.20
960	15	0.44120	0.00424	0.00341	0.00132	1.36113	2.89	51.23	7.55 ± 0.20
990	15	0.53329	0.00490	0.00340	0.00149	1.56375	3.32	53.18	9.12 ± 0.19
1010	15	0.57291	0.00525	0.00356	0.00152	1.57023	3.33	54.53	9.79 ± 0.19
1030	15	0.61596	0.00577	0.00381	0.00154	1.52447	3.23	55.90	10.53 ± 0.20
1050	15	0.63364	0.00605	0.00444	0.00152	1.48283	3.14	56.99	10.83 ± 0.19
1050	15	0.61415	0.00640	0.00440	0.00144	1.01451	2.15	57.40	10.50 ± 0.24
1050	15	0.63092	0.00638	0.00444	0.00146	0.77840	1.65	57.74	10.78 ± 0.29
1050	45	0.63890	0.00656	0.00459	0.00158	1.59250	3.38	56.30	10.92 ± 0.17
1050	45	0.67343	0.00713	0.00444	0.00178	1.07675	2.28	54.78	11.50 ± 0.25
1050	45	0.73331	0.00726	0.00444	0.00185	0.81928	1.74	56.05	12.52 ± 0.30

Appendix B: Isotopic analysis of feldspars from SE Tibet

Temperature °C	duration min	$^{40}Ar/^{39}Ar$	$^{38}Ar/^{39}Ar$	$^{37}Ar/^{39}Ar$	$^{36}Ar/^{39}Ar$	^{39}Ar 10^{-13} mol	^{39}Ar Released %	$^{40}Ar^*$ %	Age +/- 1σ Ma
1050	45	0.73974	0.00751	0.00404	0.00196	0.68316	1.45	54.80	12.63 ± 0.28
1050	120	0.77901	0.00764	0.00413	0.00206	1.40090	2.97	54.98	13.30 ± 0.38
1050	120	0.78717	0.00806	0.00419	0.00226	1.06554	2.26	53.06	13.44 ± 0.36
1050	120	0.80731	0.00836	0.00435	0.00270	0.83515	1.77	49.42	13.78 ± 0.44
1050	120	0.79083	0.00893	0.00447	0.00261	0.69891	1.48	49.72	13.50 ± 0.50
1050	120	0.79749	0.00836	0.00460	0.00318	0.60440	1.28	45.11	13.62 ± 0.69
1050	120	0.85019	0.00838	0.00443	0.00239	0.52271	1.11	53.57	14.51 ± 0.66
1050	120	0.80129	0.00875	0.00419	0.00267	0.46217	0.98	49.49	13.68 ± 0.74
1050	120	0.77977	0.00857	0.00480	0.00280	0.40797	0.87	47.68	13.32 ± 0.81
1050	120	0.80724	0.00862	0.00452	0.00231	0.31975	0.68	53.12	13.78 ± 1.02
1070	15	0.82378	0.00900	0.00611	0.00056	0.04752	0.10	80.86	14.06 ± 4.15
1090	15	0.82586	0.00951	0.00519	0.00100	0.09181	0.19	71.78	14.10 ± 2.14
1110	15	0.87620	0.01001	0.00327	0.00139	0.16808	0.36	66.61	14.95 ± 1.17
1140	15	0.89552	0.01024	0.00252	0.00168	0.37199	0.79	63.02	15.28 ± 0.55
1170	15	0.92945	0.00972	0.00313	0.00180	0.66099	1.40	62.27	15.86 ± 0.35
1200	15	0.86560	0.00956	0.00306	0.00182	0.54534	1.16	60.35	14.77 ± 0.40
1230	15	0.90341	0.00949	0.00271	0.00172	1.74843	3.71	62.68	15.42 ± 0.19
1260	15	0.78213	0.00902	0.00157	0.00155	2.08245	4.42	61.60	13.36 ± 0.18
1290	15	0.64432	0.00756	0.00125	0.00146	1.25155	2.65	58.26	11.01 ± 0.22
1320	15	0.58303	0.00691	0.00126	0.00121	0.59095	1.25	60.03	9.96 ± 0.38
1370	15	0.66943	0.00720	0.00251	0.00131	0.59356	1.26	61.67	11.44 ± 0.36
1450	15	0.95003	0.00641	0.00374	0.00165	0.08609	0.18	64.76	16.21 ± 2.30
BT-20E-02. K-feldspar; wt=0.0855 g; Irradiation: J = 0.0095; $(^{36}Ar/^{37}Ar)_{Ca} = 2.641 \times 10^{-4}$; $(^{39}Ar/^{37}Ar)_{Ca} = 6.792 \times 10^{-4}$; $(^{40}Ar/^{39}Ar)_K = 2.98 \times 10^{-2}$; $(^{38}Ar/^{39}Ar)_K = 0.01$.									
450	15	13.82956	0.02858	0.00000	0.85263	0.05785	0.13	5.20	222.69 ± 91.99
450	15	0.48746	0.00713	0.09844	0.61996	0.01980	0.04	0.27	8.34 ± 78.81
480	15	0.94298	0.00477	0.00000	0.34963	0.04532	0.10	0.90	16.09 ± 43.82
480	15	0.27168	0.00471	0.05911	0.12916	0.03025	0.07	0.71	4.65 ± 24.12
500	15	1.29929	0.00383	0.02773	0.05231	0.04530	0.10	7.74	22.13 ± 13.73
500	15	1.12190	0.00265	0.00000	0.02559	0.03480	0.08	12.87	19.13 ± 15.84
530	15	1.48182	0.00483	0.04069	0.01174	0.09575	0.22	29.76	25.22 ± 5.87
530	15	0.86091	0.00299	0.05860	0.00655	0.06890	0.16	30.46	14.69 ± 7.95
550	15	0.98315	0.00273	0.00000	0.00489	0.10790	0.24	39.98	16.77 ± 5.08

Appendix B: Isotopic analysis of feldspars from SE Tibet

Temperature °C	duration min	$^{40}Ar/^{39}Ar$	$^{38}Ar/^{39}Ar$	$^{37}Ar/^{39}Ar$	$^{36}Ar/^{39}Ar$	^{39}Ar 10^{-13} mol	^{39}Ar Released %	$^{40}Ar^*$ %	Age +/- 1σ Ma
550	15	0.80988	0.00257	0.02775	0.00382	0.08867	0.20	41.15	13.83 ± 6.15
580	15	1.09791	0.00313	0.02062	0.00267	0.21410	0.48	57.25	18.72 ± 2.57
580	15	0.84316	0.00209	0.00195	0.00151	0.16802	0.38	63.95	14.39 ± 3.25
600	15	0.88570	0.00240	0.00000	0.00110	0.25889	0.58	71.46	15.12 ± 2.12
600	15	0.89875	0.00228	0.00728	0.00085	0.22088	0.50	76.18	15.34 ± 2.48
630	15	1.03141	0.00282	0.01062	0.00104	0.52284	1.18	75.40	17.59 ± 1.07
630	15	0.92728	0.00222	0.00697	0.00052	0.41259	0.93	83.47	15.82 ± 1.33
660	15	0.98809	0.00228	0.00478	0.00041	0.82660	1.86	86.83	16.86 ± 0.71
690	15	0.99520	0.00243	0.00043	0.00038	1.26479	2.85	87.51	16.98 ± 0.49
720	15	0.98646	0.00221	0.00483	0.00032	1.53924	3.46	88.87	16.83 ± 0.42
750	15	0.99111	0.00230	0.00327	0.00024	1.59663	3.59	90.82	16.91 ± 0.41
780	15	1.00967	0.00219	0.00194	0.00023	1.59903	3.60	91.11	17.22 ± 0.41
810	15	1.02368	0.00231	0.00821	0.00015	1.50478	3.39	93.15	17.46 ± 0.43
840	15	1.03990	0.00218	0.00921	0.00014	1.35247	3.04	93.61	17.74 ± 0.46
870	15	1.05640	0.00219	0.00283	0.00020	1.23096	2.77	92.24	18.02 ± 0.50
900	15	1.07327	0.00228	0.00560	0.00017	1.12099	2.52	93.06	18.30 ± 0.54
930	15	1.08785	0.00223	0.00376	0.00028	1.07874	2.43	90.66	18.55 ± 0.56
960	15	1.11528	0.00231	0.00930	0.00030	1.05714	2.38	90.43	19.01 ± 0.56
990	15	1.13385	0.00244	0.00934	0.00035	1.06669	2.40	89.48	19.33 ± 0.56
1010	15	1.16192	0.00245	0.00661	0.00051	0.96079	2.16	86.47	19.80 ± 0.62
1030	15	1.19011	0.00246	0.00000	0.00057	0.93031	2.09	85.72	20.28 ± 0.64
1050	15	1.21878	0.00253	0.00000	0.00062	0.89044	2.00	85.12	20.77 ± 0.66
1050	15	1.19721	0.00215	0.01041	0.00058	0.71868	1.62	85.56	20.40 ± 1.11
1050	15	1.26127	0.00264	0.01723	0.00060	0.58919	1.33	85.88	21.49 ± 0.96
1050	15	1.29239	0.00291	0.00000	0.00061	0.51187	1.15	86.10	22.02 ± 1.09
1050	15	1.28966	0.00294	0.00260	0.00059	0.44905	1.01	86.38	21.97 ± 1.24
1050	45	1.30481	0.00289	0.00547	0.00075	1.10032	2.48	83.82	22.23 ± 0.28
1050	45	1.32654	0.00284	0.00019	0.00077	0.84984	1.91	83.78	22.59 ± 0.28
1050	120	1.35635	0.00282	0.00463	0.00068	1.53933	3.46	85.38	23.10 ± 0.28
1050	120	1.39604	0.00289	0.00463	0.00056	1.07094	2.41	87.66	23.77 ± 0.29
1050	120	1.41345	0.00287	0.00000	0.00042	0.79070	1.78	90.22	24.06 ± 0.32
1050	120	1.42149	0.00290	0.00157	0.00028	0.59886	1.35	92.61	24.20 ± 0.98
1050	120	1.42049	0.00300	0.01223	0.00020	0.49525	1.11	94.19	24.18 ± 0.36
1050	120	1.44106	0.00304	0.00894	0.00008	0.42527	0.96	96.49	24.53 ± 0.39

Appendix B: Isotopic analysis of feldspars from SE Tibet

Temperature °C	duration min	$^{40}Ar/^{39}Ar$	$^{38}Ar/^{39}Ar$	$^{37}Ar/^{39}Ar$	$^{36}Ar/^{39}Ar$	^{39}Ar 10^{-13} mol	^{39}Ar Released %	$^{40}Ar^*$ %	Age +/- 1σ Ma
1070	15	1.30429	0.00306	0.04994	0.00000	0.06688	0.15	97.77	22.22 ± 5.14
1090	15	1.50086	0.00290	0.00000	0.00000	0.11193	0.25	98.05	25.54 ± 3.07
1110	15	1.50724	0.00294	0.01873	0.00043	0.17090	0.38	90.57	25.65 ± 3.18
1050	15	1.22256	0.00254	0.00000	0.00000	0.04970	0.11	97.62	20.83 ± 6.92
1170	15	1.50796	0.00322	0.00879	0.00105	0.60247	1.36	81.61	25.66 ± 0.94
1200	15	1.55593	0.00359	0.00516	0.00081	0.73614	1.66	85.23	26.47 ± 0.78
1230	15	1.57773	0.00372	0.00413	0.00091	1.13120	2.55	84.06	26.84 ± 0.59
1260	15	1.59997	0.00357	0.00154	0.00106	1.70900	3.85	82.35	27.22 ± 0.43
1290	15	1.60642	0.00335	0.00396	0.00118	2.50114	5.63	80.96	27.32 ± 0.37
1320	15	1.62172	0.00336	0.00608	0.00127	3.38192	7.61	80.02	27.58 ± 0.37
1370	15	1.60349	0.00316	0.00000	0.00129	3.57547	8.05	79.62	27.27 ± 0.35
1450	15	1.57176	0.00295	0.00154	0.00145	0.84824	1.91	77.45	26.74 ± 0.71
BT-07-02. K-feldspar; wt=0.083 g; Irradiation: J = 0.0095; $(^{36}Ar/^{37}Ar)_{Ca} = 2.641 \times 10^{-4}$; $(^{39}Ar/^{37}Ar)_{Ca} = 6.792 \times 10^{-4}$; $(^{40}Ar/^{39}Ar)_K = 2.98 \times 10^{-2}$; $(^{38}Ar/^{39}Ar)_K = 0.01$.									
450	15	50.53020	0.04758	0.13950	2.03789	0.03675	0.10	7.74	707.32 ± 90.10
450	15	1.19541	0.01044	0.03345	0.62438	0.01472	0.04	0.64	20.37 ± 39.33
480	15	1.36016	0.00592	0.02477	0.13056	0.03103	0.09	3.40	23.16 ± 10.02
480	15	0.00127	0.00348	0.01847	0.03050	0.01917	0.05	0.01	0.02 ± 9.96
500	15	0.74269	0.00319	0.02211	0.01201	0.02956	0.08	17.19	12.68 ± 6.32
500	15	0.08574	0.00345	0.02017	0.00878	0.02153	0.06	3.16	1.47 ± 8.67
530	15	0.50736	0.00343	0.04372	0.00502	0.05000	0.14	25.11	8.67 ± 3.73
530	15	0.22781	0.00230	0.04902	0.00354	0.03691	0.11	17.46	3.90 ± 5.01
550	15	0.40804	0.00277	0.05426	0.00259	0.05921	0.17	33.92	6.98 ± 3.13
550	15	0.26002	0.00231	0.05198	0.00206	0.04739	0.13	28.98	4.45 ± 3.90
580	15	0.37295	0.00235	0.05062	0.00157	0.11487	0.33	43.07	6.38 ± 1.61
580	15	0.15010	0.00218	0.03934	0.00107	0.10001	0.28	30.21	2.57 ± 1.85
600	15	0.22351	0.00231	0.03182	0.00080	0.17699	0.50	45.69	3.83 ± 1.05
600	15	0.14238	0.00211	0.02501	0.00066	0.15738	0.45	38.83	2.44 ± 1.19
630	15	0.30115	0.00223	0.02225	0.00063	0.35224	1.00	58.13	5.15 ± 0.54
630	15	0.15066	0.00218	0.01738	0.00050	0.29400	0.84	45.81	2.58 ± 0.64
660	15	0.14807	0.00235	0.01476	0.00034	0.54486	1.55	53.23	2.54 ± 0.35
660	15	0.17371	0.00242	0.01225	0.00247	0.51705	1.47	18.61	2.97 ± 0.41
690	15	0.17350	0.00230	0.01115	0.00116	0.89549	2.55	31.82	2.97 ± 0.24

Appendix B: Isotopic analysis of feldspars from SE Tibet

Temperature °C	duration min	$^{40}Ar/^{39}Ar$	$^{38}Ar/^{39}Ar$	$^{37}Ar/^{39}Ar$	$^{36}Ar/^{39}Ar$	^{39}Ar 10^{-13} mol	^{39}Ar Released %	$^{40}Ar^*$ %	Age +/- 1σ Ma
690	15	0.13486	0.00241	0.01134	0.00059	0.64760	1.84	39.65	2.31 ± 0.31
720	15	0.17075	0.00226	0.01243	0.00037	0.98508	2.80	55.35	2.92 ± 0.21
720	15	0.14265	0.00244	0.01255	0.00037	0.69706	1.98	50.76	2.44 ± 0.28
750	15	0.15549	0.00225	0.01551	0.00035	0.98798	2.81	53.82	2.66 ± 0.22
750	15	0.15012	0.00229	0.01751	0.00038	0.66956	1.90	51.15	2.57 ± 0.29
780	15	0.16258	0.00225	0.02088	0.00035	0.92990	2.65	54.79	2.78 ± 0.23
810	15	0.16968	0.00231	0.02513	0.00036	1.13480	3.23	55.53	2.91 ± 0.19
840	15	0.17280	0.00228	0.02726	0.00040	1.23395	3.51	54.11	2.96 ± 0.18
870	15	0.21263	0.00224	0.03184	0.00051	1.46996	4.18	54.20	3.64 ± 0.17
900	15	0.22051	0.00226	0.03533	0.00056	1.26001	3.58	52.90	3.78 ± 0.18
930	15	0.29627	0.00236	0.03533	0.00068	1.08942	3.10	56.08	5.07 ± 0.21
960	15	0.39980	0.00241	0.03017	0.00091	1.03292	2.94	57.35	6.84 ± 0.22
990	15	0.47607	0.00232	0.02395	0.00115	1.03771	2.95	56.33	8.14 ± 0.22
1010	15	0.46687	0.00237	0.01878	0.00140	0.88530	2.52	51.29	7.98 ± 0.25
1030	15	0.49829	0.00235	0.01677	0.00165	0.88455	2.52	49.09	8.52 ± 0.26
1050	15	0.51649	0.00244	0.01665	0.00179	0.90512	2.57	47.99	8.83 ± 0.26
1050	15	0.45768	0.00238	0.01635	0.00201	0.64339	1.83	42.33	7.83 ± 0.33
1050	45	0.44174	0.00228	0.01585	0.00214	0.50973	1.45	40.06	7.56 ± 0.41
1050	45	0.44412	0.00243	0.01718	0.00233	1.10510	3.14	38.22	7.60 ± 0.24
1050	120	0.48058	0.00243	0.01789	0.00256	0.76499	2.18	37.90	8.22 ± 0.27
1050	120	0.54594	0.00241	0.02033	0.00278	1.30968	3.73	39.06	9.33 ± 0.32
1050	120	0.58695	0.00242	0.02151	0.00322	0.86221	2.45	37.39	10.03 ± 0.43
1050	120	0.64153	0.00249	0.02111	0.00349	0.63562	1.81	37.65	10.96 ± 0.56
1050	120	0.66739	0.00239	0.02236	0.00345	0.51447	1.46	38.91	11.40 ± 0.67
1050	120	0.66232	0.00263	0.02126	0.00346	0.44083	1.25	38.60	11.32 ± 0.76
1050	120	0.64993	0.00261	0.02155	0.00365	0.35126	1.00	36.99	11.10 ± 0.94
1050	120	0.62244	0.00231	0.02114	0.00072	0.19851	0.56	71.87	10.64 ± 1.59
1070	15	0.76385	0.00253	0.01683	0.00000	0.03666	0.10	96.25	13.04 ± 2.68
1090	15	0.91803	0.00243	0.01860	0.00000	0.06434	0.18	96.86	15.67 ± 1.53
1110	15	0.96850	0.00286	0.01978	0.00024	0.11671	0.33	90.52	16.52 ± 1.57
1140	15	0.98530	0.00276	0.02114	0.00041	0.27331	0.78	86.64	16.81 ± 0.69
1170	15	1.00283	0.00269	0.01943	0.00059	0.49979	1.42	83.16	17.11 ± 0.38
1200	15	0.87289	0.00254	0.01885	0.00064	0.39203	1.12	79.95	14.90 ± 0.48
1230	15	0.90647	0.00260	0.01299	0.00051	1.68720	4.80	83.45	15.47 ± 0.16

Appendix B: Isotopic analysis of feldspars from SE Tibet

Temperature °C	duration min	$^{40}Ar/^{39}Ar$	$^{38}Ar/^{39}Ar$	$^{37}Ar/^{39}Ar$	$^{36}Ar/^{39}Ar$	^{39}Ar 10^{-13} mol	^{39}Ar Released %	$^{40}Ar^*$ %	Age +/- 1σ Ma
1260	15	0.70416	0.00249	0.00871	0.00037	2.20466	6.27	83.36	12.03 ± 0.15
1290	15	0.65163	0.00239	0.00892	0.00039	1.32298	3.76	81.91	11.13 ± 0.18
1320	15	0.58428	0.00245	0.01114	0.00045	0.68843	1.96	78.26	9.99 ± 0.29
1370	15	0.64488	0.00250	0.01417	0.00103	1.07065	3.05	65.85	11.02 ± 0.22
1450	15	1.67072	0.00299	0.02711	0.01766	0.10765	0.31	24.15	28.41 ± 2.08

Margaret A. Malloy

Background Born in Waukesha, WI on July 15, 1980 to John and Joyce Malloy.

Education

M.S., Earth and Environmental, Prospected 2004, Lehigh University
GPA: 3.71/4.0

B.S., Geological Sciences, 2002, University of South Carolina, Columbia
GPA: 3.68/4.0, Graduated Cum Laude

Expertise & skills I have been actively working since age 15. Through grants and wages earned, I was able to pay for all of my own education. I specialized in geology in both Undergraduate and Graduate work. I have worked both as a member as a team, as well as independently on numerous research projects in the past 4 years.

Professional experience

2002-present, Lehigh University, Bethlehem, PA
Research and Teaching Assistant
In addition to schooling, I was working 20 hours+ per week as a researcher/teaching assistant.
Teaching
Introduction to Planet Earth Laboratory TA: 2003/2004
Physical Geology and Geomorphology in the Rocky Mountains TA: 2002
Research
Erosion and Exhumation at the Namche Barwa Knickpoint, Tibet. (Graduate Thesis)
Age-elevation Relationships of zircons near Nanga Parbat, Pakistan (Assistant Investigator)
Tectonic Processes, Geochronology, Stable Isotope Geochemistry, Hydrogeology, and Paleoclimatology (Graduate Level Classes)

2000-2002, University of South Carolina, Columbia, SC
Undergraduate Research Assistant
In addition to obtaining my undergraduate degree, I worked 20 hours a week doing active research with my department.
Research
Rare Earth Element Interactions during Metamorphism (Assistant Investigator)
Groundwaters from Coastal Soils as Sources of Dissolved Organic Matter (Assistant Investigator)
Amazon Deep Sea Fan: An organic geochemical study of tropical paleoclimate (Assistant Investigator)

1999-2000, Modern Machine Works, Orangeburg, SC
Administrative Staff

I was a member of a five person administrative staff. For two years I worked part time during the school year and full time during the summer and vacation breaks. Modern Machine Works was a 200+ people manufacturer of automotive components.

1997-2000, Lake Park Golf Course, Germantown, WI

Bartender/Food Preparation

This was a second job taken during summers in High School/College

1996-1998, Andersons Fine Dining, Germantown, WI

Buser/Hostess

I started Busing sophomore year of high school. Worked ~20 hours a week throughout high school.

Professional membership & service

Member, American Geophysical Union: 2002-2004

Founder/ President, University of South Carolina Geology Club: 2002

Computer skills

Macintosh, Windows, Office (Word, Excel, PowerPoint), Adobe Illustrator and Photoshop, geochronology age modeling programs (Arvert and Lovera)

Publications

Kohn, M. J., and **Malloy, M. A.**, 2004, Formation of monazite via prograde metamorphic reactions among common silicates: Implications for age determinations: *Geochimica et Cosmochimica Acta*, v., 68, p. 101-113.

Malloy, M. A., Zeitler, P. K., Idleman, B. D., Reiners, P. W., and Zheng, L., 2003, Rapid Erosion at the Tsangpo Knickpoint and Exhumation of Southeastern Tibet: *2003 AGU Fall Meeting*

Awards

Joseph R. LeConte Outstanding Senior Award (in Geological Sciences), University of South Carolina, 2002

Joseph R. LeConte Outstanding Junior Award (in Geological Sciences), University of South Carolina, 2001

Stephan Taber Award, University of South Carolina, 2000

END OF TITLE